

University of Alabama in Huntsville

LOUIS

Theses

UAH Electronic Theses and Dissertations

2011

Initial design process for a pulsed thermonuclear fusion reaction engine

Ross Jared Cortez

Follow this and additional works at: <https://louis.uah.edu/uah-theses>

Recommended Citation

Cortez, Ross Jared, "Initial design process for a pulsed thermonuclear fusion reaction engine" (2011).

Theses. 575.

<https://louis.uah.edu/uah-theses/575>

This Thesis is brought to you for free and open access by the UAH Electronic Theses and Dissertations at LOUIS. It has been accepted for inclusion in Theses by an authorized administrator of LOUIS.

**INITIAL DESIGN PROCESS FOR A PULSED THERMONUCLEAR
FUSION REACTION ENGINE**

by

ROSS JARED CORTEZ

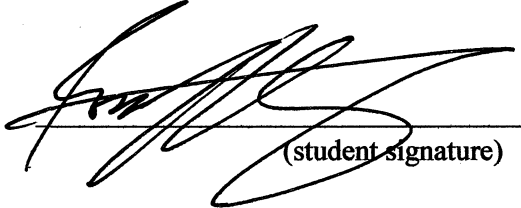
A THESIS

**Submitted in partial fulfillment of the requirements
for the degree of Master of Science in Engineering
in
The Department of Mechanical and Aerospace Engineering
to
The School of Graduate Studies
of
The University of Alabama in Huntsville**

HUNTSVILLE, ALABAMA

2011

In presenting this thesis in partial fulfillment of the requirements for a master's degree from The University of Alabama in Huntsville, I agree that the Library of this University shall make it freely available for inspection. I further agree that permission for extensive copying for scholarly purposes may be granted by my advisor or, in his/her absence, by the Chair of the Department or the Dean of the School of Graduate Studies. It is also understood that due recognition shall be given to me and to The University of Alabama in Huntsville in any scholarly use which may be made of any material in this thesis.


(student signature)

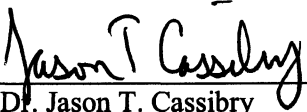
8/9/11

(date)


THESIS APPROVAL FORM

Submitted by Ross Jared Cortez in partial fulfillment of the requirements for the degree of Master of Science in Engineering and accepted on behalf of the Faculty of the School of Graduate Studies by the thesis committee.

We, the undersigned members of the Graduate Faculty of The University of Alabama in Huntsville, certify that we have advised and/or supervised the candidate on the work described in this thesis. We further certify that we have reviewed the thesis manuscript and approve it in partial fulfillment of the requirements for the degree of Master of Science in Engineering.

 7/11/11 Committee Chair


Dr. Jason T. Cassibry (Date)

 7/25/2011

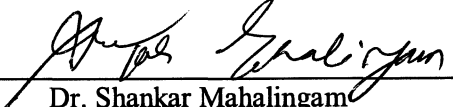
Dr. Robert B. Adams

 7/19/2011

Dr. Robert A. Frederick

 7/19/2011 Department Chair

Dr. Robert A. Frederick

 07/26/11 College Dean

Dr. Shankar Mahalingam

 8/9/11 Graduate Dean

Dr. Rhonda K. Gaede

ABSTRACT
The School of Graduate Studies
The University of Alabama in Huntsville

Degree Master of Science in Engineering College/Dept. Engineering/Mechanical and
Aerospace Engineering

Name of Candidate Ross Jared Cortez

Title Initial Design Process for a Pulsed Thermonuclear Fusion Reaction Engine

This thesis aims to illustrate the development and implementation of parametric cycle analysis based on the thermodynamic Otto cycle and then applies that analysis to pulsed fusion reaction engines. This method of analysis is intended to facilitate the design and development of fusion propulsion systems for future in-space mission requirements. Performance results are presented for different cases of initial fuel mass, ignition temperature, initial radius, system length, and dwell time. These results are then used to show how one may then estimate required system design points such as required driver storage energy, work input required to achieve ignition, liner implosion velocity, etc. Implications of the model results and the focus of future development and use of the model are discussed.

Abstract Approval: Committee Chair Jason T Cassalry
 Department Chair Robert O'Frederick M.
 Graduate Dean Rhonda Kay Baede 8/9/11

ACKNOWLEDGMENTS

I am deeply indebted to God for creating me to do this work and giving me this calling. Indeed, it was not I who did this, but Him.

Additionally, a number of people have supported me and put up with my nonsense through this endeavor. First, I want to thank my advisor, Dr. Jason Cassibry, for giving me a chance to do something worthwhile in the first place when we met almost 4 years ago. Without him, I wouldn't have made it past "go". I also want to thank Dr. William Seidler for his patience and willingness to provide guidance to our team here in the Propulsion Research Center, as well as his indispensable, indeed, seemingly inexhaustible, knowledge of the field we work in. My deepest gratitude also goes out to Dr. Robert Adams, who took me in and taught me the "Art of Systems Integration," and his wonderful guidance and friendship. Many thanks also go out to the rest of the team at the Advanced Concepts Office at Marshall Space Flight Center for their support and the challenging questions they asked that helped make this project what it has become. I would also like to thank Seth Thompson for his friendship, his time, and his amazing resilience when putting up with my shenanigans and complaints throughout this entire process. This work was supported by the Alabama Space Grant Consortium, contract #NNX10AJ80H. I am thankful to them for the support they have provided me so that I could dive into this headfirst. My heartfelt gratitude also goes out to my closest friends and my church family, without whom I never would have held onto the inspiration that has kept me going for so long. Thank you for all of your hard work and support in all of this.

Finally, I would like to thank the most wonderful family anyone could ever be blessed to have. Without you, I would have been hopeless. Without you, this would be meaningless. I am humbled by the way you have prayed for me, listened to me whine, and given me unhesitating support without asking anything in return. Your love graces each of these pages.

TABLE OF CONTENTS

| | |
|--|------------|
| LIST OF FIGURES | x |
| LIST OF TABLES | xii |
| Chapter | |
| 1 INTRODUCTION..... | 1 |
| 1.1 MOTIVATION | 1 |
| 1.2 THERMONUCLEAR FUSION TECHNOLOGY..... | 3 |
| 1.2.1 <i>Necessity of Confinement</i> | 4 |
| 1.2.2 <i>Gravitational Confinement</i> | 5 |
| 1.2.3 <i>Electrostatic Confinement</i> | 7 |
| 1.2.4 <i>Inertial Confinement</i> | 8 |
| 1.2.5 <i>Magnetic Confinement</i> | 9 |
| 1.2.6 <i>Magneto-Inertial Fusion (MIF)</i> | 10 |
| 1.3 PARAMETRIC CYCLE ANALYSIS | 11 |
| 1.4 FUSION PROPULSION SYSTEMS | 12 |
| 1.5 ROADMAP | 13 |
| 2 FUSION PROPULSION SYSTEM RESEARCH & DEVELOPMENT..... | 14 |
| 2.1 RELEVANCE OF MAGNETO-INERTIAL FUSION..... | 14 |
| 2.2 Z-PINCH RESEARCH & DEVELOPMENT | 15 |
| 2.2.1 <i>Relevant Z-Pinch Research</i> | 16 |
| 2.2.2 <i>Instability Mitigation Methods: Sheared Axial Flow</i> | 18 |
| 2.2.3 <i>Instability Mitigation Methods: Structured Gas-Puff Loads</i> | 21 |
| 2.3 Z-PINCH FUSION PROPULSION SYSTEM | 23 |

| | | |
|----------|---|-----------|
| 3 | FUSION REACTION ENGINE CYCLE ANALYSIS MODEL..... | 26 |
| 3.1 | ANALYTICAL MODELS & THEIR VALUE | 26 |
| 3.2 | THE OTTO CYCLE | 27 |
| 3.3 | FUSION REACTION ENGINE CYCLE | 29 |
| 3.4 | PERFORMANCE & FIGURES OF MERIT..... | 35 |
| 3.4.1 | <i>Exhaust Velocity & I_{sp}</i> | 36 |
| 3.4.2 | <i>Thrust Power</i> | 38 |
| 3.4.3 | <i>Efficiencies</i> | 39 |
| 3.4.4 | <i>Fusion Gain</i> | 40 |
| 4 | Z-PINCH FUSION REACTION ENGINE CYCLE ANALYSIS..... | 41 |
| 4.1 | BASIC Z-PINCH OPERATION | 41 |
| 4.2 | Z-PINCH CYCLE ANALYSIS & DESIGN PARAMETERS..... | 44 |
| 4.2.1 | <i>Work Input & Current Required</i> | 45 |
| 4.2.2 | <i>Liner Implosion Velocity & Exhaust Velocity</i> | 47 |
| 4.2.3 | <i>Gain</i> | 51 |
| 4.3 | SUMMARY OF EQUATIONS—Z-PINCH FUSION REACTION ENGINE | 52 |
| 5 | RESULTS & DISCUSSION..... | 55 |
| 5.1 | INTRODUCTION | 55 |
| 5.2 | MODEL PARAMETER SPACE..... | 55 |
| 5.3 | DEFINITION OF CASES..... | 57 |
| 5.4 | CASE STUDY I: PERFORMANCE RESULTS..... | 58 |
| 5.5 | CASE STUDY II: PERFORMANCE RESULTS | 63 |
| 5.6 | CASES I & II: DESIGN REQUIREMENTS | 68 |
| 5.6.1 | <i>Input Current</i> | 68 |
| 5.6.2 | <i>Driver Charging Energy</i> | 70 |
| 5.6.3 | <i>Liner Velocity</i> | 72 |
| 5.7 | CASE STUDY: Z-PINCH FUSION REACTION ENGINE VEHICLE DESIGN | 75 |

| | |
|--|------------|
| 6 CONCLUSIONS | 80 |
| 6.1 MODEL PERFORMANCE | 80 |
| 6.2 MODEL DEVELOPMENT & FUTURE WORK..... | 81 |
| 6.2.1 <i>Liner Properties</i> | 82 |
| 6.2.2 <i>Inductively Coupled Geometries: The θ-Pinch</i> | 83 |
| 6.3 FINAL THOUGHTS | 85 |
| APPENDIX A: Z-PINCH CYCLE SCRIPT: GO.M..... | 88 |
| APPENDIX B: Z-PINCH CYCLE INPUT FUNCTION: IN.M..... | 96 |
| APPENDIX C: Z-PINCH CYCLE CALCULATION FUNCTION: ZCYCLE.M..... | 103 |
| REFERENCES | 112 |

LIST OF FIGURES

| Figure | Page |
|---|------|
| 1.1: Inertial Electrostatic Fusion (IEF) device being developed at EMC2 [49]..... | 7 |
| 1.2: Inertial confinement fusion [50] | 8 |
| 1.3: Tokamak [51]..... | 9 |
| 1.4: MTF schematic showing plasma formation region and liner implosion section [6]..... | 10 |
| 2.1: Z-pinch instabilities. (a) $m = 0$ sausage mode and (b) $m = 1$ kink mode [52] | 19 |
| 2.2: Nonlinear simulation results showing pressure contours in a z-pinch. The results for each simulation time are aligned vertically. (a) No equilibrium axial flow is initialized. The plasma quickly develops an $m = 0$ mode and loses confinement. (b) An equilibrium axial flow with a uniform shear through the pinch is initialized. The $m = 0$ mode is significantly less developed than the static plasma case. (c) An equilibrium axial flow with a shear increasing towards the plasma edge is initialized. The stabilizing effect is again evident [27] | 20 |
| 2.3: Photograph of a double shell gas nozzle. The inner and outer radii of the outer nozzle exit are 3 and 4 cm; the inner nozzle exit radii are 1 and 2 cm [54] | 21 |
| 2.4: Schematic diagram of “shell-on-shell” nozzle: (1) outer plenum gas inlet, (2) inner plenum gas inlet, (3) breakdown pin output, (4) hammer, (5) hammer reset spring, (6) solenoid, (7) poppet, (8) poppet reset spring, (9) sliding seal, (10) outer nozzle, and (11) inner nozzle [55] | 22 |
| 2.5: Z-pinch thruster concept drawing 1. | 23 |
| 2.6: Z-pinch thruster concept drawing 2. | 24 |
| 3.1: Otto cycle P-V diagram. | 28 |
| 3.2: Fusion reaction engine cycle..... | 37 |
| 4.1: Stages of z-pinch formation..... | 42 |
| 5.1: Thrust per unit frequency vs. specific impulse for D-T fuel mixture. | 58 |

| | |
|--|----|
| 5.2: Thrust per unit frequency vs. specific impulse for D- ³ He fuel mixture..... | 60 |
| 5.3: Thrust per unit frequency vs. specific impulse for D-D fuel mixture..... | 60 |
| 5.4: Gain curves for D-T fuel mixture..... | 61 |
| 5.5: Gain curves for D- ³ He fuel mixture..... | 61 |
| 5.6: Gain curves for D-D fuel mixture..... | 62 |
| 5.7: Thrust per unit frequency vs. specific impulse for D-T fuel mixture..... | 63 |
| 5.8: Thrust per unit frequency vs. specific impulse for D- ³ He fuel mixture..... | 64 |
| 5.9: Thrust per unit frequency vs. specific impulse for D-D fuel mixture..... | 64 |
| 5.10: Gain curves for D-T fuel mixture..... | 65 |
| 5.11: Gain curves for D- ³ He fuel mixture..... | 65 |
| 5.12: Gain curves for D-D fuel mixture..... | 66 |
| 5.13: Input current required for D-T fuel mixture..... | 69 |
| 5.14: Input current required for D- ³ He fuel mixture..... | 69 |
| 5.15: Input current required for D-D fuel mixture..... | 70 |
| 5.16: Driver charging energy required for D-T fuel mixture..... | 71 |
| 5.17: Driver charging energy required for D- ³ He fuel mixture..... | 71 |
| 5.18: Driver charging energy required for D-D fuel mixture..... | 72 |
| 5.19: Exhaust/liner velocity vs. compression ratio for D-T fuel mixture..... | 73 |
| 5.20: Exhaust/liner velocity vs. compression ratio for D- ³ He fuel mixture..... | 73 |
| 5.21: Exhaust/liner velocity vs. compression ratio for D-D fuel mixture..... | 74 |
| 5.22: Thrust per unit frequency vs. specific impulse for NASA design study..... | 76 |
| 5.23: Gain curves for NASA design study..... | 77 |
| 5.24: Required input current for NASA design study..... | 78 |
| 5.25: Exhaust/liner velocity vs. compression ratio for NASA design study..... | 78 |
| 5.26: Charging energy required for NASA design study..... | 79 |

LIST OF TABLES

| Table | Page |
|----------------------------------|------|
| 1.1: Fusion fuel cycles [1]..... | 6 |
| 5.1: Fuel Compositions | 56 |
| 5.2: Model Parameter Space | 56 |
| 5.3: Representative Cases | 57 |

This work is dedicated to the One who saved me.

*“His lightnings enlightened the world;
the earth saw, and trembled.”*

Psalm 97:4

Chapter 1

Introduction

1.1 Motivation

On July 20, 1969, the story of man's endeavor to conquer the wilderness came to a spectacular climax as Apollo 11 landed on the surface of the moon. Like the initial flight of the Wright brothers over sixty years previously, the first steps of one man upon an alien world marked the beginning of a new age in our exploration of the universe we inhabit and, by extension, our relationship to the immeasurable expanse of heaven. Such was the grace of a star-faring culture in its infancy.

It has been over forty years since that historic landing, with the last propitious steps taken just over three years later on December 7, 1972. Although this did not end man's presence in space, the loss of interest in one of history's greatest adventures via the somniferous events of politics became palpable as the world moved on. Since then, multiple technological breakthroughs have been achieved as the space program extended our reach beyond low earth orbit with robotic satellites and marvels such as the Hubble space telescope.

The dream of human space exploration and colonization still persists, and as time progresses, technological development makes the prospect of space travel increasingly achievable. Furthermore, due to this development, the pursuit of an objective as difficult as sending humans to Mars warrants more consideration. There are multiple reasons for this consideration: first, the development of a program to do so would require vast amounts of human capital and ingenuity, thus requiring the generation of multiple jobs in industry and subsequently an educated workforce to fill this need. Second, such an endeavor would enable access to vast

amounts of resources in the solar system. Simultaneously, these resources would cause an unprecedented expansion of the global economy. Third, the ability to travel to Mars quickly and efficiently provides an impetus for the development of advanced technologies and capabilities that will drive this new economy onward. Dr. Terry Kammash framed this discussion quite succinctly:

Although the debate on the wisdom of such an undertaking rages on between those who bemoan the prohibitive cost of such a venture and those who boast of the economic benefits that may accrue from reaping the riches of Mars and other planets, the fact remains that without a frontier to conquer humanity will be doomed to stagnation, will lose its spirit of creativity and inquisitiveness, and ultimately surrender the buoyancy and exuberance that seem to come only from the freedom associated with the existence of frontiers... Yet to secure these riches people on Earth must become spacefaring for which suitable transportation must be developed and perfected [1].

The ability to create and further develop new transportation systems to accomplish such lofty goals, as with any other engineering achievement, is the first major obstacle to be overcome. In order to do so, it is advantageous to have simple models that can predict the performance of multiple new systems based on specific design parameters and limitations that are common to those systems. Engineering development is replete with examples of this process. Consider, for instance, the design and evolution of the gas turbine engine and the subsequent design of turbojets, turbofans, etc. This process is based upon the basic thermodynamic Brayton cycle. The performance trends are similar across the different types of engine because they operate by the same physical principles while their differences arise due to specifics in system geometry, component performance, etc. [2]. The explosion of highly sophisticated jet propulsion systems and the continual increase in performance of these engines provides firm testimony for this fact. Although this may be true for turbojets and other familiar engineering systems, it comes as somewhat of a surprise that these same effective design principles have not been applied to new systems in order to analyze, develop and compare them based on similar design points. More specifically, it is surprising to find this absence of a simple design process in the rather mature

field of nuclear fusion propulsion research and development. For the multitude of fusion propulsion system designs that are in existence today, there is a corresponding multitude of models that describe only the unique engine they were specifically created for. This not only makes it impossible to compare any two engines with a respectable level of objectivity and accuracy, it impedes any progress that might be made in the design and development of new fusion propulsion systems for specific mission requirements due to the seeming lack of any common basis on which to perform an analysis.

To remedy this problem, a common basis must be found that will enable the design engineer to develop multiple fusion systems that utilize different methods of operation in varying levels of complexity. The objective of this thesis is to present the starting point for this ability by using the four-step thermodynamic Otto cycle to enumerate a design process for pulsed nuclear fusion reaction engines. As presented below, the class of pulsed fusion confinement systems can be described using the same thermodynamic arguments that describe internal combustion engines. Furthermore, the design parameters and performance trends resultant from this model will be used to design an experiment to test and develop the concepts described below using a ~500 kJ pulsed power facility, to be described later. The remainder of this chapter will describe the nature of thermonuclear fusion confinement technology, further description of the analysis process upon which the framework of this model is built, the class of fusion propulsion systems to be analyzed, and the structure of the rest of this thesis.

1.2 Thermonuclear Fusion Technology

Since the advent of the hydrogen bomb and the pursuit of controlled nuclear fusion reactions in the following decades, much has been learned about the processes involved in creating and confining fusion plasmas. Research outside of defense applications has focused on terrestrial power and propulsion, due to its potential to meet much of the world's energy needs for centuries. One of the major challenges to thermonuclear fusion is confinement of the gases with

temperatures that far exceed the thermal limits of any material. Given the myriad of approaches devised over the decades for containing these gases, fusion reactors are frequently categorized according to their respective confinement mechanisms. For completeness, the following sections describe the necessity of fusion confinement and a brief review of the physics involved in each confinement process.

1.2.1 Necessity of Confinement

The acquisition of a sufficiently high reaction rate density is a requirement of all energy systems. In contrast with nuclear fission reactions, the reactants in a fusion system are positively charged and therefore have to overcome their electrostatic repulsion in order to be close enough for the nuclear strong force to dominate. In this sense, the requirement to overcome the Coulomb barrier with a sufficiently high kinetic energy of the reacting nuclei becomes the essential condition for fusion ignition to occur [1] [3]. Those fusion reactions most often mentioned in the context of terrestrial power or propulsion applications are listed along with their reaction products and the energy produced in Table 1.1. The achievement of the ion energies required to overcome the Coulomb barrier is not difficult; however, as experience has shown with initial beam/target approaches to fusion, the tendency of incident particles to scatter upon reaching a target tends to render further fusion reactions unlikely [3].

More promising approaches soon began to emerge with the initiation of experiments taking advantage of the electromagnetic effects of fusion plasmas to contain the reactions. Beginning with a combination of deuterium (2_1H) and tritium (3_1H) atoms in a confined space and heating the mixture to cause ionization and high temperatures to occur, the resulting plasma is then able to attain thermodynamic equilibrium resulting from random collisions. The critical requirement is thus the sustainment of a high temperature ($\sim 10^8$ K) plasma over a sufficiently long period of time (dwell time) within a sufficiently small reaction volume in order for such a

concept to be energetically feasible [3]. [3][1] Therefore, the confinement of the fuel ions by some means becomes crucial to the operational viability of a fusion system.

1.2.2 Gravitational Confinement

The use of fusion energy and its prospect as the ultimate terrestrial energy source finds its origins in an intriguing and rather significant observation: life on Earth is sustained as a consequence of fusion reactions in the sun [3]. Although such a spectacular display of power and enormity is far detached from the everyday experience of life, the operation of our first and most important energy source relies on the *gravitational* confinement of nuclear fusion reactions. The formation of stars occurs by the accumulation of large amounts of gas over time through gravitational attraction where, once the density of this gas reaches a certain critical point, the overwhelming gravitational pressure causes large enough temperature rise in the core to result in the ignition of fusion reactions. The consequent burning of fusile material in the core of the star leaks through the surface of the star by radiation; however, the core of the star consistently exists in thermodynamic equilibrium. Although this method of confinement is by far the most favorable and efficient in nature, the sheer dimensions of stars and the amount of mass required are evidence enough that confinement by gravity is inappropriate for use in fusion energy systems.

Table 1.1: Fusion fuel cycles [1].

| Reaction | Fusion fuel cycles, MeV | Ignition temperature, °C |
|----------|--|--------------------------|
| 1a | ${}^2_1\text{H} + {}^2_1\text{H} \xrightarrow{50\%} {}^3_1\text{H}(1.01) + p (3.02)$ | 300×10^6 |
| 1b | ${}^2_1\text{H} + {}^2_1\text{H} \xrightarrow{50\%} {}^3_2\text{He} (0.82) + n (2.45)$ | |
| 2 | ${}^2_1\text{H} + {}^3_1\text{H} \xrightarrow{50\%} {}^4_2\text{He} (3.5) + n (14.1)$ | 50×10^6 |
| 3 | ${}^2_1\text{H} + {}^3_2\text{He} \longrightarrow {}^4_2\text{He} (3.6) + p (14.7)$ | 500×10^6 |
| 4 | ${}^3_1\text{H} + {}^3_1\text{H} \longrightarrow {}^4_2\text{He} + 2n + 11.3$ | |
| 5a | ${}^3_2\text{He} + {}^3_1\text{H} \xrightarrow{51\%} {}^4_2\text{H} + p + n + 12.1$ | |
| 5b | ${}^3_2\text{He} + {}^3_1\text{H} \xrightarrow{43\%} {}^4_2\text{He} (4.8) + {}^2_1\text{H} (9.5)$ | |
| 5c | ${}^3_2\text{He} + {}^3_1\text{H} \xrightarrow{6\%} {}^3_2\text{He} (2.4) + p (11.9)$ | |
| 6 | $p + {}^6_3\text{Li} \longrightarrow {}^4_2\text{He} (1.7) + {}^3_2\text{He} (2.3)$ | |
| 7a | $p + {}^7_3\text{Li} \xrightarrow{\sim 20\%} 2({}^4_2\text{He}) + 17.3$ | |
| 7b | $p + {}^7_3\text{Li} \xrightarrow{\sim 80\%} {}^3_4\text{Be} + n - 1.6$ | |
| 8 | ${}^2_1\text{H} + {}^6_3\text{Li} \longrightarrow 3({}^4_2\text{He}) + 22.4$ | |
| 9 | $p + {}^{11}_5\text{B} \longrightarrow 3({}^4_2\text{He}) + 8.7$ | |
| 10 | $n + {}^6_3\text{Li} \longrightarrow {}^3_1\text{H} + {}^4_2\text{He} + 4.8$ | |
| 11 | $n + {}^7_3\text{Li} \longrightarrow {}^3_1\text{H} + {}^4_2\text{He} - 2.5$ | |

1.2.3 Electrostatic Confinement

Another possible approach to the confinement of fusion reactions arises by the observation that ions are affected by the existence of electrostatic fields. An example of such a reactor currently in development can be seen in Figure 1.1. This device is denoted as an inertial-electrostatic-fusion (IEF) device, and it is being developed by the Energy Matter Conversion Corporation (EMC2) in Santa Fe, NM. One of the most interesting approaches to this confinement concept is the use of an outer metallic anode emitting deuteron ions towards the



Figure 1.1: Inertial Electrostatic Fusion (IEF) device being developed at EMC2 [49].

center. The ions pass through a spherical negatively charged cathode grid that is designed to be transparent to the converging ions. When the positively charged ions reach the center a space charge forms, and establishes a positive ion shell inside the cathode. This positive ion shell may be called a “virtual anode.” The inner cathode also emits electrons towards the center of this device. After passing through the virtual anode, the electrons form a “virtual cathode” further within the center. This progressive formation of virtual cathodes and anodes forms an increasing density gradient toward the center of the device where fusion reactions are then expected to occur [3] [1]. In general, the problems associated with this approach include the high probability of

discharge breakdown in the process, the magnitude of the electric fields required, and the problems of geometrical restriction.

1.2.4 Inertial Confinement

In the method of inertial confinement of fusion reactions, no externally applied means (e.g., magnetic fields) are needed to confine the plasma since energy production occurs on a very short time scale ($\sim 10^{-9}$ sec) [1]. The most common process involves the compression of a small fusion fuel pellet to high density and temperature by external laser or ion beams (Figure 1.2). The external driver delivers a pulse of energy to its target, heating and expanding the ablator, and the inner shell is compressed due to momentum conservation. The compression work by the outward momentum of the ablator increases the temperature at the center of the target, which results in a self-sustained burn of the fuel. The term inertial confinement is thus appropriate for this approach due to the inward directed momentum of the pellet mass providing the necessary force to confine the explosive effect of fusion reaction and target disassembly.

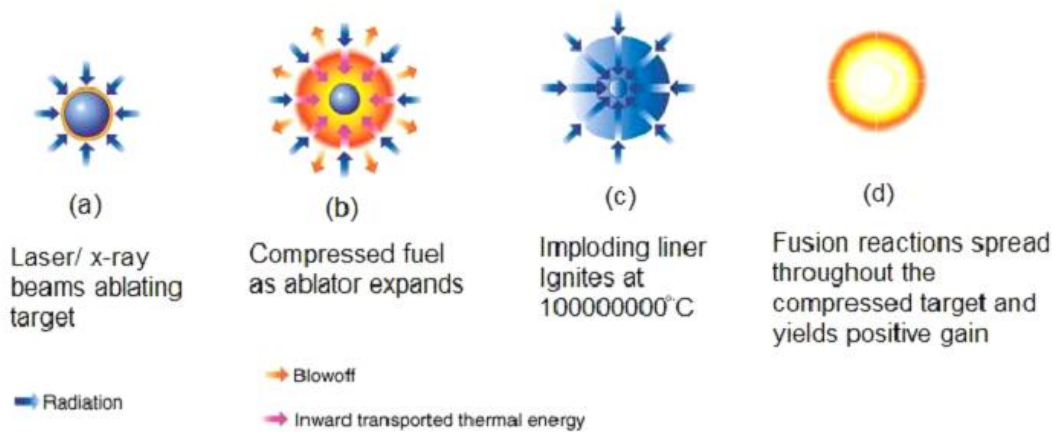


Figure 1.2: Inertial confinement fusion [50].

1.2.5 Magnetic Confinement

Confining a plasma at temperatures sufficient for fusion reactions to occur necessitates the need for one of two design requirements: (1) materials to confine the reaction that are capable of handling inordinately high temperatures, or (2) the ability to confine the plasma away from the material walls so that the plasma does not cool and the reactor does not melt down. This requirement drives the idea behind Magnetic Confinement Fusion (MCF), which takes advantage of the charged nature of the plasma components and their response to the presence of a magnetic field. Multiple configurations exist for this confinement method, but the most common is a toroidal configuration known as a *tokamak* (Figure 1.3). In this configuration, rather than rapidly increasing the density of the fuel in order to achieve ignition, the toroidal magnetic field confines a lower density plasma for a longer period of time (multiple seconds) in order to increase the likelihood of initiating a fusion reaction.

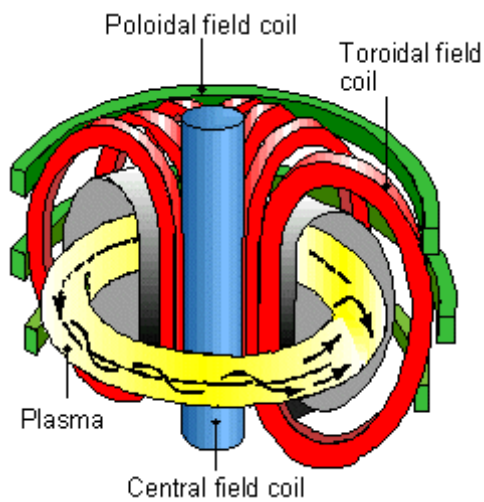


Figure 1.3: Tokamak [51].

1.2.6 Magneto-Inertial Fusion (MIF)

Magneto-Inertial Fusion (MIF) or Magnetized Target Fusion (MTF) is a hybrid approach to fusion confinement that takes place in the intermediate density regime and time scale between MCF and ICF [4]. This method of confinement uses a magnetic field in an inertially confined fusion plasma to reduce thermal losses and to enhance alpha particle self-heating of the fuel. This reduces the areal density (ρR) threshold for ignition allowing lower implosion velocities or alternatively higher gain for a given implosion velocity [5]. There are two major embodiments for MIF, distinguished by the liner material, geometry, and compression scheme:

1. Solid liner MIF (Figure 1.4) utilizes a cylindrical metal shell to implode a simply connected magnetized plasma known as a compact toroid (CT). The shell implodes by running a large current ($\sim 10^6$ A) through the shell, causing self-compression by the induced Lorentz force ($\mathbf{j} \times \mathbf{B}$) [6][4][7]. Solid liner implosion technology is a fairly mature research effort. Most recently, the first successful demonstration of an imploding solid liner with geometric scale lengths and compression ratios suitable for compressing a field reversed configuration target was achieved. Radiographs indicated a 13 times radial

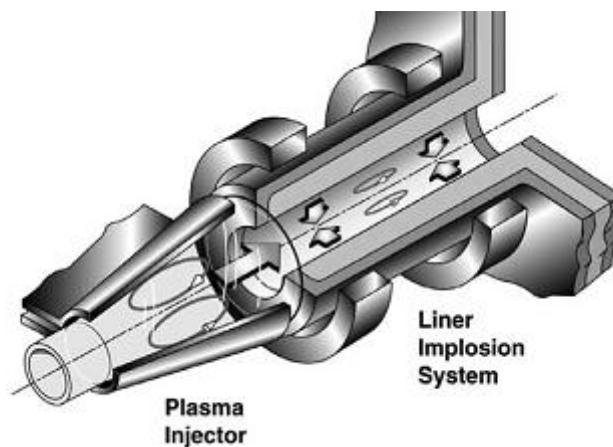


Figure 1.4: MTF schematic showing plasma formation region and liner implosion section [6].

compression ratio with no observable instability growth. But solid liners may suffer from potential engineering difficulties in the context of a reactor concept due to reasons such as nonreusability, manufacturing costs, and debris deposits along the interior of the wall [5].

2. Plasma liner driven MIF (PLMIF) aims to overcome the problems associated with the solid liner approach at the expense of requiring a higher implosion velocity and lower hydrodynamic efficiency due to increased liner thickness. Primarily, PLMIF has the benefit of potentially allowing all the driver hardware to be situated far enough away so that they are not destroyed during each shot, i.e., imploding plasma liners are a possible solution to the “stand-off” problem [5].

1.3 Parametric Cycle Analysis

As stated by Dr. Jack Mattingly:

Cycle analysis studies the thermodynamic changes of a working fluid (air and products of combustion in most cases) as it flows through the engine, and it is typically divided into two types: parametric cycle analysis (or design-point analysis) and engine performance analysis (or off-design analysis). Parametric cycle analysis seeks to determine the performance of engines at different flight conditions, values of design choice (e.g., compressor pressure ratio), and design limit (e.g., combustor exit temperature) parameters. Engine performance analysis determines the performance of a specific engine at all flight conditions and throttle settings. In both forms of the analysis, the components of an engine are characterized by the change in properties they produce. In addition to this, a specific engine's behavior is determined by its geometry [2].

The advantage of parametric analysis is its independence from specific geometries so that a given analysis can represent a whole ‘family’ of engines. Therefore, the plots of specific performance properties such as thrust or fuel consumption vs. values of a design choice like compressor pressure ratio do not portray the behavior of a specific engine; furthermore, each point on such a plot will represent a different engine [2]. In addition, the value of parametric

cycle analysis depends on the realism with which the engine components are characterized. Therefore, for any conclusions of such an analysis to be useful, a realistic variation of component efficiency with a design point such as total pressure ratio or compression ratio must be included in the analysis.

1.4 Fusion Propulsion Systems

For the analysis presented in this thesis, we examine the method of parametric cycle analysis as it pertains to the fusion propulsion system geometry known as a z-pinch, which derives its operation from the MIF regime by using an azimuthal magnetic field to compress the fusion fuel to ignition conditions. The concept to be described here is novel not in its configuration or geometry, but in the method of implementation by which ignition is achieved and utilized. The short confinement time required for this approach, on the order of 10^{-9} seconds, and those for other configurations in the MIF regime may extend up to 10^{-6} seconds. Due to the short timescales and the necessarily pulsed nature of MIF concepts in general, we will from here on denote this type of engine a *pulsed fusion reaction engine*.

It is also important to note that, although the propulsion system design examined here is confined to a cylindrical geometry, the analysis process is *not* restricted by such constraints. The parametric analysis is generic enough so that it may be applied to all system designs of this class (and very possibly others), yet it can then be narrowed down to examine individual system geometries, sizes, etc., as will be shown in Chapter 4.

1.5 Roadmap

A description of the aforementioned system configuration will be given in Chapter 2 along with an overview of the research & development work performed thus far for the given system design. Chapter 3 will present and discuss the general thermodynamic model based on the Otto cycle and will develop the cycle analysis for a general pulsed fusion reaction engine. This analysis will then be broken down for the z-pinch fusion reaction engine in Chapter 4, followed by the results of the model and their implications in Chapter 5. Finally, Chapter 6 will discuss further development of the model and future work to be performed, the conclusions that may be drawn from the thermodynamic model, and its implications for further use.

Chapter 2

Fusion Propulsion System Research & Development

2.1 Relevance of Magneto-Inertial Fusion

There exists a general perception in the fusion community that fusion research is inherently expensive. MCF and ICF are the dominant approaches being pursued [7]. However, the fusion parameter space is a continuum between (and beyond) these two extremes and the associated costs may be reduced drastically through alternative means. One approach to this cost reduction exists in the advent of Magneto-Inertial Fusion due to its combination of the potentially favorable aspects of both inertial and magnetic confinement concepts; we remark that the pulsed z-pinch is such an approach.

The essential ideas of MIF have existed for quite some time and provide an appealing option to address the fundamental issues of controlled thermonuclear fusion [8][9]. By considering the intermediate regime of MIF with, for example, fuel mass 1.7 mg, number density $10^{20}/\text{cm}^3$, temperature 8 keV, and magnetic field strength 1 MG (100 T), as resulting from a quasi-adiabatic compression of a magnetized plasma by a liner, and limiting the radial compression ratio to 10, Lindemuth and Siemon [7] show that a plasma with an initial density, temperature, and magnetic field of $10^{18}/\text{cm}^3$, 371 eV, and 100 kG (10 T), respectively, would be required. By emphasizing that existing technology might allow access to an intermediate density space that covers several orders of magnitude, and that such facilities already exist, the costs of accessing this parameter space become significantly reduced. Lindemuth and Siemon also stipulate that in addition to the aspect of cost, the intermediate MIF regime has many attractive attributes when compared to ICF, including larger and more easily fabricated targets, reduction of the required radial compression ratio, no driver pulse shaping, longer burn times (dwell times),

and enhanced alpha particle deposition. Furthermore, since the technology required to access this regime already exists, magnetized target fusion reactors should not require high gain values as is essential for conventional ICF targets [7].

The energy losses from tokamak plasmas are more than an order of magnitude higher than predicted based on the classical thermal conductivity used in the analysis performed by Lindemuth and Siemon[7]; correspondingly, the possibility of increased losses in the intermediate density range of MIF cannot be discounted. However, the losses are unlikely to be larger than Bohm losses [7]. Bohm thermal conductivity is fatal at densities representative of MCF, and for the MIF regime the loss ratio, defined as the energy lost through radiation, thermal conduction, etc. divided by the total energy output of the fusion reactions, increases to ~ 0.37 . To reduce this would cause corresponding increases in energy and cost unless the magnetic field is increased. Even with the Bohm losses mentioned, the region of the density-temperature space where the cost is minimized still corresponds to a region that is equivalent to the geometric mean between MCF and ICF [7][8]. Accordingly, the parameter space in which the costs are less than \$1B covers an expansive density-temperature range. In addition, the required implosion velocities are significantly lower than those required for ICF [7].

2.2 Z-Pinch Research & Development

The field of z-pinch research and development has a long history and has recently received renewed vitality via dramatic advances in pulsed-power technology, computational and modeling capabilities, and plasma physics understanding [10]. In its simplest form, a z-pinch is a radial implosion of a cylindrical or annular plasma under the influence of a strong magnetic field produced by current flowing down the length of the plasma; it usually involves the ionization and subsequent implosion of a gas for time-scales on the order of microseconds. The concept originated in the 1930s when Tonks suggested the term “z-pinch” [11] and it is widely used in the field of Nuclear Weapons Effects (NWE) testing in the defense industry, as well as fusion energy

research. Facilities of note include the Z Machine at Sandia National Laboratories (SNL) [12][13] [13][2], MAGPIE at Imperial College, London [14][15][16], Atlas, which was located at Los Alamos National Laboratory (LANL) [17][18] and DECADE, previously located at the Arnold Engineering Development Center (AEDC) in Tullahoma, Tennessee [19]. Z-pinches have a wide range of applications because they are a highly efficient and cost effective technique to heat a small mass to very high temperatures. However, z-pinches are susceptible to the Magnetic Rayleigh-Taylor (MRT) instability over the timescales of interest in nuclear fusion applications; this instability must be mitigated in order for z-pinches to be utilized effectively.

In what follows, we discuss z-pinch research performed previously, along with the studies that are relevant to the propulsion system configuration used in the current study. This will be followed by an overview of the MRT instability and the methods that can be used to mitigate it.

2.2.1 Relevant Z-Pinch Research

At SNL, z-pinches are driven by the Z Machine, which delivers 20 MA of current through a cylindrical array of tungsten wires with ~ 2 cm radius. The wires vaporize and form a uniform plasma sheath, which summarily implodes under its own magnetic field onto a low-density foam or annular foil, achieving temperatures up to 230 eV (2.7 million °C), and thermal x-rays emitted containing up to 1.8 MJ of total energy [20][21]. The fast z-pinch technology differs from the classical concept since it can create high-level radiation environments on time scales similar to those created in indirect-drive laser hohlraums or ion-beam ICF drivers. Simple scaling from current and previous pulsed power z-pinch machines indicate that a next generation z-pinch driver which generates ~ 60 MA of load current could produce almost 10 MJ of x-ray energy for driving an ICF capsule [20]. It is also estimated that final yields will be in the range of 3-12 GJ, and individual chamber rep-rate will have to be < 0.1 Hz with multiple chambers required from the perspective of plant maintenance and operation.

The design of modern z-pinch facilities is typically determined by the initial load configuration, and the available pulsed power energy source; the former may be represented as a gas column, a solid cryogenic fiber, a metal wire or wire array, a laser-produced ionized channel in a gas, an annular metal foil, or an annular gas jet [10]. Today, most pulsed power drivers have a current drive time scale within the range of 50-150 ns in order to limit the growth of magnetohydrodynamic (MHD) instabilities. Many of the difficulties found in z-pinch load fabrication are greatly reduced with higher current drivers.

Significantly, the dynamics and stability of z-pinch are very closely related. As an example, the MRT instability will develop as the pinch plasma is accelerated to the axis, resulting in destruction of its cylindrical symmetry before any equilibrium steady state is achieved [10][22][23][24]. Susceptibility to the MRT instability is a primary cause of the difficulty in utilizing the z-pinch as a confinement method to produce fusion energy consistently and effectively. Multiple studies have been performed on this instability [25][26] and its mitigation [27][28]. In the more prominent case of wire array z-pinch implosions, the mitigation of the MRT instability can be made by decreasing the gap between the wires to reduce any initial asymmetries, or by the use of nested wire arrays.

Although useful for wire array pinches, the methods mentioned above have no application in the realm of gas-puff z-pinch configurations. Since no wires are involved, the gas-puff method requires more innovative approaches to guard against the MRT instability. Two methods have been devised previously: the use of axial velocity shear profiling, and structuring of the gas-puff load by multiple gas shells. These methods will be described below, followed by a discussion of the z-pinch propulsion concept to be examined in this thesis.

2.2.2 Instability Mitigation Methods: Sheared Axial Flow

For the system configurations studied here, wire arrays prove to be impractical due to the need to provide cartridges, or some other form of replacement, for the pinch electrodes between each shot. The use of a gas-puff configuration can help remedy this problem, but the methods by which one might alleviate the onset of the MRT instability require more innovation. Shumlak et al. have demonstrated the first favorable method on the ZaP experiment at the University of Washington [27][29]. Spawned by the success of using sheared axial flows to stabilize steady state pinches their application to stabilize the MRT instability in z-pinch implosions was then investigated.

For the system configurations studied here, wire arrays prove to be impractical due to the need to provide cartridges, or some other form of replacement, for the pinch electrodes between each shot. The use of a gas-puff configuration can help remedy this problem, but the methods by which one might alleviate the onset of the MRT instability require more innovation. Shumlak et al. have demonstrated the first favorable method on the ZaP experiment at the University of Washington [27][29]. Spawned by the success of using sheared axial flows to stabilize steady state pinches their application to stabilize the MRT instability in z-pinch implosions was then investigated.

Classically, the z-pinch is unstable to the $m = 0$ sausage and $m = 1$ kink modes (Figure 2.1). Conventional techniques to provide stability include limiting the pressure gradient of the plasma and the application of an axial magnetic field. Controlling the pressure profile is difficult, and it does not stabilize the kink mode. The strength of applied axial magnetic fields limits the possible plasma current and pressure according to the Kruskal-Shafranov limit and furthermore opens all field lines and connects the electrodes to all regions of the plasma, which is not desirable in the context of a hot fusion plasma [27]. Flow shear stabilizes the MHD modes without the accompanying drawbacks of the conventional approaches (Figure 2.2). Analyses

conducted by Shumlak et al. demonstrate the stabilizing effect of sheared axial flow on the kink mode instability when the shear exceeds some threshold value corresponding to the relation $dV_z/dr > 0.1kV_A$, where k is the axial wave number and $V_A \equiv B/\sqrt{\mu_0\rho}$ is the Alfvén velocity [30]. This threshold is computed based on measurements in the ZaP experiment of the plasma equilibrium using plasma density from interferometry, and magnetic field extrapolated from magnetic probes in the outer electrode [27][29]. Furthermore, the analyses presented by Zhang et al. on the effects of compressibility on the MRT instability [26] show that with uniform current, axial perturbations deform the plasma, compressing the magnetic field inside so that the magnetic pressure contributes to the overall stability of the plasma.

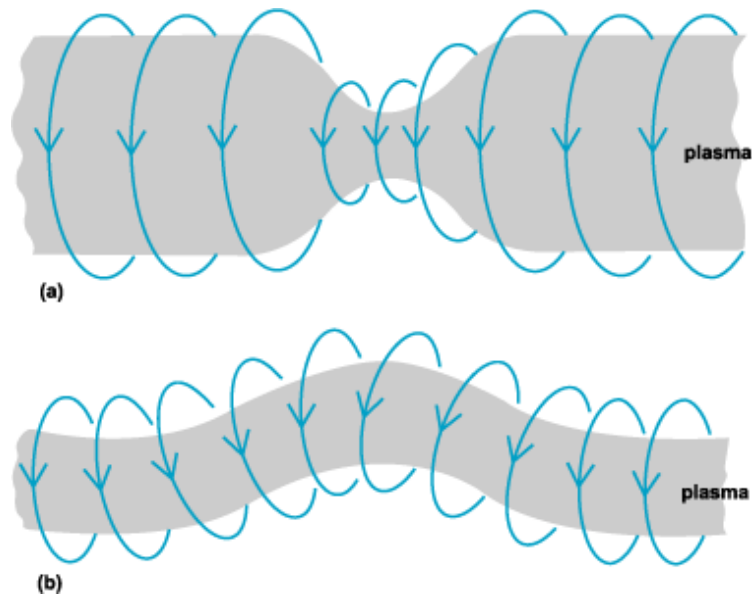


Figure 2.1: Z-pinch instabilities. (a) $m = 0$ sausage mode and (b) $m = 1$ kink mode [52].

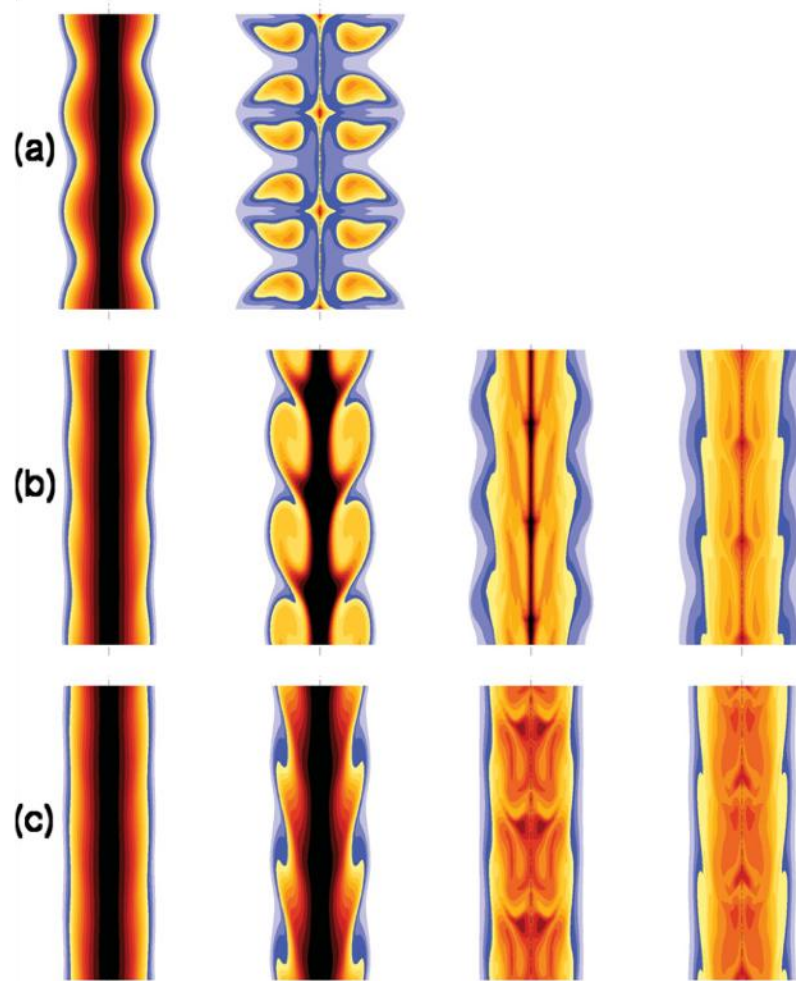


Figure 2.2: Nonlinear simulation results showing pressure contours in a z-pinch. The results for each simulation time are aligned vertically. (a) No equilibrium axial flow is initialized. The plasma quickly develops an $m = 0$ mode and loses confinement. (b) An equilibrium axial flow with a uniform shear through the pinch is initialized. The $m = 0$ mode is significantly less developed than the static plasma case. (c) An equilibrium axial flow with a shear increasing towards the plasma edge is initialized. The stabilizing effect is again evident [27].

2.2.3 Instability Mitigation Methods: Structured Gas-Puff Loads

The second method by which the deleterious effects of the MRT instability can be mitigated is the use of “structured” z-pinch loads. Rather than the approach of using “solid filled” loads requiring placement of a wire on the axis of the pinch, this method applies multiple gas shells (Figure 2.3) to achieve a uniform mass distribution throughout the pinch. This method was studied initially for application to plasma radiation sources (PRS) used for NWE testing. More importantly, structured loads are shown to enable higher coupling efficiencies between the driver and the PRS [31].

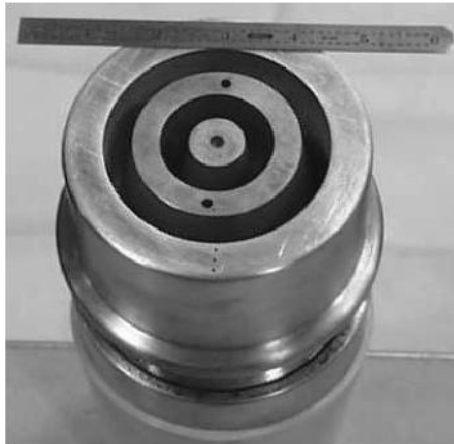


Figure 2.3: Photograph of a double shell gas nozzle. The inner and outer radii of the outer nozzle exit are 3 and 4 cm; the inner nozzle exit radii are 1 and 2 cm [54].

In studies performed on the Double-EAGLE pulsed power facility at L-3 Pulse Sciences in San Leandro, CA this approach was demonstrated to overcome the MRT instability enhancing the energy coupling, and lead to a high yield, high compression z-pinch. Nozzles were then constructed to create a gas-puff load consisting of a “pusher,” outer region plasma that carries the current and couples energy from the driver, a “stabilizer,” inner region plasma that mitigates the MRT growth, and a “radiator,” high-density center jet plasma that is heated and compressed to radiate (Figure 2.4) [32]. The studies were performed with multiple combinations of the inner,

outer, and jet initial density profiles. By examining the evolution of the z-pinch implosions with and without a stabilizing inner gas shell, it was found that the inner shell provides an intermediate zone to decelerate and smooth out the unstable current sheath. Further, the sheath then implodes at nearly constant velocity while maintaining good axial uniformity upon its approach to the jet zone and stagnation. This method of implosion is found to be consistently reproducible, and the dynamics are determined by the current and mass profile [28].

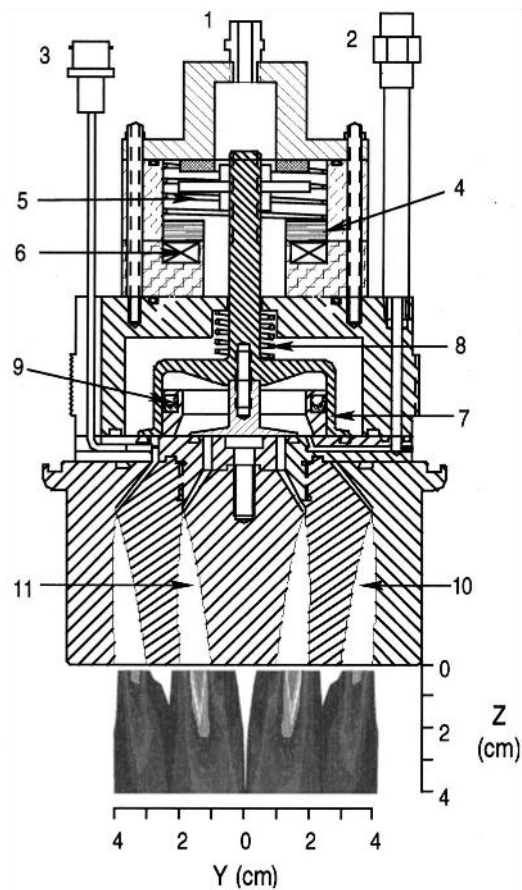


Figure 2.4: Schematic diagram of “shell-on-shell” nozzle: (1) outer plenum gas inlet, (2) inner plenum gas inlet, (3) breakdown pin output, (4) hammer, (5) hammer reset spring, (6) solenoid, (7) poppet, (8) poppet reset spring, (9) sliding seal, (10) outer nozzle, and (11) inner nozzle [55].

2.3 Z-Pinch Fusion Propulsion System

The z-pinch propulsion system configuration examined in this study utilizes the two methods of instability mitigation mentioned above by combining the structured gas puff load with the favorable effects of sheared axial flow to produce a unique configuration. Using an annular nozzle to create a structured load and focusing it in a conical shape may achieve this. As noted by Shumlak and Roderick [30], the use of a conical shape would generate an axial flow and the thickness of the outer layer can be adjusted to produce a simultaneous arrival on axis of the plasma mass.

This novel system configuration would utilize a lithium-6/7 mixture in the outer layer while the inner shell and center jet would feature a fusion fuel mixture such as a 50/50 deuterium-tritium mixture. By focusing the configuration in a conical manner, the two mixtures meet at a specific point that acts as a “virtual cathode” (Figure 2.5) such that the lithium mixture can serve as a current return path to complete the circuit, rather than a material cathode that would have to be replaced between each shot.

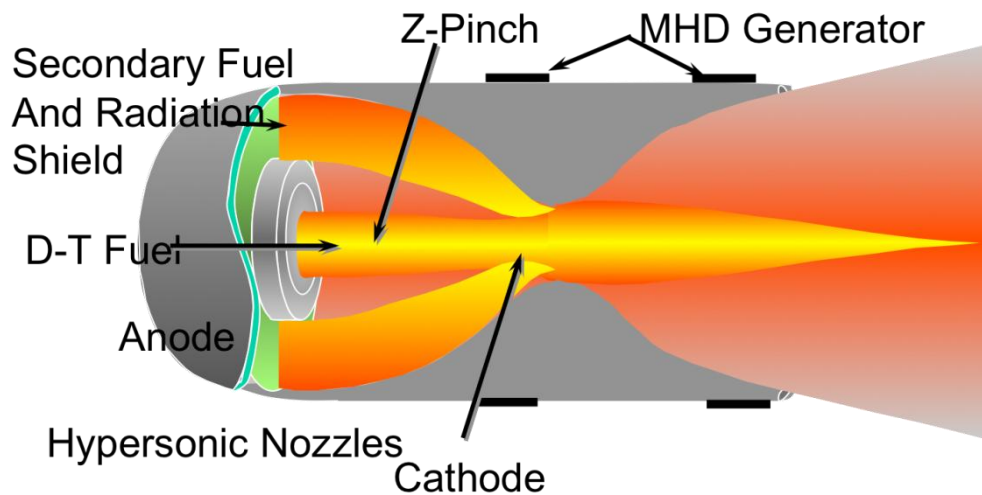


Figure 2.5: Z-pinch thruster concept drawing 1.

In addition to serving as a current return path (Figure 2.6), the lithium liner also serves as a radiation shield. The advantage of this configuration is the reaction between neutrons and lithium-6 resulting in the production of tritium, thus adding further fuel to the fusion reaction, and

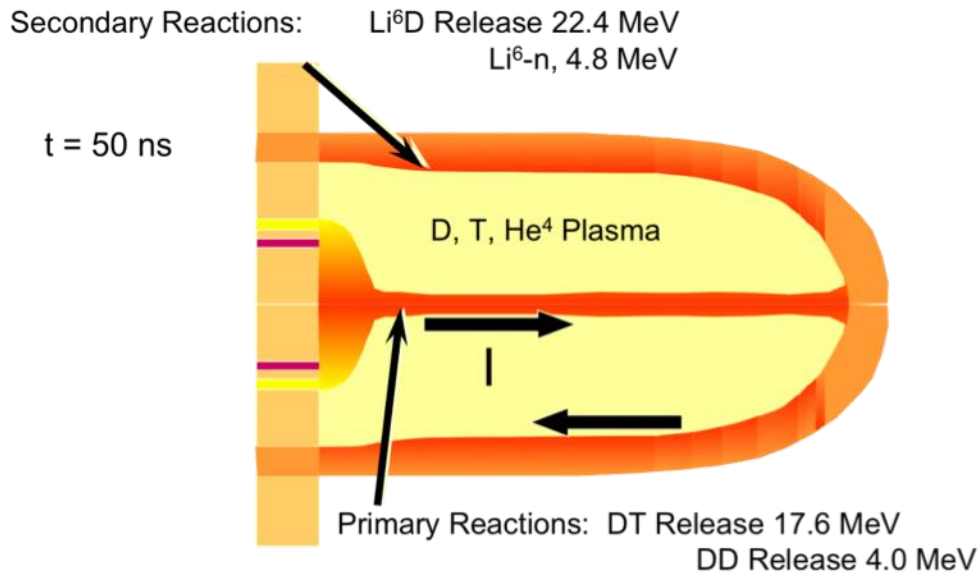


Figure 2.6: Z-pinch thruster concept drawing 2.

boosting energy output. By utilizing this method of fusion for propulsion to achieve extremely high exhaust kinetic energies, one can produce very high thrusts by adding additional fuel or liner mass, and/or specific impulse impulse due to the higher exhaust velocities that are a logical consequence of such high kinetic energies.

There is also an important question to consider when examining the feasibility of this configuration: if the current flow returns through the liner in a coaxial manner as depicted here, then will the current not be cancelled out such that there is no net magnetic field outside the liner, and therefore no net pressure to compress the liner itself? This will indeed be the case if the current in the pinch is equal to the return current through the liner. However, if the overall

configuration is in a conical shape this will also affect the current flow through the liner. Furthermore, this point will affect the actual method by which the thruster nozzle configuration is designed. Although this problem is not addressed explicitly in this study, it will become important in later stages of analysis when we begin to look at the dynamics of the liquid liner compression and how it affects the performance of the system. This will be another layer of complexity to be added to the model at a later stage, but must be mentioned ahead of time since it will heavily affect whether the “virtual cathode” is a feasible design or has to be changed to enable the liner compression to proceed. In the intermittent period between now and then, we accept it as a caveat to the design and assume that the liner compression proceeds without hindrance.

Chapter 3

Fusion Reaction Engine Cycle Analysis Model

3.1 Analytical Models & Their Value

Modeling and analysis of fusion plasmas and their dynamics is a very large field in which multiple approaches have been taken to gain insight into how the fusion process proceeds according to the dynamics of an implosion, laser/plasma interaction, etc. The difficulties and complications involved in modeling magnetohydrodynamic (MHD) flows, as well as the fusion reactions themselves, are legion, necessitating the formulation of very simple models and approximations to facilitate our understanding. Computational studies, performed with complex programs and large amounts of computing power, have tremendous value in the fusion community due to the wealth of quantitative data they provide. Although this may be true, the intrinsic value of very simple, analytical models must not be overlooked due to their ability to quickly impart qualitative understanding of a concept. It is therefore advantageous to have these models to describe fusion processes as well.

An example of the wealth of qualitative information such simple models may provide is given by the air-standard analysis of an internal-combustion engine, also known as an Otto engine. The combustion of fuel within the engine makes the analysis of such a process exceedingly complicated. In addition to this, fuel and air flow steadily into the engine while combustion products flow steadily out of it such that no working medium undergoes a cyclic process. However, we can make a simple analysis by imagining a cyclic engine with air as the working fluid that is equivalent in performance to actual internal-combustion engines. Furthermore, the step involving combustion is replaced by the addition of an equivalent amount of heat to the air at a constant volume.

Likewise, a similar approximation may be made to develop a qualitative understanding of multiple fusion ignition processes. Thus, within the framework of thermodynamics, it is possible to develop a straightforward engineering cycle analysis in similar fashion to those developed for the internal-combustion engine. In what follows, we develop the ideal thermodynamic model that describes the Otto cycle followed by the development of the general framework for a fusion reaction engine.

3.2 The Otto Cycle

The Otto cycle takes place in a four step, or four-stroke process, for which the working fluid is air, considered an ideal gas with constant heat capacities [33]. The process is illustrated in Figure 3.1, and proceeds in four steps as follows:

Process 1-2: Isentropic compression

Process 2-3: Constant Volume heat addition

Process 3-4: Isentropic expansion

Process 4-1: Constant volume heat rejection

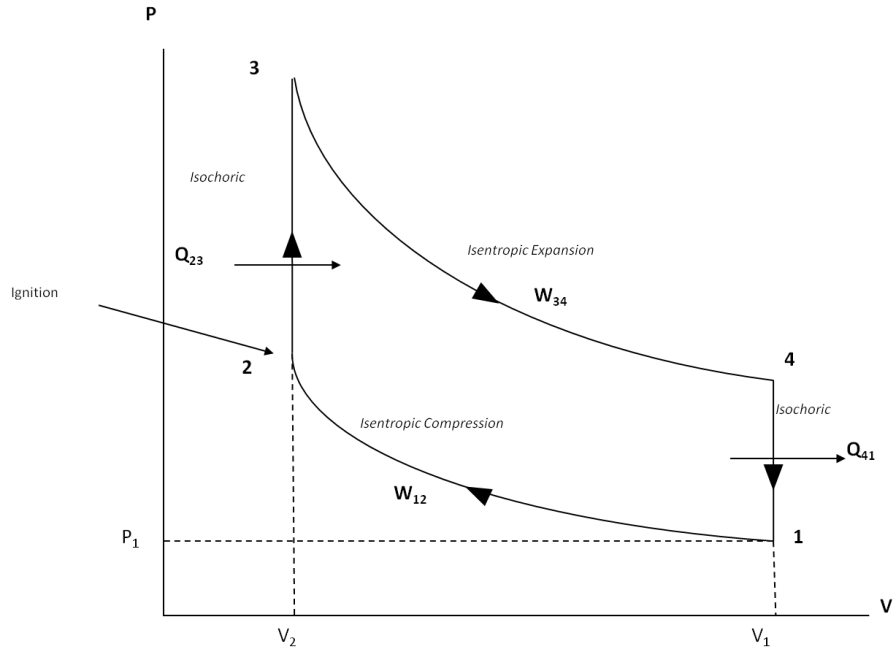


Figure 3.1: Otto cycle P-V diagram.

A simple energy balance $(Q_{in} - Q_{out}) + (W_{in} - W_{out}) = \Delta U$ gives the following for each of the processes listed above:

$$\begin{aligned}
 [1-2]: W_{in} &= U_2 - U_1 \\
 [2-3]: Q_{in} &= U_3 - U_2 \\
 [3-4]: W_{out} &= U_3 - U_4 \\
 [4-1]: Q_{out} &= U_4 - U_1
 \end{aligned} \tag{3.1}$$

The thermal efficiency of the cycle is defined as

$$\eta_T = \frac{\dot{W}_{net}}{\dot{Q}_{in}}, \tag{3.2}$$

and, using the isentropic relations, $\frac{T_2}{T_1} = \left(\frac{V_1}{V_2}\right)^{\gamma-1} = r^{\gamma-1}$, where r is the volumetric compression ratio $r \equiv V_1/V_2$, and γ is the ratio of specific heats, it can be shown that [3]

$$\eta_T = 1 - \left(\frac{1}{r}\right)^{\gamma-1}. \quad (3.3)$$

3.3 Fusion Reaction Engine Cycle

As stated above, similar approximations may be made that will illuminate a qualitative understanding of multiple fusion ignition processes. We stress that while some of the assumptions may introduce marked departures from real systems, the simplifications retain the qualitative behavior. The value in doing this is two fold. First, we gain invaluable insights with the power of studying performance across a broad fusion parameter space. Second, the simplifications make the approach accessible to a wide audience, at the level of senior level undergraduates and first year grad students. For a generic pulsed fusion reaction engine, we apply the general cycle analysis equation (3.1) to gain expressions for the work input (process [1-2]), heat added (process [2-3]), and work output (process [3-4]) where the working fluid consists of the fusion fuel mass m_f and some liner mass m_l .

Beginning with process [1-2] for the required work input, we may write

$$W_{12} = W_{in} = U_2 - U_1 = m_f c_{vf} (T_2 - T_1)_f + m_l c_{vl} (T_2 - T_1)_l, \quad (3.4)$$

where c_{vf} and c_{vl} are the constant volume specific heats for the fuel and liner, respectively.

Equation (3.4) illustrates the simple juxtaposition of the internal energies of the fuel and the liner, taking into account the fact that their respective properties vary thus necessitating the distinction

between the temperature of the liner and the temperature of the fuel at states 1 and 2. This equation can be simplified so that

$$W_{12} = m_f c_{vf} T_{2f} \left[1 - \frac{T_1}{T_2} \right]_f + m_l c_{vl} T_{2l} \left[1 - \frac{T_1}{T_2} \right]_l, \quad (3.5)$$

or, since

$$\frac{T_1}{T_2} = \left(\frac{1}{r} \right)^{\gamma-1}, \quad (3.6)$$

it follows that

$$W_{12} = m_f c_{vf} T_{2f} \left[1 - \left(\frac{1}{r} \right)^{\gamma-1} \right]_f + m_l c_{vl} T_{2l} \left[1 - \left(\frac{1}{r} \right)^{\gamma-1} \right]_l. \quad (3.7)$$

To make this expression more general, we make a few simplifying assumptions: (1) the mass of the liner can be expressed as proportional to the fuel mass via the “fractional liner mass”, $\phi \equiv m_l / m_f$. This fractional liner mass can range from 10 times the fuel mass all the way up to 1000 times the fuel mass. (2) The temperature of the liner can also be expressed in proportion to that of the fuel. The reasoning for this assumption is two-fold: first, the liner itself in the compression process is not being heated to the ignition temperature required by the fuel; second, the liner is also undergoing an isentropic compression process that will raise its temperature by the amount ΔT_l . This temperature rise will be proportional to the temperature rise of the fuel in the same amount that the liner mass is proportional to the fuel mass. In other words,

$$T_{2l} = \frac{T_{2f}}{\phi}. \quad (3.8)$$

We note that actual devices will depart from both the proportionality of temperatures and isentropic compression process. In the former, the relatively high mass of the liner and lower current density in the liner will result in less compression, meaning that less work will be done on the liner. In the latter assumption, Ohmic dissipation, radiation, thermal transfer, and shock heating will all cause departures from isentropic behavior. If we use these two simplifying assumptions in (3.7) above, then

$$W_{12} = m_f c_{vf} T_{2f} \left[1 - \left(\frac{1}{r} \right)^{\gamma-1} \right]_f + (\phi m_f) c_{vl} \left(\frac{T_{2f}}{\phi} \right) \left[1 - \left(\frac{1}{r} \right)^{\gamma-1} \right]_l; \quad (3.9)$$

therefore,

$$W_{12} = m_f c_{vf} T_{2f} \left[1 - \left(\frac{1}{r} \right)^{\gamma-1} \right]_f + m_f c_{vl} T_{2f} \left[1 - \left(\frac{1}{r} \right)^{\gamma-1} \right]_l. \quad (3.10)$$

Next we consider the compression ratio for the fuel and that for the liner to see what assumptions and constraints will exist if they are equivalent. In order for the assumption of an isentropic compression to hold, we have to assume that the thickness of the liner will be negligible compared to its radius. The volumetric compression ratio for a z-pinch will be based on the cylindrical geometry, i.e.,

$$r \equiv \frac{V_1}{V_2} = \frac{\pi R_1^2 l}{\pi R_2^2 l} = \frac{R_1^2}{R_2^2}, \quad (3.11)$$

where R_1 and R_2 are the radii of the fuel at states 1 and 2. If we assume, for simplicity, that the inner radius of the liner is equal to the radius of the fuel, and the liner has thickness δ_1 and δ_2 at states 1 and 2, respectively, then the compression ratio for the liner will be

$$r_l = \frac{V_{1l}}{V_{2l}} = \frac{\pi \left[(R_1 + \delta_1)^2 - R_1^2 \right] l}{\pi \left[(R_2 + \delta_2)^2 - R_2^2 \right] l} = \frac{(R_1^2 + 2R_1\delta_1 + \delta_1^2) - R_1^2}{(R_2^2 + 2R_2\delta_2 + \delta_2^2) - R_2^2} = \frac{2R_1\delta_1 + \delta_1^2}{2R_2\delta_2 + \delta_2^2} \quad (3.12)$$

$$\delta_{1,2} \ll R_{1,2} \Rightarrow r_l = \frac{2R_1\delta_1}{2R_2\delta_2} = \frac{R_1\delta_1}{R_2\delta_2} \quad (3.13)$$

since $\delta_{1,2}^2$ is much smaller than the quantity $2R_{1,2}\delta_{1,2}$.

If the compression ratios of the liner and fuel are equivalent, then

$$\frac{R_1\delta_1}{R_2\delta_2} = r_l = r = \frac{R_1^2}{R_2^2}; \quad (3.14)$$

therefore,

$$\frac{\delta_1}{\delta_2} = \frac{R_1}{R_2}. \quad (3.15)$$

Thus, if the two compression ratios are to be equivalent, we find the requirement that the proportionality of the thickness of the liner and the fuel radii at states 1 and 2 must be equivalent as well. It is important to note, however, that this design requirement also creates a subsequent design constraint: as the compression ratio increases, one must keep in mind that the density of the liner itself can surpass solid densities, i.e., it becomes “super-critical.” The point where this transition occurs for a given system is important since the model, at this level of analysis, does not account for the complexity introduced by the liner when this happens. When designing such a system in this configuration, the design engineer must be careful to consider what the liner will do when it undergoes such high compressions.

Keeping (3.15) in mind, we can then simplify (3.10) to

$$W_{12} = m_f (c_{vf} + c_{vl}) T_2 \left[1 - \left(\frac{1}{r} \right)^{\gamma-1} \right]. \quad (3.16)$$

The accuracy of this statement can be verified by comparing it with the calculation made in equation (3.10) where we use a 50% Deuterium, 50% Tritium fuel with mass $m_f = 10^{-4}$ kg, fractional liner mass $\phi = 200$, fuel ignition temperature $T_{2f} = 10$ keV, liner “ignition” temperature $T_{2l} = \frac{T_{2f}}{\phi} = 50$ eV, compression ratio $r = 10$, $c_{vf} = 4986.21$ J/kg · K and $c_{vl} = 2077.586$ J/kg · K. Using equation (3.10), we calculate $W_{12} \cong 64.328$ MJ; using equation (3.16), we calculate $W_{12} \cong 64.33$ MJ. As one can see, these two calculations are within much less than 1% of each other.

Process [2-3] accounts for the constant volume heat addition process in the Otto cycle. In the traditional use of this thermodynamic cycle, the heat addition comes from the combustion process in a car engine, for example. In our case, this process is represented by the fusion burn process initiated by the compressional work input in process [1-2]. This can be justified since the typical dwell time (the time spent burning the fuel) for a pulsed fusion reaction engine is on the nano/micro-second scale, and thus is very short in comparison to the rest of the cycle.

Quantitatively, we may write this as

$$Q_{in} = Q_{23} = U_3 - U_2 = E_{fus} = (m_f c_{vf} + m_l c_{vl}) (T_3 - T_2), \quad (3.17)$$

where there is no distinction between the fuel and liner temperatures since, at ignition, they may be considered as a mixture.

In this study, the fusion energy is calculated using cross-section data from the Evaluated Nuclear Data File (ENDF) database [4] to compute the reaction rate for species a, b:

$$R_{ab}(\mathbf{r}, t) = N_a N_b \langle \sigma \mathbf{v} \rangle_{ab}(\mathbf{r}, t), \quad (3.18)$$

where $N_{a,b}$ are the population counts for species a and b in the reaction, and the quantity $\langle \sigma \mathbf{v} \rangle$ represents the average of the product $\sigma_{ab}(|\mathbf{v}_a - \mathbf{v}_b|)|\mathbf{v}_a - \mathbf{v}_b|$ with two “weighting” functions which, in this case, are the two population counts $N_{a,b}$ [3]. The fusion power, then, is written as

$$P_{fus} = N_a N_b \langle \sigma \mathbf{v} \rangle_{ab} Q_{ab}, \quad (3.19)$$

where Q_{ab} is the reaction “Q-value”, typically given in MeV. Then the fusion energy will be

$$E_{fus} = N_a N_b \langle \sigma \mathbf{v} \rangle_{ab} Q_{ab} \tau_d, \quad (3.20)$$

where τ_d is the dwell time of the fusion burn.

Knowing the fusion energy added to the mixture during this process, we may solve for the temperature at state 3:

$$T_3 = \frac{E_{fus} + m_f (c_{vf} + c_{vl}) T_2}{m_f (c_{vj} + c_{vl})} \quad (3.21)$$

or

$$T_3 = \frac{N_a N_b \langle \sigma \mathbf{v} \rangle_{ab} Q_{ab} \tau_d + m_f (c_{vf} + c_{vl}) T_2}{m_f (c_{vj} + c_{vl})}. \quad (3.22)$$

Although we fix the value of the temperature at state 2, fixing a temperature at state 3 (after expansion of the reacting plasma) would seem to be superfluous due to the ambiguity of the

properties of the plasma after the explosion. This is also an obvious problem since a real fusion reaction engine would not be a closed system. However, rather than choosing an arbitrary temperature to fix the end state of the process, we are now able to calculate that temperature by knowing the nature of how the fusion reactions in the plasma proceed.

For process [3-4], we utilize the same arguments used for process [1-2] so that we may write an expression for the useful work output from the fusion burn:

$$W_{34} = m_f (c_{vf} + c_{vl}) T_3 \left[1 - \left(\frac{1}{r} \right)^{\gamma-1} \right], \quad (3.23)$$

where we keep with the convention of the Otto cycle analysis by assuming the volume that the fusion output expands into is the same as the volume at state 1. This is obviously not true since the explosion that occurs after the fusion fuel is ignited will expand rapidly without containment, preferably directed out of a nozzle for thrust. Although this may be true, consider this a pessimistic assumption for the model in order that the resulting calculations will be truly conservative in nature since the full expansion of the fusion explosion is not utilized completely.

Process [3-4] implies that the expanding plasma is doing work on the surroundings. We borrow the term “work” loosely here merely to advance the discussion. In reality, there are several processes for the energy available at state 3 to be converted to other forms such as work in compressing an external field, expansion into kinetic energy of the plasma, and thermal conduction and radiation losses. In the subsequent analysis we account for the total energy from [3-4] as W_{34} to indicate the potential for doing work, to retain the analogy to the Otto cycle.

3.4 Performance & Figures of Merit

The following discussion will give an overview of the development of the performance equations for a generic pulsed fusion reaction engine, and expressions for figures of merit such as

gain, propulsive efficiency, etc. We begin with a short discussion of exhaust velocity and specific impulse.

3.4.1 Exhaust Velocity & I_{sp}

To find an expression for the exhaust velocity of the fusion products out of the explosion, we equate the total work output from process [3-4] with the exhaust kinetic energy and the energy needed to re-charge the driver. In this way, we account for the fact that we have to extract energy from the exhaust plume to add energy to the charging circuit. In addition to this, the efficiency of this conversion from total work output to exhaust kinetic energy plus circuit re-charge energy will be accounted for in the expression developed for propulsive efficiency. To begin,

$$W_{34} = (KE)_{ex} + E_c, \quad (3.24)$$

where E_c is the required charging energy, and $(KE)_{ex}$ is the exhaust kinetic energy. If we examine the required amount of energy to be stored in the driver at any given time, we note that the output energy of the driver must be enough to initiate a fusion reaction, but it will be less than the initial energy stored in the driver due to some coupling efficiency, η_χ , and some transfer efficiency of the circuit, η_t . This coupling efficiency gives a measure of how well the liner energy is transformed into thermal energy of the plasma, while the transfer efficiency will account for any losses in the circuit incurred when transferring the energy from the driver to the circuit load (the pinch, for example). These processes are represented diagrammatically in Figure 3.2. The energy required to re-charge the driver, then, will be

$$E_D = \eta_c E_c \quad (3.25)$$

so that

$$E_c = \frac{E_D}{\eta_c} = \frac{W_{12}}{\eta_c}, \quad (3.26)$$

where the energy input into the system from the driver is manifest in the expression for the work required to compress the plasma, W_{12} . With this expression for the required charging energy and equation (3.24), we may write

$$W_{34} = \frac{1}{2}(m_f + m_l)u_e^2 + \frac{W_{12}}{\eta_c} = \frac{1}{2}m_f(\phi + 1)u_e^2 + \frac{W_{12}}{\eta_c}; \quad (3.27)$$

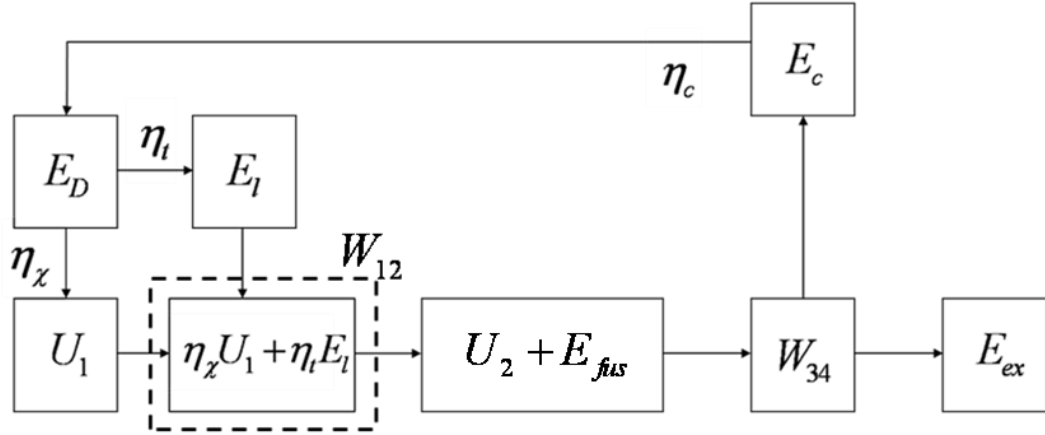


Figure 3.2: Fusion reaction engine cycle.

also,

$$W_{34} = E_{fus} \left[1 - \left(\frac{1}{r} \right)^{\gamma-1} \right] + m_f (c_f + c_{cl}) T_2 \left[1 - \left(\frac{1}{r} \right)^{\gamma-1} \right] \quad (3.28)$$

or

$$W_{34} = \eta E_{fus} + W_{12}. \quad (3.29)$$

Equating (3.27) with (3.29),

$$W_{34} = \frac{1}{2} m_f (\phi + 1) u_e^2 + \frac{W_{12}}{\eta_c} = \eta_T E_{fus} + W_{12} \quad (3.30)$$

and solving for u_e ,

$$u_e = \left\{ \frac{2}{m_f (\phi + 1)} \left[\eta_T E_{fus} + W_{12} \left(1 - \frac{1}{\eta_c} \right) \right] \right\}^{\frac{1}{2}}. \quad (3.31)$$

Thus we see that the exhaust velocity will be inversely dependent upon the fuel and liner mass, which is appropriate since an increased mass flow rate corresponds to a lower specific impulse,

$$I_{sp} = \frac{u_e}{g_0} \quad (3.32)$$

and a higher thrust, via the rocket equation

$$F = \dot{m} u_e = m_f (\phi + 1) f u_e, \quad (3.33)$$

where f is the pulse frequency of the system.

3.4.2 Thrust Power

The thrust power is formulated as

$$P = \frac{1}{2} \dot{m} u_e^2 = \frac{1}{2} m_f (\phi + 1) f u_e^2 = \frac{1}{2} F u_e, \quad (3.34)$$

so

$$P = f \left[\eta_T E_{fus} + W_{12} \left(1 - \frac{1}{\eta_c} \right) \right]. \quad (3.35)$$

3.4.3 Efficiencies

The propulsive efficiency of the cycle is a measure of how efficiently the energy released during the heating process (like combustion) is converted to propulsive energy. A better way to state this, for more clarity, is the ratio of the useful power output to the total power output of the engine:

$$\eta_p = \frac{\text{useful power output}}{\text{total power output}} = \frac{\dot{W}_p}{\dot{W}_{out}}, \quad (3.36)$$

so the useful power output will be the power available to be used as thrust (after extracting the energy needed to re-charge the driver) and the total power output of the engine will be the work output of process [3-4], which accounts for the heat added by fusion and the energy added to the plasma in the ignition phase of process [1-2]. Therefore,

$$\eta_p = \frac{P}{W_{34}} = \frac{\eta_T E_{fus} + W_{12} \left(1 - \frac{1}{\eta_c}\right)}{\eta_T E_{fus} + W_{12}}. \quad (3.37)$$

The overall efficiency of the system will be

$$\eta_o = \eta_T \eta_i \eta_\chi \eta_c \eta_p, \quad (3.38)$$

where η_T is the thermal efficiency, η_i is the transfer efficiency, η_χ is the coupling efficiency, and η_c is the charging efficiency. The transfer efficiency is determined via analysis of the circuit providing the power for the load, and for most pulsed power facilities the value is typically ~ 0.8 depending on impedance matching of the transmission line with the load. The coupling efficiency will be dependent upon the individual system geometry and how the driver transfers the energy to the plasma. This has to be determined for the specific system to be analyzed. The

charging efficiency, like the transfer efficiency, also hovers around ~ 0.8 depending on the system impedance matching and the method used to extract the electrical energy from the flow.

3.4.4 Fusion Gain

The expression for the fusion gain follows from the expressions above, knowing

$$G \equiv \frac{E_{fus}}{U_1 + W_{12}}. \quad (3.39)$$

The initial thermal energy of the plasma can be written as

$$U_1 = m_f c_{vf} T_1 = m_f c_{vf} T_2 \left(\frac{1}{r} \right)^{\gamma-1} \quad (3.40)$$

so that

$$U_1 + W_{12} = m_f c_{vf} T_2 \left(\frac{1}{r} \right)^{\gamma-1} + m_f (c_{vf} + c_{vl}) T_2 \left[1 - \left(\frac{1}{r} \right)^{\gamma-1} \right], \quad (3.41)$$

which may be simplified to

$$U_1 + W_{12} = m_f (c_{vf} + \eta_T c_{vl}) T_2. \quad (3.42)$$

Then, using the expression for the gain in (3.39) and equation (3.17) above,

$$G = \frac{E_{fus}}{U_1 + W_{12}} = \frac{m_f (c_{vf} + \phi c_{vl}) (T_3 - T_2)}{m_f (c_{vf} + \eta_T c_{vl}) T_2} = \frac{(c_{vf} + \phi c_{vl})}{(c_{vf} + \eta_T c_{vl})} \frac{T_3 - T_2}{T_2}; \quad (3.43)$$

therefore,

$$G = \frac{(c_{vf} + \phi c_{vl})}{(c_{vf} + \eta_T c_{vl})} \left(\frac{T_3}{T_2} - 1 \right). \quad (3.44)$$

Chapter 4

Z-Pinch Fusion Reaction Engine Cycle Analysis

4.1 Basic Z-Pinch Operation

A z-pinch is a radial implosion of a cylindrical or annular plasma under the influence of a strong magnetic field produced by current flowing down the length of the plasma; it usually involves the ionization and subsequent implosion of a gas for time-scales on the order of microseconds. The process can be broken down into a number of steps that occur in the following order (Figure 4.1):

1. Gas injection/preionization
2. Compression/implosion
3. Stagnation/burn
4. Expansion/explosion

By closely examining this process, one might observe that it is strikingly similar to the operation of an Otto cycle. We can therefore make the following correlations:

- 1) The gas injection/preionization phase can be considered in similar fashion to the valve intake process of an internal-combustion engine
- 2) Compression/implosion can be correlated to Process 1-2 of the Otto cycle, making similar assumptions: approximate the plasma as an ideal gas, with constant specific heats and composition.
- 3) Stagnation/burn is the stage in which the plasma reaches fusion conditions thus causing fusion reactions to occur. In this case, like the normal combustion process, the fusion reactions can be considered to occur rapidly enough such that the process

takes place at constant volume. This stage can therefore be approximated as a constant volume heat addition like Process 2-3 of the Otto cycle.

- 4) Expansion/explosion, like Process 3-4 of the Otto cycle, can also take place

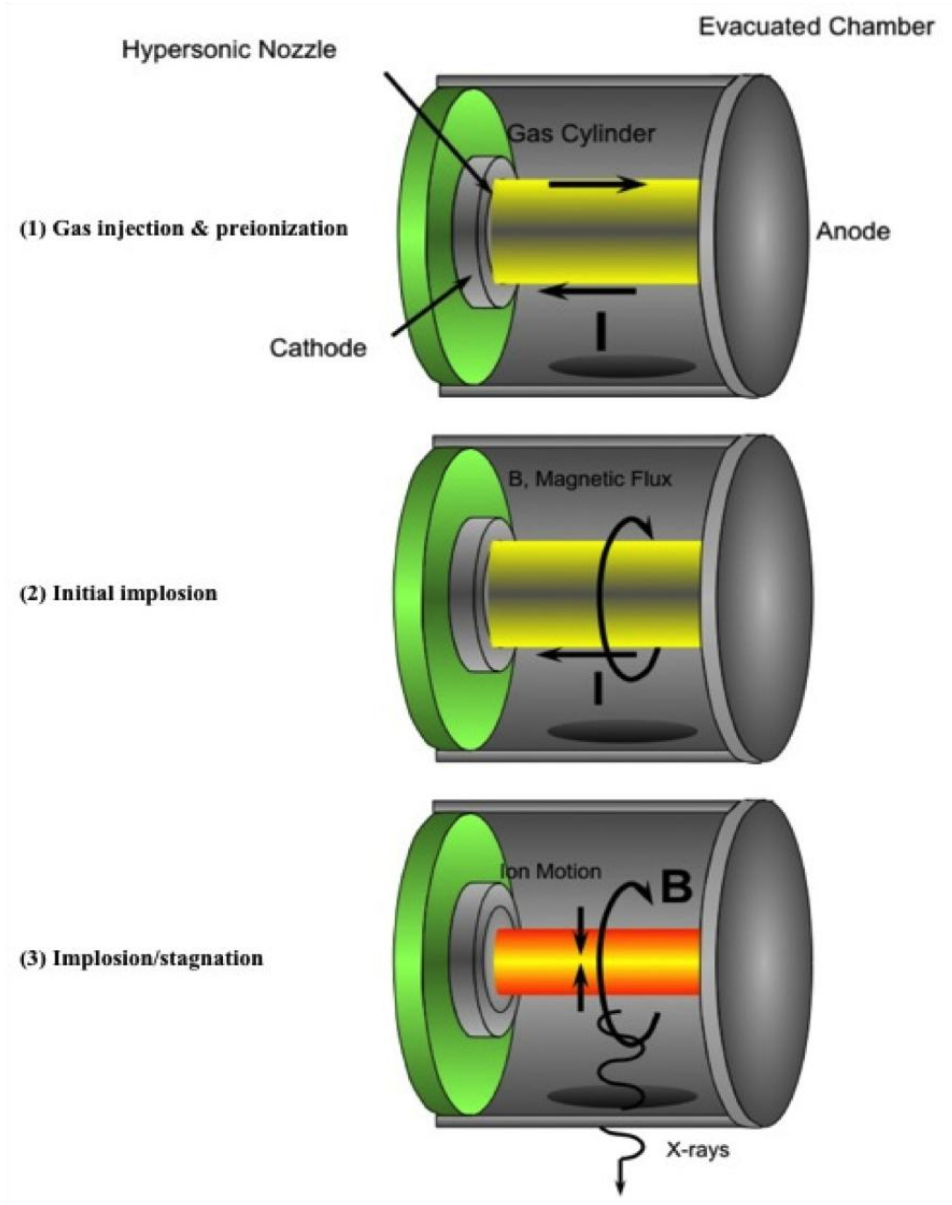


Figure 4.1: Stages of z-pinch formation.

isentropically under the same assumptions. For our particular propulsion application, this process takes place by expanding the plasma out of a magnetic nozzle into vacuum.

- 5) Process 4-1 of the Otto cycle can be incorporated into the fusion reaction engine model as well by assuming constant volume heat rejection from the plasma, thus returning to state 1. Like the Otto cycle, this does not necessarily reflect reality, but it is nonetheless useful when considering the general performance of an engine.

Using the correlations stated above, we can construct a useful thermodynamic model incorporating simple plasma physics arguments to describe the performance of a z-pinch fusion reaction cycle.

Before further developing the thermodynamic analysis of the z-pinch system, there are a few important notes to consider involving the formation process. First, the z-pinch process proceeds by pulsing very large currents through the gas being used. Therefore, electrostatics plays a significant role in the performance of the system. Due to this simple fact, we must incorporate the effects of electric and magnetic field dynamics into the model. Second, the representation of this cycle analysis can only be made by considering the state of the system at each individual step of the process. The complicating effects of the electric and magnetic fields must therefore be somehow discretized so that we can consider each state individually, disregarding the dynamics in between. A simple pressure balance model used to describe z-pinch stability facilitates this by assuming the pinch to be a cylindrical column of fully ionized gas with an axial electric field, producing an axial current density, \mathbf{j} , and an associated azimuthal magnetic field, \mathbf{B} . As this current flows through its own magnetic field, it produces an inward radial force density $\mathbf{F}_r = \mathbf{j} \times \mathbf{B} = (j_z \hat{\mathbf{z}}) \times (B_\theta \hat{\theta})$ such that $\mathbf{F}_r = -j_z B_\theta \hat{\mathbf{r}}$. The pressure balance is achieved by matching the internal gas pressure with the pressure of the magnetic field compressing the column, which can be shown to be $p = B^2/2\mu_0$.

Finally, by focusing on the energy states of each process and knowing certain criteria, such as temperature, composition, and geometry of the system, we can determine the input requirements of the system to achieve ignition. For example, if we wish to ignite a 50/50 Deuterium-Tritium gas mixture, we know we require the minimum temperature at state 2 (compressed state) to be at least 10 keV. Knowing this temperature, and the mixture composition, we can back out the magnetic field strength (and therefore current) required for ignition via simple thermodynamic arguments. Thus the input parameters we use to design the system can be simplified to simple functions of the ignition temperature, compression ratio, and mass of the fuel we are using. This will be further explored in the next section.

As noted previously in Chapter 2, the z-pinch propulsion concept studied here is modified from a typical z-pinch confinement scheme by using a liquid lithium mixture to serve as the current return path for the circuit. This serves two purposes: (1) the lithium acts as a partial shield to capture neutrons from the D-T reaction, releasing further energy in the reaction as well as helping to reduce the burden of the neutron load on the surrounding nozzle structure, and (2) it will add mass to the exhaust of the rocket causing increased mass flow and therefore increased thrust. In the model depicted here, the lithium liner mass is defined to be a function of the fuel mass (see Chapter 3) in order to determine its effect on the overall performance of the system. Indeed, by plotting parameters such as specific impulse, thrust and acceleration as functions of the fractional liner mass the results show a significant dependence upon the liner mass and therefore the fuel mass and composition.

4.2 Z-Pinch Cycle Analysis & Design Parameters

We begin by re-stating the steps of the Otto cycle and writing the energy balance for each:

Process 1-2: Isentropic compression

$$W_{in} = U_2 - U_1$$

Process 2-3: Constant Volume heat addition

$$Q_{in} = U_3 - U_2$$

Process 3-4: Isentropic expansion

$$W_{out} = U_3 - U_4$$

Process 4-1: Constant volume heat rejection

$$Q_{out} = U_4 - U_1$$

For process 1-2, knowing the ignition temperature we require, we can back out a value for the initial temperature of the plasma since

$$T_1 = T_2 \left(\frac{1}{r} \right)^{\gamma-1}. \quad (4.1)$$

It follows, then, that we can determine the internal energy needed in the plasma at state 1:

$$U_1 = m_f c_{vf} T_1. \quad (4.2)$$

4.2.1 Work Input & Current Required

In order to determine the input current needed to achieve ignition conditions at state 2, we consider the work input required for ignition in relation to the compression work by the liner on the plasma. In other words, we begin with the well-known expression

$$W_{12} = -p\Delta V. \quad (4.3)$$

This expression can then be written as

$$W_{12} = -p(V_2 - V_1) = -p\left(\frac{V_1}{r} - V_1\right) = -pV_1\left(\frac{1}{r} - 1\right) = pV_1\left(\frac{r-1}{r}\right). \quad (4.4)$$

Knowing the magnetic pressure at state 1 will be $p = B_1^2 / 2\mu_0$, we may write this as

$$W_{12} = \frac{B_1^2}{2\mu_0} V_1 \left(\frac{r-1}{r} \right). \quad (4.5)$$

From Ampere's Law, $\nabla \times \mathbf{B} = \mu_0 \mathbf{j}$, we know that for a current I running through a cylindrical volume of length l with cross-sectional area πR_1^2 the azimuthally induced magnetic field will be

$$B_1 = \frac{\mu_0 I_1}{2\pi R_1} \quad (4.6)$$

such that (4.5) becomes

$$W_{12} = \frac{\mu_0 I_1^2}{8\pi^2 R_1^2} V_1 \left(\frac{r-1}{r} \right). \quad (4.7)$$

Taking the initial plasma volume to be $V_1 = \pi R_1^2 l$, expression (4.7) then simplifies to

$$W_{12} = \frac{\mu_0 l}{8\pi} I_1^2 \left(\frac{r-1}{r} \right). \quad (4.8)$$

Recalling our general expression for the work input from equation (3.16) and equating it with this expression,

$$\frac{\mu_0 l}{8\pi} I_1^2 \left(\frac{r-1}{r} \right) = W_{12} = m_f (c_{vf} + c_{vl}) T_2 \left[1 - \left(\frac{1}{r} \right)^{\gamma-1} \right], \quad (4.9)$$

we then solve for the current at state 1,

$$I_1^2 = \frac{8\pi m_f}{\mu_0 l} T_2 (c_{vf} + c_{vl}) \left(\frac{r}{r-1} \right) \left[1 - \left(\frac{1}{r} \right)^{\gamma-1} \right]. \quad (4.10)$$

Thus, we have a relationship for the current required for ignition as a function of compression ratio, fuel mass, ignition temperature, and system length.

This expression can then enable us to determine other design parameters for the system such as the transfer efficiency of the circuit and the properties of the driver (e.g., capacitance,

voltage, energy density). As an example, the transfer efficiency of the transmission line in a discharge circuit is taken as the ratio of the power transferred to the load divided by the power output from the transmission line. This efficiency is dependent upon the matching of the impedance of the transmission line, Z_0 with that of the circuit load, R_L [35]. Even if these impedances are not perfectly matched, there exists a broad maximum in the transfer efficiency from 0.5 to ~ 1.5 in the ratio of R_L/Z_0 where the efficiency is ~ 0.8 . By knowing the current required for ignition, this simple property of the transfer efficiency of the transmission line can be utilized to design the power circuit of the system. This in turn enables us to back out the properties for the driver and, going further, the properties of the auxiliary power supply in the system as well as the properties of the recharge circuit.

4.2.2 Liner Implosion Velocity & Exhaust Velocity

Starting with the work input required for ignition W_{12} and referring to Figure 3.2 we may write

$$W_{12} = \eta E_t + \eta_\chi U_1 = \eta E_t + \eta_\chi m_f c_{vf} T_1 = \eta E_t + \eta_\chi m_f c_{vf} T_2 \left(\frac{1}{r}\right)^{\gamma-1} \quad (4.11)$$

or

$$W_{12} = \frac{1}{2} \eta_t m_l v_l^2 + \eta_\chi m_f c_{vf} T_2 \left(\frac{1}{r}\right)^{\gamma-1}, \quad (4.12)$$

where the first term is the kinetic energy of the liner, and the second term is the internal energy of the plasma at state 1 as a function of the ignition temperature at state 2 and the volumetric compression ratio. Equation (4.12) can be simplified to

$$W_{12} = m_f \left[\frac{\phi}{2} \eta_t v_l^2 + \eta_\chi c_{vf} T_2 \left(\frac{1}{r}\right)^{\gamma-1} \right] = m_f (c_{vf} + c_{vl}) T_2 \left[1 - \left(\frac{1}{r}\right)^{\gamma-1} \right] \quad (4.13)$$

or

$$\frac{\phi}{2}\eta_t v_l^2 + \eta_\chi c_{vf} T_2 \left(\frac{1}{r}\right)^{\gamma-1} = (c_{vf} + c_{vl}) T_2 \left[1 - \left(\frac{1}{r}\right)^{\gamma-1}\right]. \quad (4.14)$$

Then,

$$\frac{\phi}{2}\eta_t v_l^2 = (c_{vf} + c_{vl}) T_2 \left[1 - \left(\frac{1}{r}\right)^{\gamma-1}\right] - \eta_\chi c_{vf} T_2 \left(\frac{1}{r}\right)^{\gamma-1} \quad (4.15)$$

and after further manipulation, solving for the squared liner velocity, normalized to the ignition temperature T_2 ,

$$\frac{v_l^2}{T_2} = \frac{2}{\phi \eta_t} \left\{ c_{vl} \left[1 - \left(\frac{1}{r}\right)^{\gamma-1}\right] + c_{vf} \left[1 - (1 + \eta_\chi) \left(\frac{1}{r}\right)^{\gamma-1}\right] \right\} \quad (4.16)$$

or

$$\frac{v_l^2}{T_2} = \frac{2}{\phi \eta_t} \left\{ c_{vl} \eta_t + c_{vf} \left[1 - (1 + \eta_\chi) \left(\frac{1}{r}\right)^{\gamma-1}\right] \right\}. \quad (4.17)$$

Equation (4.17) gives us a relationship between the liner velocity (or kinetic energy) scaled with the ignition temperature at state 2 which is dependent upon liner mass fraction, transfer efficiency, thermal efficiency, coupling efficiency and compression ratio.

Continuing this trend, and examining the energy output from the fusion explosion, the energy available for work is

$$W_{34} = E_{ex} + E_c = \frac{1}{2} (m_f + m_t) u_e^2 + E_c = \frac{1}{2} m_f (\phi + 1) u_e^2 + E_c. \quad (4.18)$$

Since the propulsive efficiency is a measure of the kinetic energy of the exhaust, and therefore thrust, compared with the energy available from fusion, then, using (4.18),

$$\eta_p = \frac{E_{ex}}{W_{34}} \Rightarrow \frac{E_{ex}}{\eta_p} = W_{34} = E_{ex} + E_c \quad (4.19)$$

so that

$$\frac{E_c}{E_{ex}} = \left(\frac{1 - \eta_p}{\eta_p} \right). \quad (4.20)$$

The energy that makes it to the driver (re-charge energy) from the charging energy is

$$E_D = \eta_c E_c, \quad (4.21)$$

and the energy released from the driver is just the input work, so

$$E_D = \eta_c E_c = W_{12} \Rightarrow E_c = \frac{W_{12}}{\eta_c} \quad (4.22)$$

and (4.20) becomes

$$\frac{E_{ex}}{W_{12}} = \frac{1}{\eta_c} \left(\frac{\eta_p}{1 - \eta_p} \right). \quad (4.23)$$

Re-writing (4.23),

$$\frac{E_{ex}}{W_{12}} = \frac{\frac{1}{2} m_f (\phi + 1) u_e^2}{m_f (c_{vf} + c_{vl}) T_2 \eta_T} = \frac{(\phi + 1) u_e^2}{2 (c_{vf} + c_{vl}) T_2 \eta_T}, \quad (4.24)$$

so

$$\frac{(\phi+1)u_e^2}{2(c_{vf} + c_{vl})T_2\eta_T} = \frac{1}{\eta_c} \left(\frac{\eta_p}{1-\eta_p} \right). \quad (4.25)$$

Solving for u_e^2/T_2 gives

$$\frac{u_e^2}{T_2} = \frac{2(c_{vf} + c_{vl})\eta_T}{(\phi+1)\eta_c} \left(\frac{\eta_p}{1-\eta_p} \right). \quad (4.26)$$

From equation (3.37) for the propulsive efficiency we may write

$$\frac{\eta_p}{1-\eta_p} = \frac{\eta_c\eta_TE_{fus} + W_{12}(\eta_c - 1)}{W_{12}} = \frac{\eta_c(\eta_TE_{fus} + W_{12}) - W_{12}}{W_{12}}, \quad (4.27)$$

where $(\eta_TE_{fus} + W_{12})$ is just W_{34} so that (4.27) becomes

$$\frac{\eta_p}{1-\eta_p} = \frac{\eta_c W_{34} - W_{12}}{W_{12}} = \eta_c \frac{W_{34}}{W_{12}} - 1. \quad (4.28)$$

From our previous expression for W_{12} and W_{34} we may write this as

$$\frac{\eta_p}{1-\eta_p} = \eta_c \frac{m_f(c_{vf} + c_{vl})T_3}{m_f(c_{vf} + c_{vl})T_2} - 1 = \eta_c \frac{T_3}{T_2} - 1. \quad (4.29)$$

Plugging this expression back into (4.26) above,

$$\frac{u_e^2}{T_2} = 2 \frac{(c_{vf} + c_{vl})\eta_T}{(\phi+1)\eta_c} \left(\eta_c \frac{T_3}{T_2} - 1 \right) \quad (4.30)$$

or

$$\frac{u_e^2}{T_2} = 2\eta_T \frac{(c_{vf} + c_{vl})}{(\phi + 1)} \left(\frac{T_3}{T_2} - \frac{1}{\eta_c} \right). \quad (4.31)$$

This gives us an expression for the exhaust kinetic energy scaled with ignition temperature that is therefore based on both the volumetric compression ratio, implicit in the thermal efficiency η_T , the liner mass fraction, and the temperature at state 3.

The relationship between the exhaust velocity and liner implosion velocity can be found by dividing equation (4.31) by equation (4.17). Although a bit messy, the scaling that emerges of the exhaust velocity with the liner implosion velocity can be a useful design tool. This will be further explored in Chapter 5.

4.2.3 Gain

An expression for the fusion gain of the system may be obtained that is connected back to the basic design parameters (compression ratio, liner mass fraction) and other design parameters such as the input current and the system length. To find this relationship, we begin with the general expression for the gain developed in Chapter 3:

$$G = \left(\frac{c_{vf} + \phi c_{vl}}{c_{vf} + \eta_T c_{vl}} \right) \left(\frac{T_3}{T_2} - 1 \right). \quad (4.32)$$

Utilizing our expression for T_3 in equation (3.21), we may write this as

$$\begin{aligned} G &= \left(\frac{c_{vf} + \phi c_{vl}}{c_{vf} + \eta_T c_{vl}} \right) \left[\frac{E_{fus} + m_f (c_{vf} + c_{vl}) T_2}{m_f (c_{vf} + c_{vl}) T_2} - 1 \right] = \left(\frac{c_{vf} + \phi c_{vl}}{c_{vf} + \eta_T c_{vl}} \right) \left[\frac{E_{fus}}{m_f (c_{vf} + c_{vl}) T_2} + 1 - 1 \right] \\ &= \left(\frac{c_{vf} + \phi c_{vl}}{c_{vf} + \eta_T c_{vl}} \right) \left(\frac{E_{fus}}{m_f (c_{vf} + c_{vl}) T_2} \right) = \left(\frac{c_{vf} + \phi c_{vl}}{c_{vf} + \eta_T c_{vl}} \right) \eta_T \frac{E_{fus}}{W_{12}}. \end{aligned} \quad (4.33)$$

Inserting equation (4.8) into this expression gives

$$G = \left(\frac{c_{vf} + \phi c_{vl}}{c_{vf} + \eta_T c_{vl}} \right) \eta_T E_{fus} \left[\frac{8\pi}{\mu_0 l} \frac{1}{I_1^2} \left(\frac{r}{r-1} \right) \right] \quad (4.34)$$

or

$$G = \frac{8\pi}{\mu_0 l} \eta_T \left(\frac{c_{vf} + \phi c_{vl}}{c_{vf} + \eta_T c_{vl}} \right) \frac{E_{fus}}{I_1^2} \left(\frac{r}{r-1} \right). \quad (4.35)$$

4.3 Summary of Equations—Z-Pinch Fusion Reaction Engine

A summary of the inputs, outputs, and equations of the z-pinch cycle analysis is given below after the convenient form used by Mattingly in *Elements of Propulsion: Gas Turbines and Rockets* [2].

INPUTS: T_2 (keV, K), r , l (m), R_1 (m), τ_d (s), τ_i (s), f (Hz)

Fuel: z , m_f (kg), c_{vf} (J/kg•K), R_f (J/kg•K), m_{if} (fuel ion mass) (kg)

Liner: m_l (kg), $\phi = \frac{m_l}{m_f}$, c_{vl} (J/kg•K), R_l (J/kg•K)

OUTPUTS: u_e (m/s), I_{sp} (s), F (N), P (W), G , E_{fus} (J), η_p , η_T , η_t , η_χ , η_c , f_b (burn fraction), N_n (# neutrons), E_n (J), E_c (J), I_1 (A), B_1 (T)

EQUATIONS:

$$V_1 = \pi R_1^2 l \quad (4.36)$$

$$V_2 = \frac{V_1}{r} \quad (4.37)$$

$$n_1 = \frac{m_f}{m_{if}V_1} \quad (4.38)$$

$$n_2 = n_1 r \quad (4.39)$$

$$\eta_T = 1 - \left(\frac{1}{r}\right)^{\gamma-1} \quad (4.40)$$

$$W_{12} = m_f (c_{vf} + c_{vl}) T_2 \left[1 - \left(\frac{1}{r}\right)^{\gamma-1} \right] \quad (4.41)$$

$$I_1 = \left\{ \frac{8\pi}{\mu_0 l} m_f T_2 (c_{vf} + c_{vl}) \left(\frac{r}{r-1}\right) \left[1 - \left(\frac{1}{r}\right)^{\gamma-1} \right] \right\}^{\frac{1}{2}} \quad (4.42)$$

$$B_1 = \frac{\mu_0 I_1}{2\pi R_1}; B_2 = B_1 \sqrt{r} \quad (4.43)$$

$$Q_{23} = E_{fus} = m_f (c_{vf} + c_{vl}) (T_3 - T_2) \quad (4.44)$$

$$T_3 = \frac{E_{fus} + m_f (c_{vf} + c_{vl}) T_2}{m_f (c_{vf} + c_{vl})} \quad (4.45)$$

$$W_{34} = m_f (c_{vf} + c_{vl}) T_3 \left[1 - \left(\frac{1}{r}\right)^{\gamma-1} \right] \quad (4.46)$$

$$E_c = \frac{W_{12}}{\eta_c} \quad (4.47)$$

$$u_e = \left\{ \frac{2}{m_f (\phi + 1)} \left[\eta_T E_{fus} + W_{12} \left(1 - \frac{1}{\eta_c} \right) \right] \right\}^{\frac{1}{2}} \quad (4.48)$$

$$\frac{u_e^2}{T_2} = 2\eta_T \left(\frac{c_{vf} + c_{vl}}{\phi + 1} \right) \left(\frac{T_3}{T_2} - \frac{1}{\eta_c} \right) \quad (4.49)$$

$$\frac{v_l^2}{T_2} = \frac{2}{\phi \eta_t} \left\{ c_{vl} \eta_T + c_{vf} \left[1 - (1 + \eta_\chi) \left(\frac{1}{r} \right)^{\gamma-1} \right] \right\} \quad (4.50)$$

$$I_{sp} = \frac{u_e}{g_0} \quad (4.51)$$

$$F = m_f (\phi + 1) f u_e \quad (4.52)$$

$$P = \frac{1}{2} F u_e \quad (4.53)$$

$$G = \frac{E_{fus}}{W_{12}} = \frac{8\pi}{\mu_0 l} \eta_T \left(\frac{c_{vf} + \phi c_{vl}}{c_{vf} + \eta_T c_{vl}} \right) \frac{E_{fus}}{I_1^2} \left(\frac{r}{r-1} \right) \quad (4.54)$$

$$\eta_p = \frac{\eta_T E_{fus} + W_{12} \left(1 - \frac{1}{\eta_c} \right)}{\eta_T E_{fus} + W_{12}} \quad (4.55)$$

$$\eta_o = \eta_T \eta_t \eta_\chi \eta_c \eta_p \quad (4.56)$$

Chapter 5

Results & Discussion

5.1 Introduction

The results of the model will be presented and discussed below. In what follows, we will examine the effects of changes in the system geometry, fuel mass and composition, and dwell time have on the performance of the z-pinch propulsion system. In addition, we will view the basic system design requirements that are derived from these parameter changes. Two representative cases are chosen and examined in order to illustrate the range of design possibilities. We have also included a short case study that reviews the results of the model that were utilized in a recent NASA design study for an in-space propulsion system [36].

5.2 Model Parameter Space

The parameter space explored in this design analysis was chosen based on a few underlying assumptions:

1. Depending on the composition of the fuel, the required ignition temperature will be in the range from 10 keV up to 30 keV.
2. The current state of the art in z-pinch research and development utilizes system geometries with lengths of ~5 cm all the way up to 1 m, and radii between ~1 cm up to 20 cm.
3. The amount of mass used in a typical z-pinch is generally less than 10 mg.
4. Dwell times for most z-pinches are typically in the 100's of nanoseconds range.

With these assumptions in mind, we choose a parameter space to investigate that will push the bounds of current technology while also examining the parameters that are currently achievable. This enables us to have a way to check the model to ensure its accuracy.

The different fuel compositions examined in this study are given in Table 5.1 and the parameter space in its entirety is given in Table 5.2. Reviewing the results for all of these mixtures in a thorough way would take an inordinate amount of time and is therefore outside the scope of this study. However, we will examine two “representative” cases that illustrate the range of design possibilities in the model. These cases will be explained in the next section. In order to be relevant and comparable to other fusion propulsion system studies, we will examine fuel mixtures 1, 2, and 3 from Table 5.1 below.

Table 5.1: Fuel Compositions

| Mole Fraction | 1 | 2 | 3 | 4 | 5 | 6 |
|----------------------|----------|----------|----------|----------|----------|----------|
| χ_D | 0.5 | 0.5 | 1.0 | 0.5 | 0.5 | 0.5 |
| χ_T | 0.5 | 0.0 | 0.0 | 0.25 | 0.35 | 0.15 |
| χ_{He^3} | 0.0 | 0.5 | 0.0 | 0.25 | 0.15 | 0.35 |

Table 5.2: Model Parameter Space

| | | | | | | |
|---------------|------|------|------|------|------|------|
| T_2 [keV] | 10 | 15 | 20 | 25 | 30 | 35 |
| m_f [mg] | 10 | 50 | 100 | 500 | 1000 | - |
| L [m] | 0.05 | 0.25 | 0.45 | 0.65 | 0.85 | 1.0 |
| R_1 [m] | 0.05 | 0.1 | 0.15 | 0.2 | - | - |
| τ_d [ns] | 100 | 200 | 500 | 1000 | 1500 | 2000 |

5.3 Definition of Cases

The representative cases chosen for this study are represented by the 5 variables in the model parameter space, namely, ignition temperature at state 2, fuel mass, system length, initial system radius, and dwell time. As one might see upon viewing Table 5.2, there are 4320 different permutations of all of the parameters that can be examined in this parameter space. In order to see the basic effects of different combinations of these parameters, we choose the two cases below in Table 5.3 to investigate.

Table 5.3: Representative Cases

| Case | I | II |
|---------------|----------|-----------|
| T_2 [keV] | 10, 25 | 10, 25 |
| m_f [mg] | 10 | 100 |
| l [m] | 0.05 | 0.45 |
| R_1 [m] | 0.05 | 0.10 |
| τ_d [ns] | 100 | 100 |

Case I is the “baseline” case, where all the parameters are set to their lowest values. The second case represents what might be the “middle” case where the system geometry is larger than most typical z-pinchs and the amount of fuel mass is somewhat higher than the typical value as well. The performance values of the thruster are calculated and plotted as functions of volumetric compression ratio, r , and fractional liner mass, ϕ , in the ranges 10 -10000 and 10 - 1000, respectively. The dwell time was kept to 100 ns so that we could remain on the conservative side when calculating the amount of fusion energy released in the reaction. In addition, it is important to note that when calculating the fusion energy release, and therefore the gain, the energy released purely by neutrons was *not* included, thus making the calculation even more conservative. We

will appraise the performance results from each case in the next two sections. Following this we will then compare the design requirements for each case.

5.4 Case Study I: Performance Results

Referring to Table 5.3 above, the parameter values for this case study were $T_2 = 10$, 25 keV, $m_f = 10$ mg, $l = 0.05$ m, $R_1 = 0.05$ m, and $\tau_d = 100$ ns. First, we review the performance of the system for the three fuel mixtures noted above due to these parameters followed by the design requirements of the system.

Figure 5.1, Figure 5.2, and Figure 5.3 are useful illustrations of the performance of the system for the given parameters. They show the thrust per unit frequency versus specific impulse

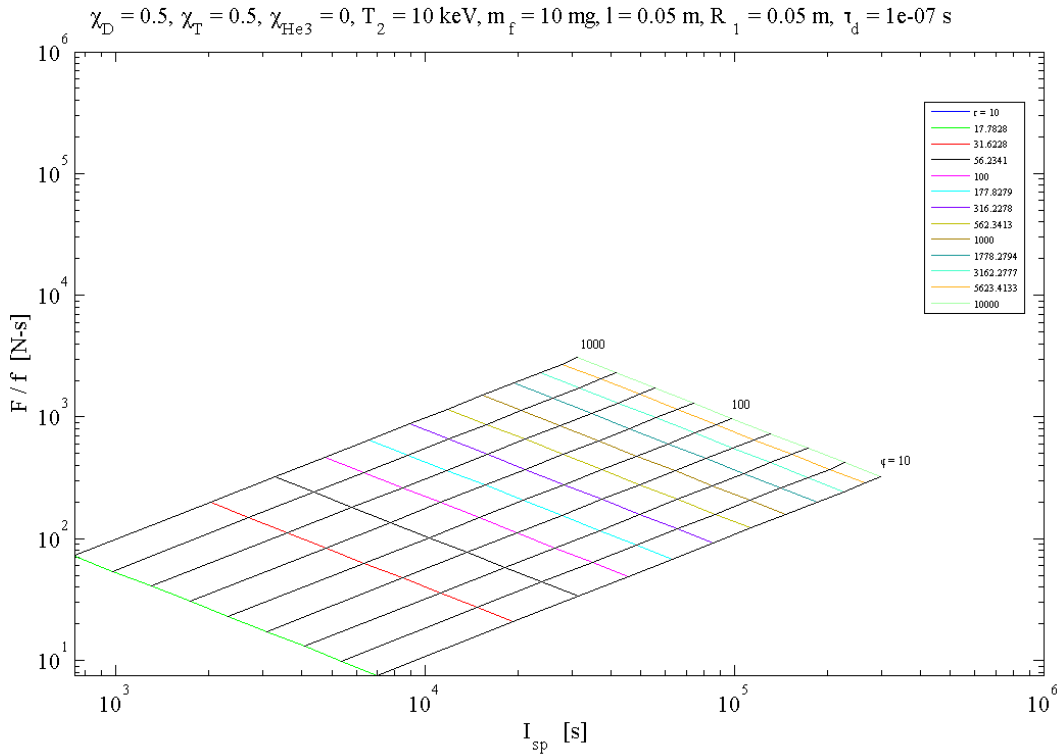


Figure 5.1: Thrust per unit frequency vs. specific impulse for D-T fuel mixture.

for each compression ratio and fractional liner mass. These plots are called “carpet plots,” and they are incredibly useful for defining an initial baseline design based on a set of given mission requirements.

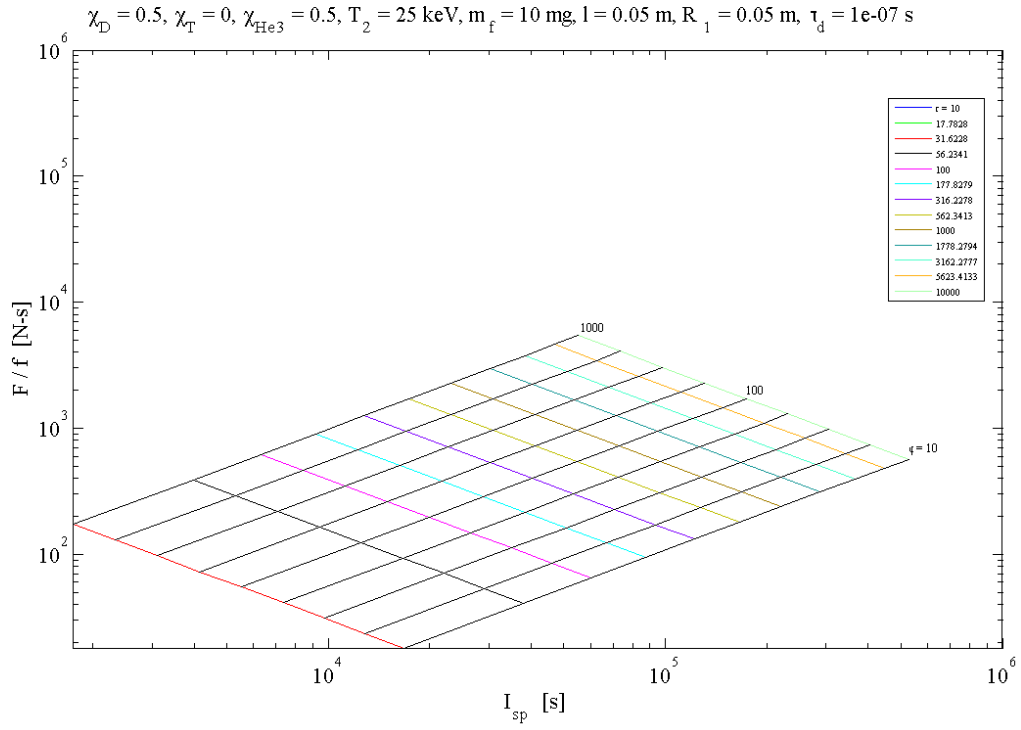


Figure 5.2: Thrust per unit frequency vs. specific impulse for D-³He fuel mixture.

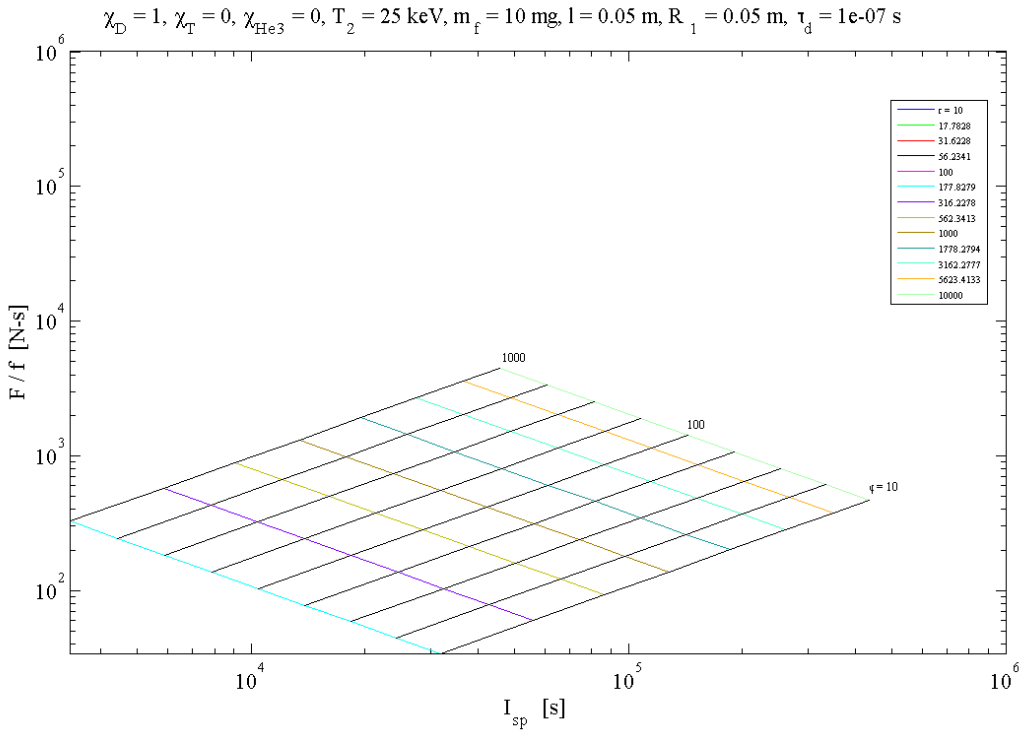


Figure 5.3: Thrust per unit frequency vs. specific impulse for D-D fuel mixture.

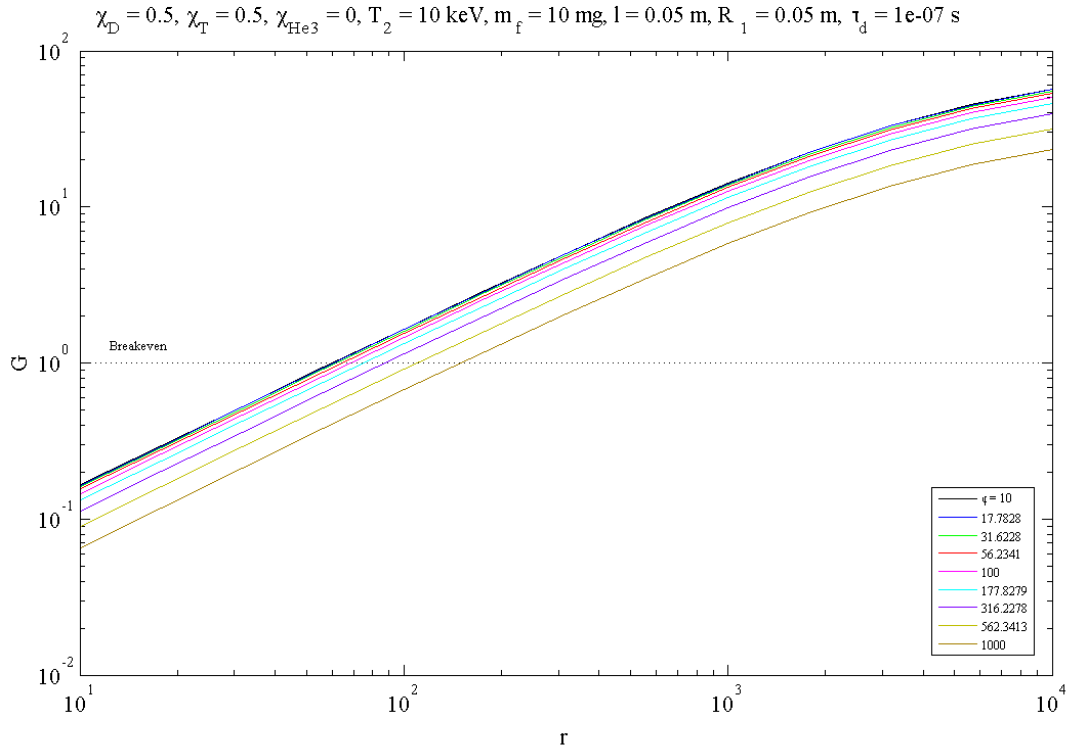


Figure 5.4: Gain curves for D-T fuel mixture.

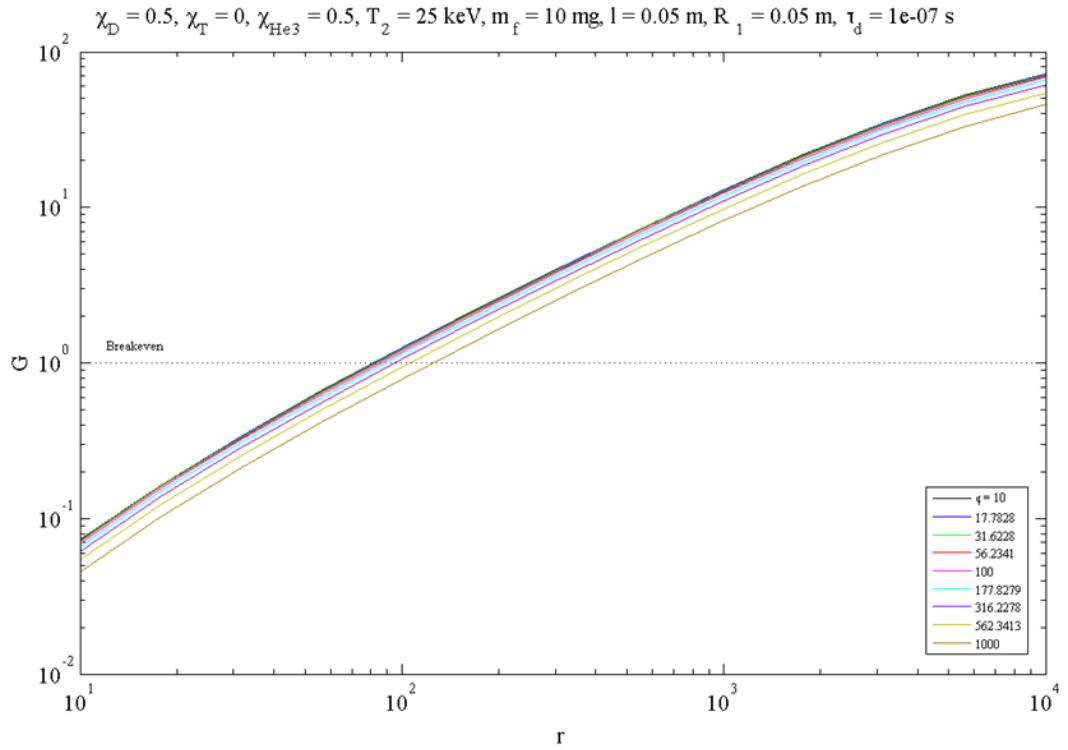


Figure 5.5: Gain curves for D-³He fuel mixture.

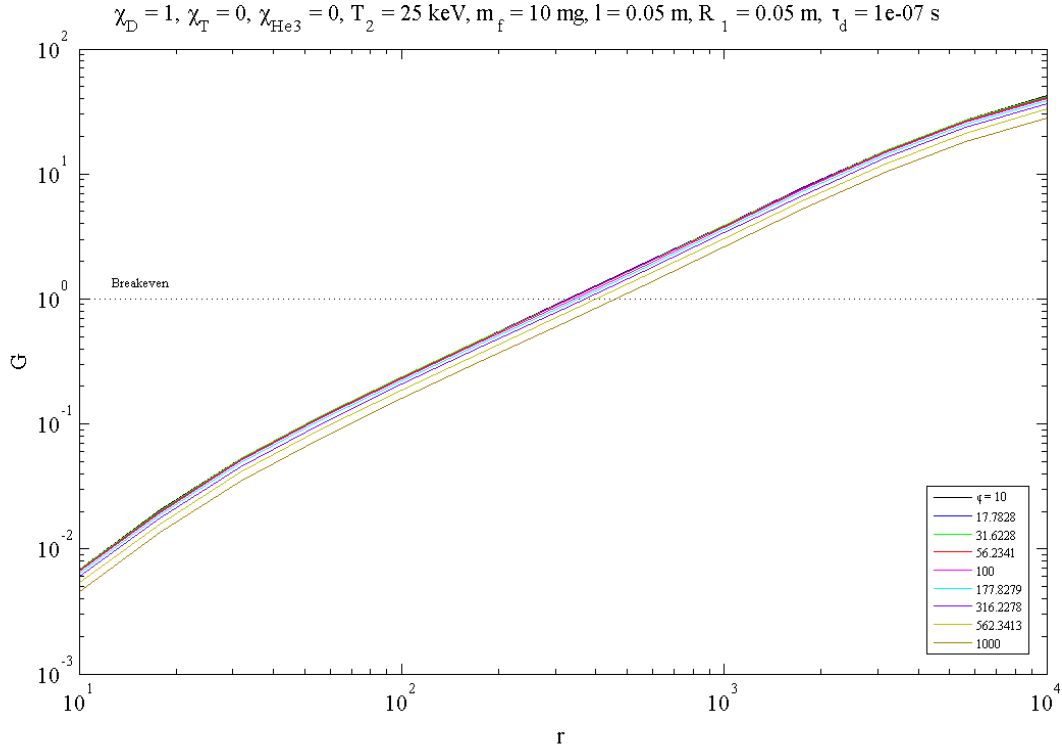


Figure 5.6: Gain curves for D-D fuel mixture.

One will notice that in order to reach breakeven ($G = 1$) for this case, the required volumetric compression ratio, r , is overall lower (<100) for D-T at a given liner mass whereas for D-³He and D-D the required compression ratio is ~ 100 and ~ 400 , respectively. The performance abilities of the system, however, change more subtly for each fuel composition. As expected, the D-³He fuel mixture tends to have a higher range of performance because it is a more energetic reaction. Although this may be true, in this case the D-T and D-D fuel mixtures perform admirably with thrust values at a pulse frequency 10 Hz and $I_{sp} \sim 10000$ s of 2 kN for both fuel mixtures. In the particular case just mentioned, both fuel mixtures require a liner mass 200 times the fuel mass, or 2 g. The difference lies in the volumetric compression ratio required: 100 for D-T and ~ 200 for D-D. For comparison, the D-³He fuel mixture at the same values requires a lower compression ratio of ~ 60 . Note that the required compression ratios for these performance

parameters for the D-³He and D-D fuel mixtures do not quite reach their respective thresholds for breakeven status.

5.5 Case Study II: Performance Results

Referring to Table 5.3 above, the parameter values for this case study were

$T_2 = 10,25$ keV, $m_f = 100$ mg, $l = 0.45$ m, $R_1 = 0.10$ m, and $\tau_d = 100$ ns. The pinch size in this

case is quite a bit larger than what is currently considered “common” in the z-pinch field.

However, z-pinch thruster concepts for deep space propulsion have recently achieved stable system sizes up to 1 meter in length and ~10 cm in diameter [37][27]. Thus, system geometries of this size for space propulsion systems are not altogether unreasonable choices. The carpet plots for the three fuel mixtures are illustrated in Figure 5.7, Figure 5.12, and Figure 5.13 below, followed by the corresponding gain curves for each mixture.

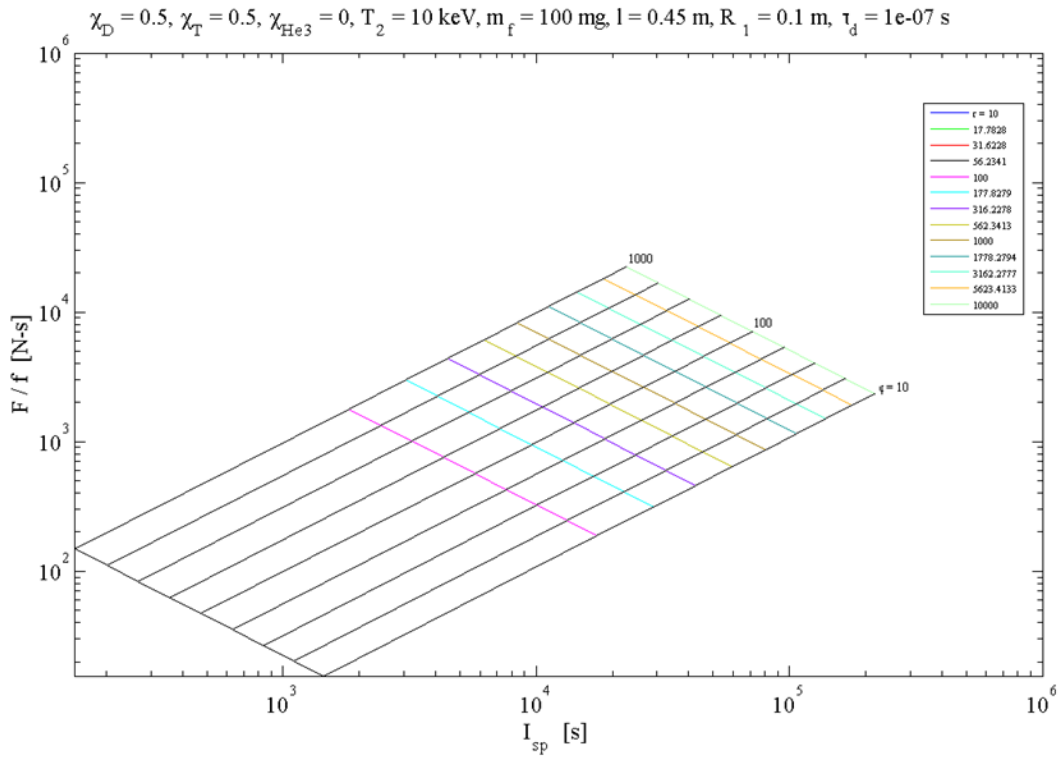


Figure 5.7: Thrust per unit frequency vs. specific impulse for D-T fuel mixture.

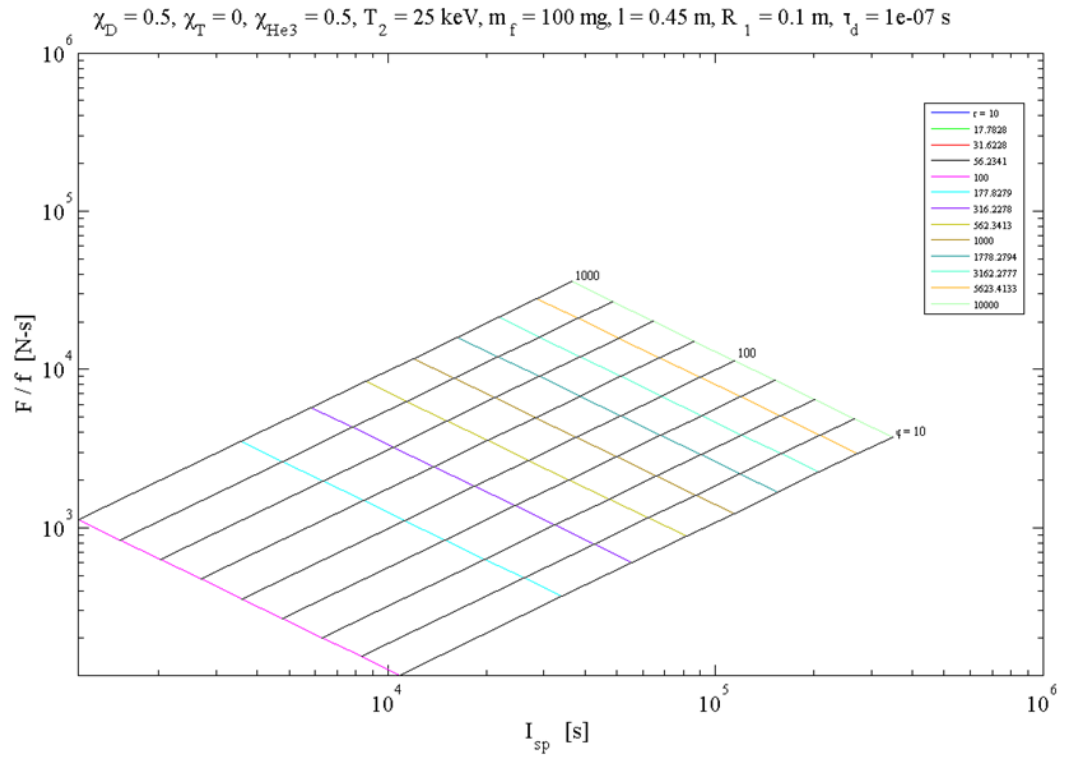


Figure 5.8: Thrust per unit frequency vs. specific impulse for D-³He fuel mixture.

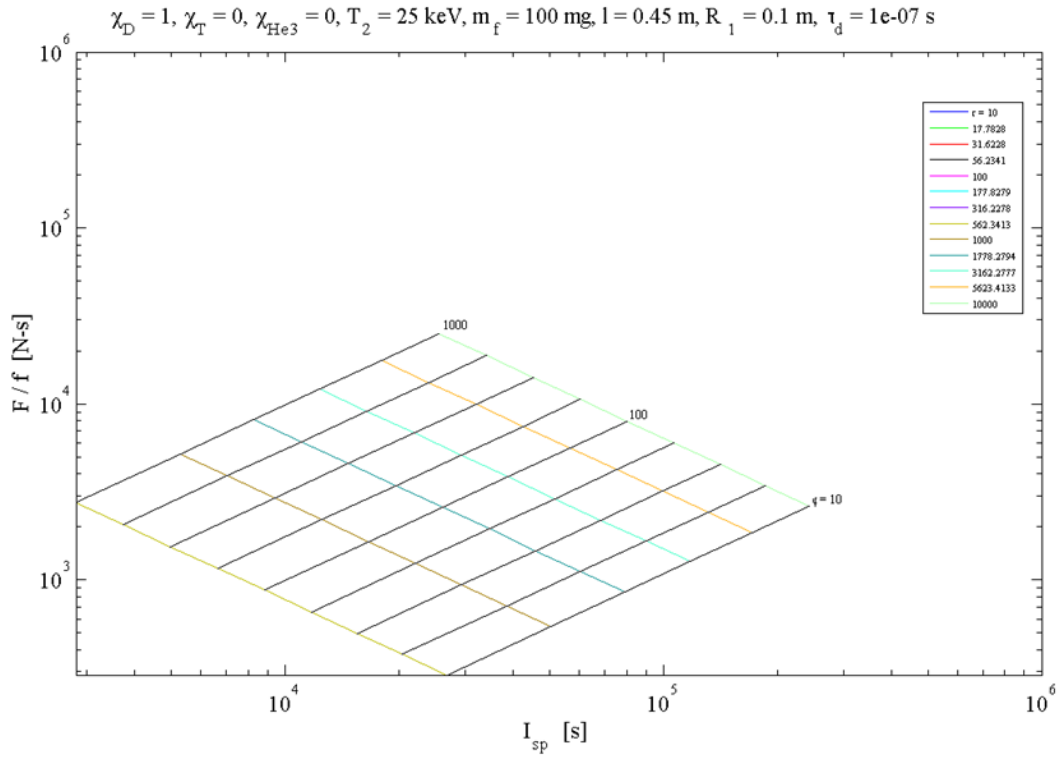


Figure 5.9: Thrust per unit frequency vs. specific impulse for D-D fuel mixture.

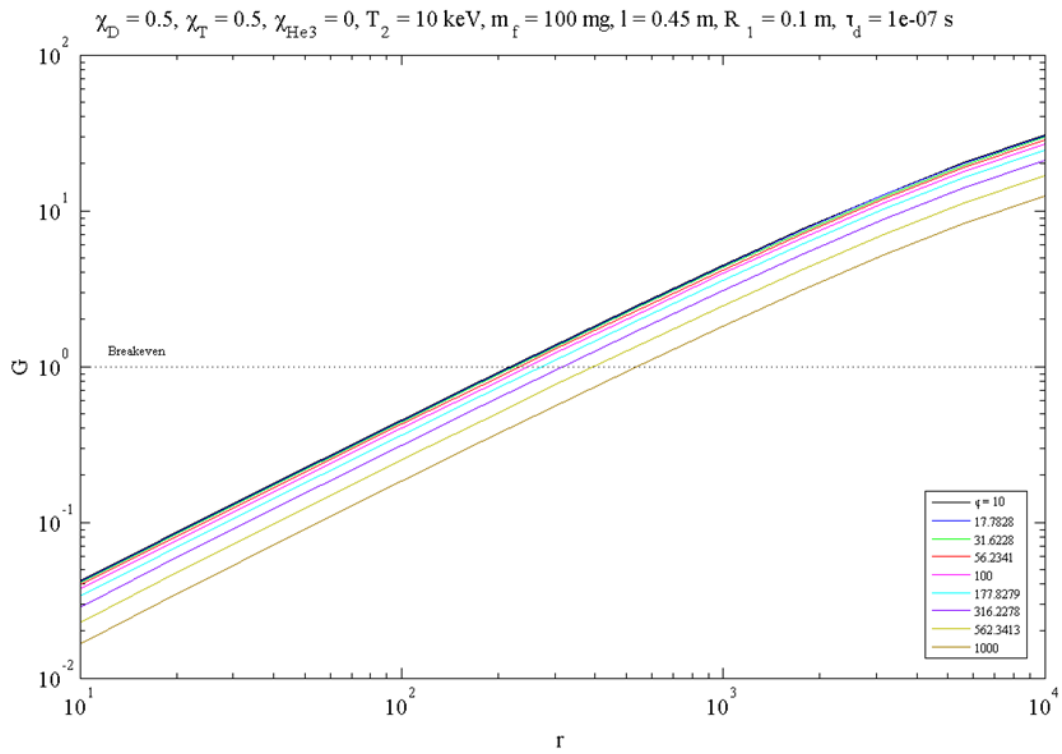


Figure 5.10: Gain curves for D-T fuel mixture.

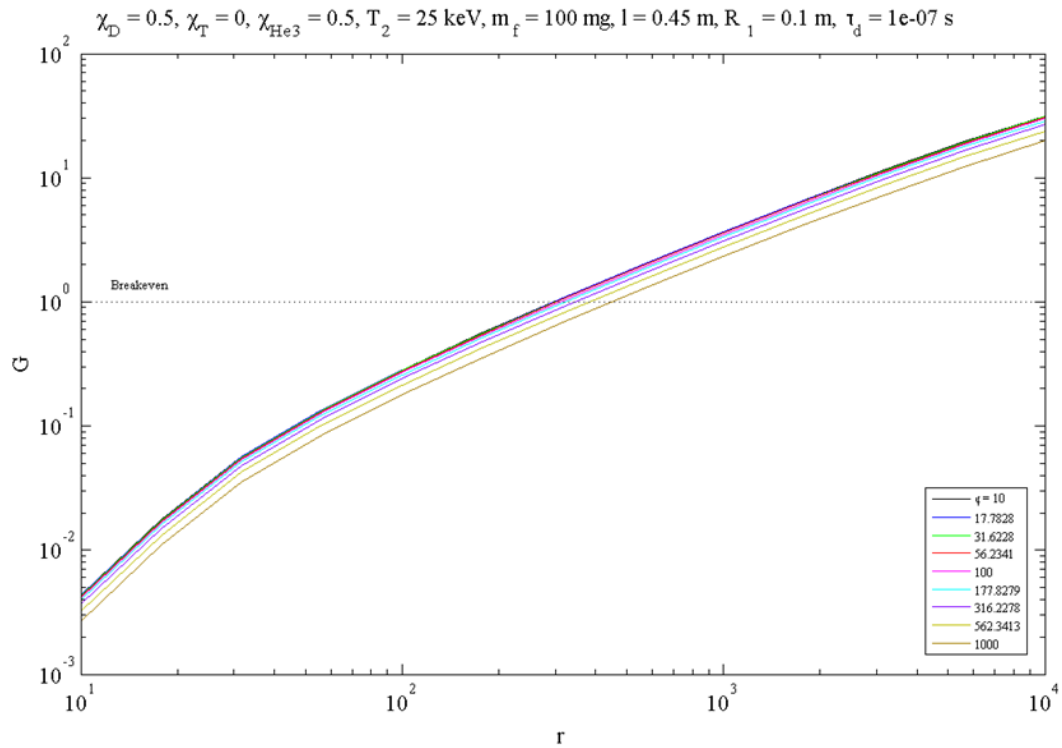


Figure 5.11: Gain curves for D-³He fuel mixture.

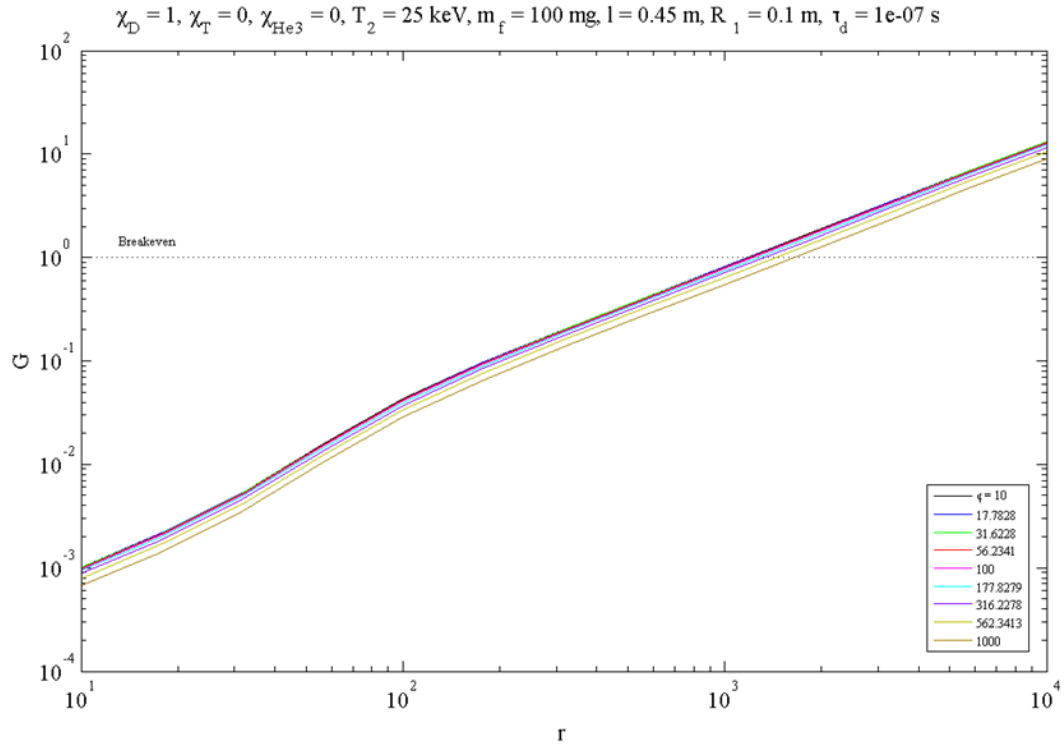


Figure 5.12: Gain curves for D-D fuel mixture.

Here we note that the required volumetric compression ratios for breakeven status for each of the three fuel mixtures are from ~ 200 - 700 for D-T, ~ 300 for D- ^3He , and ~ 1500 for D-D. Examining the same performance parameters from Case I for comparison (pulse frequency 10 Hz, $I_{sp} \sim 10000 \text{ s}$) with a liner mass 200 times that of the fuel mass ($\phi=200$) so that $m_l=20 \text{ g}$, we see that the thrust values for each fuel mixture are $\sim 50 \text{ kN}$, $\sim 70 \text{ kN}$, and $\sim 60 \text{ kN}$ for D-T, D- ^3He , and D-D, respectively. The corresponding compression ratios for each of these thrusts are ~ 200 for D-T, ~ 200 for D- ^3He and ~ 800 for D-D. The only fuel mixture with these particular parameters that could make breakeven status would be the D-T fuel mixture.

The lower compression ratio mentioned above is due to the fact that the temperature required for fusion ignition in the D-T fuel mixture is lower than the ignition temperature required for the other two fuel mixtures. This lower temperature thus necessitates a smaller initial

energy investment to reach ignition. With a smaller initial energy investment comes a smaller work input requirement to reach the ignition temperature at state 2 in the process. Since less work is required to achieve ignition, it follows that the required compression ratio does not need to be quite so high. This also affects the other design parameters of the system as will be seen in the next section.

5.6 Cases I & II: Design Requirements

Here we will examine and compare the system design points that arise from the fusion reaction engine model. Although the design of a fusion propulsion system is much more complicated, this model gives us a method of simplifying the design process by illustrating the qualitative trends and trade-offs that are derived from a given set of mission requirements. In other words, with a starting point such as a desired specific impulse and thrust level, we can narrow down a general system configuration that will further lead to the design points required to build the system, such as the input current required for the compression, driver charging energy, the liner implosion velocity, etc.

5.6.1 Input Current

Below, in Figure 5.13, Figure 5.14, and Figure 5.15, we plot the required input current as a function of compression ratio for cases I & II. Notice that the required current for both cases increases for each fuel mixture from D-T and D-³He to its highest point for D-D. Note also that for D-D the required current remains relatively constant for all compression ratios. The overall trend for the three fuel mixtures in either case shows that the required current, with an assumed transfer efficiency of 80%, tends toward 100 MA, which is an expected result. It is important to recognize, however, that although the current input for a given system takes a specific value here, in a practical setting the current profile is often changed by pulse shaping and thus the current calculated here would be considered the maximum value in such a circumstance.

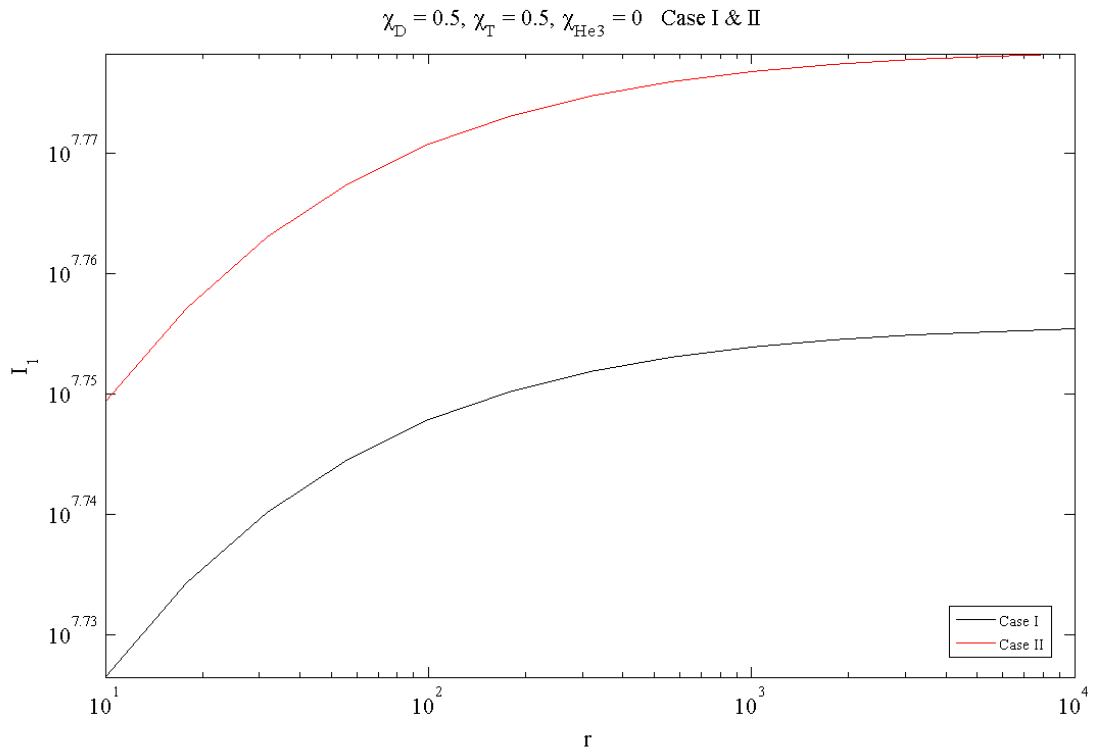


Figure 5.13: Input current required for D-T fuel mixture.

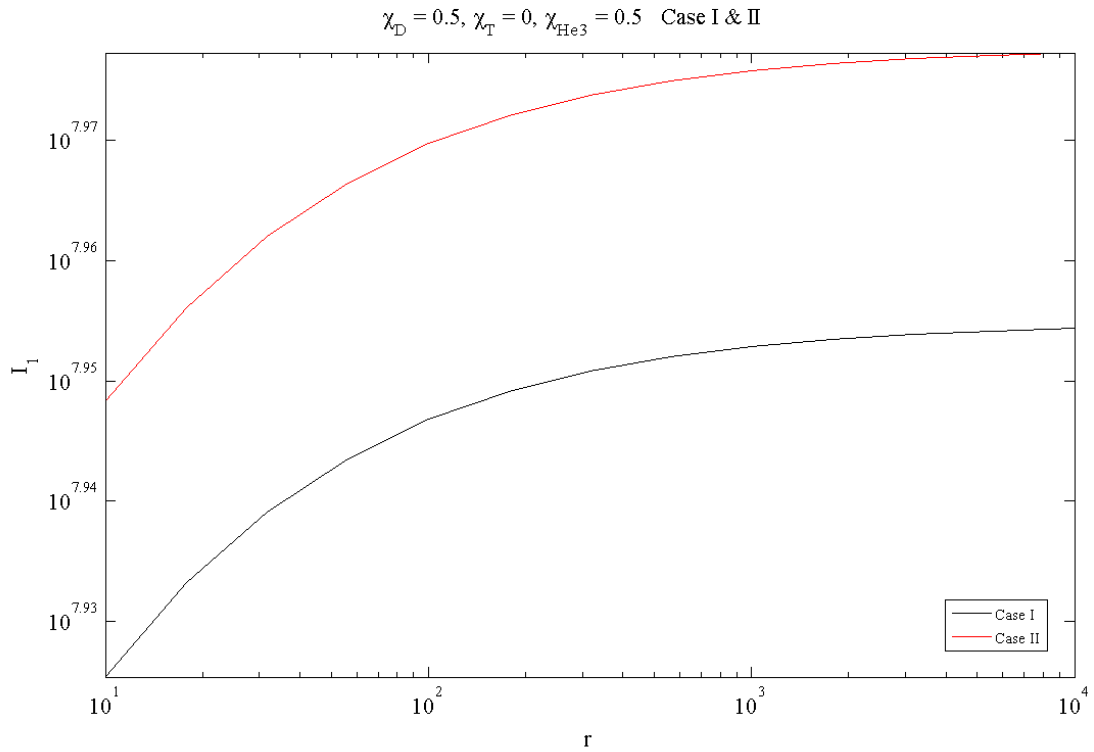


Figure 5.14: Input current required for D-³He fuel mixture.

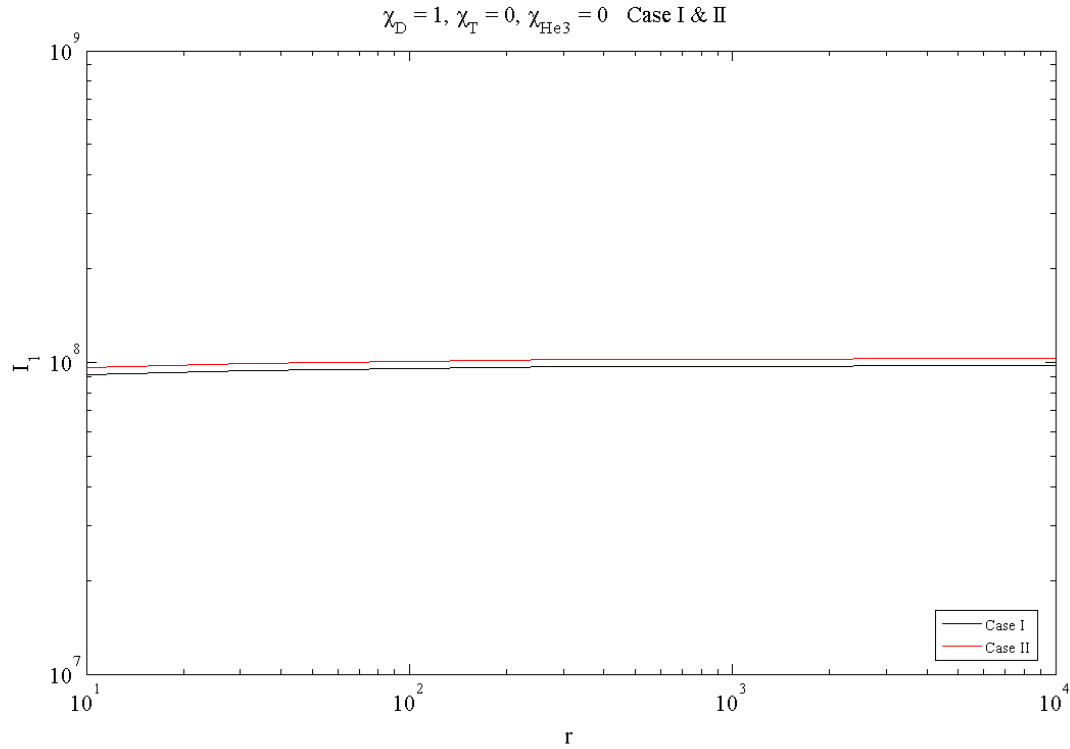


Figure 5.15: Input current required for D-D fuel mixture.

5.6.2 Driver Charging Energy

The required driver charging energies for each fuel mixture are shown in Figure 5.17 to Figure 5.18. For this study it was assumed that the efficiency of the charging circuit to the driver was 80%. This value in any given system can change due to issues such as impedance matching, among other considerations, in the same way that the transfer efficiency of the load circuit can change. Therefore we chose this value for simplicity to remain within the scope of this study. When designing the full propulsion system it will also become important to consider the coupling efficiency of the exhaust plume with the nozzle circuitry, which extracts the energy to charge the driver. For each case it can be seen that the size of the pinch significantly increases the amount of energy required to achieve ignition. The reason for this is mainly due to the change in the amount of work required to compress the plasma for a given compression ratio. Obviously, if the system is larger, then it will take more work at a given compression ratio to achieve the same goal.

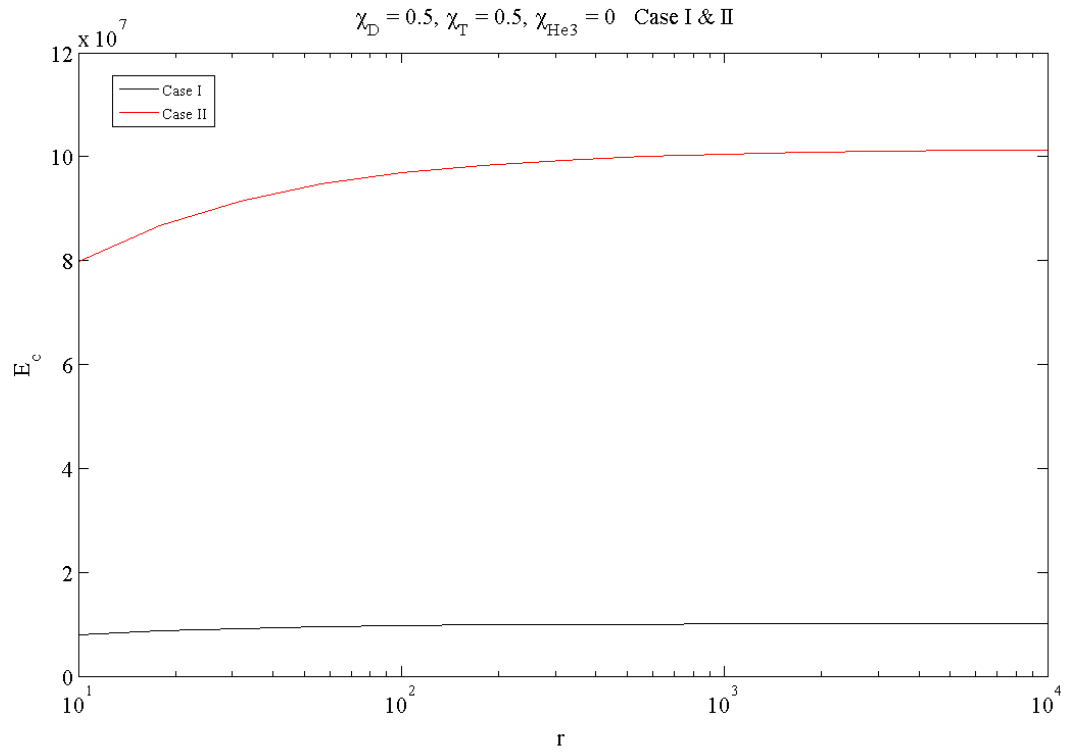


Figure 5.16: Driver charging energy required for D-T fuel mixture.

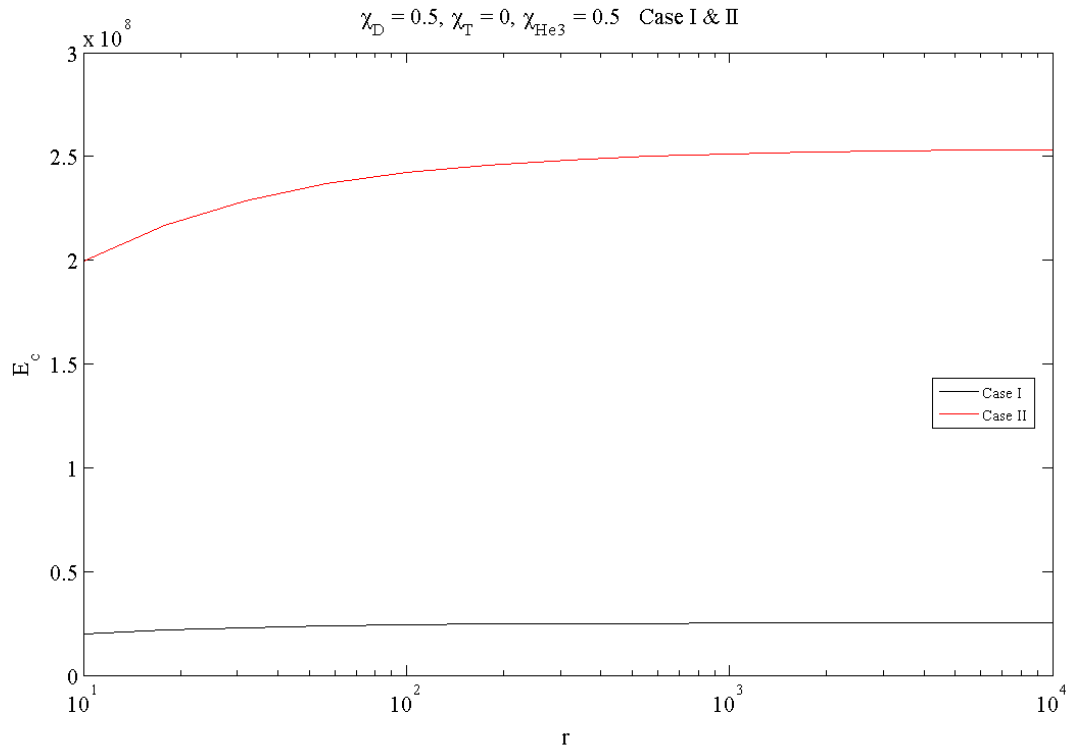


Figure 5.17: Driver charging energy required for D-³He fuel mixture.

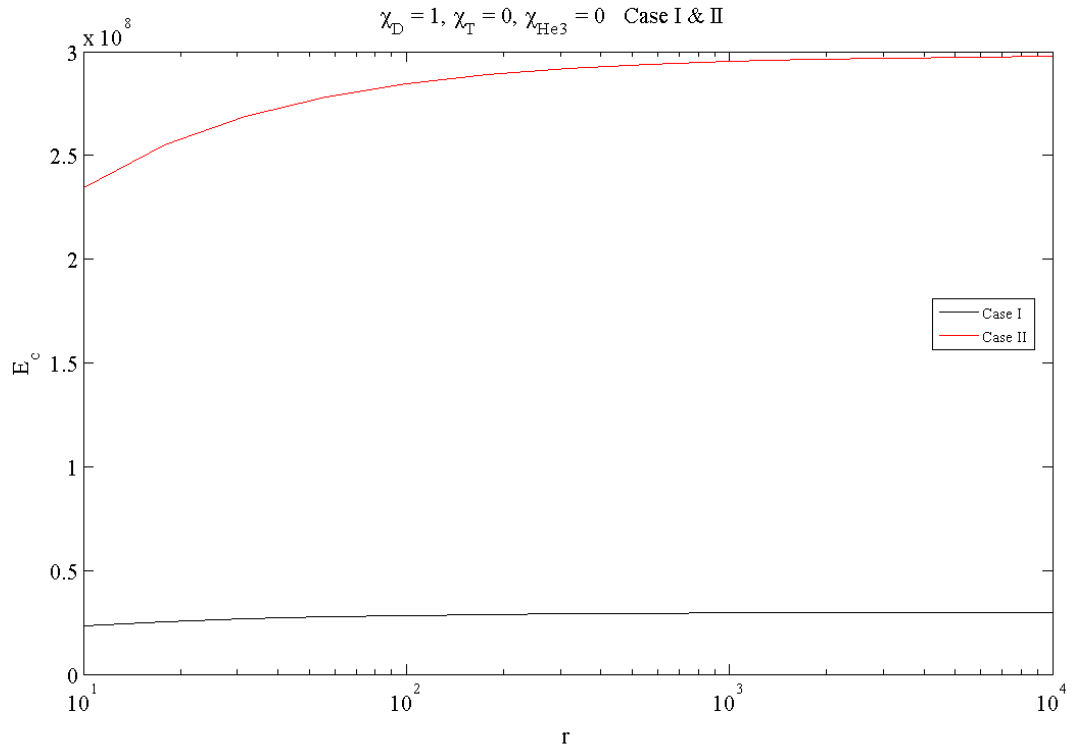


Figure 5.18: Driver charging energy required for D-D fuel mixture.

5.6.3 Liner Velocity

The design of the liner for the z-pinch thruster concept depicted here is more complicated than a simple cylindrical implosion. However, it is useful to have an idea of the required liner velocities that must be achieved for a given system size. In this study, we connect the liner implosion velocity with the exhaust velocity of the system. In doing so, we have a non-dimensional quantity, u_e/v_l , that enables us to back out the magnitude of the liner velocity that is needed for a given exhaust velocity, or specific impulse. Plots of this quantity as a function of compression ratio are shown in Figure 5.20 through Figure 5.21.

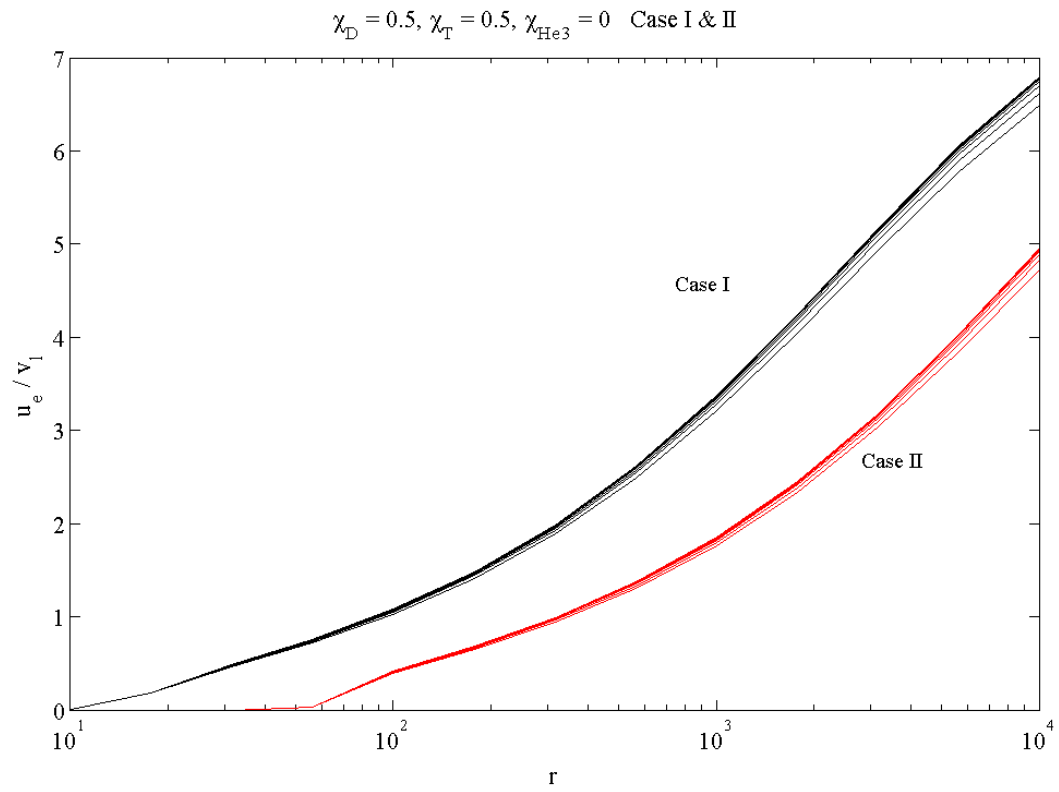


Figure 5.19: Exhaust/liner velocity vs. compression ratio for D-T fuel mixture.

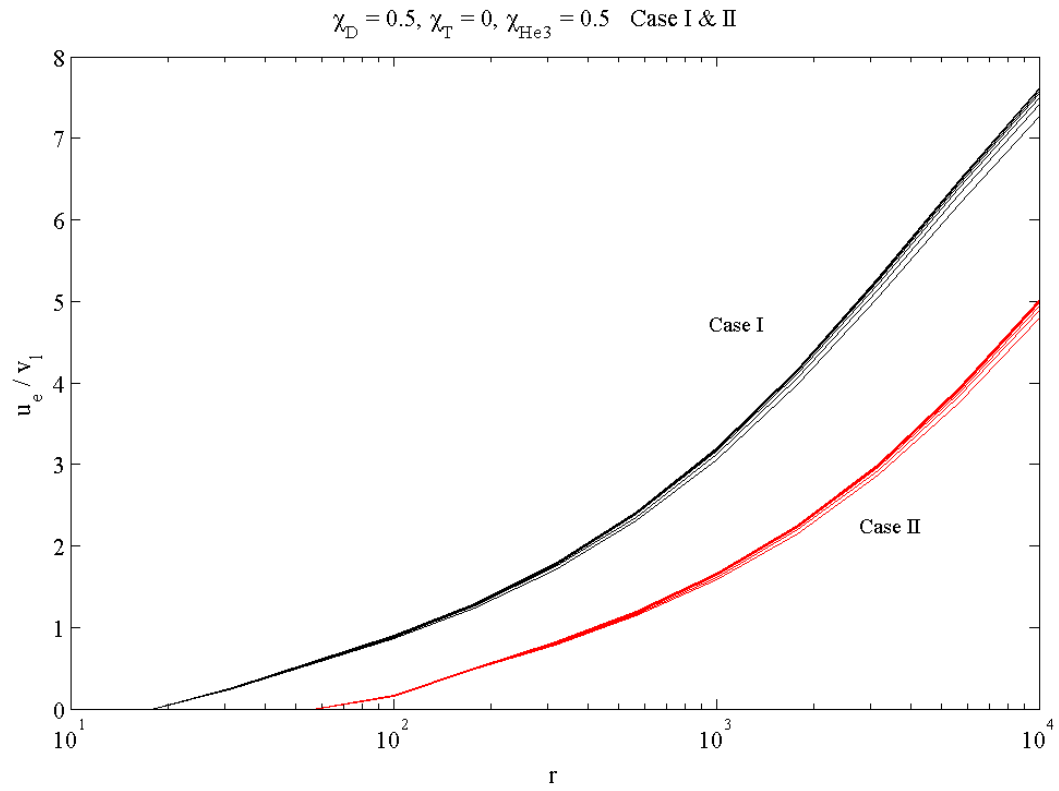


Figure 5.20: Exhaust/liner velocity vs. compression ratio for D-³He fuel mixture.

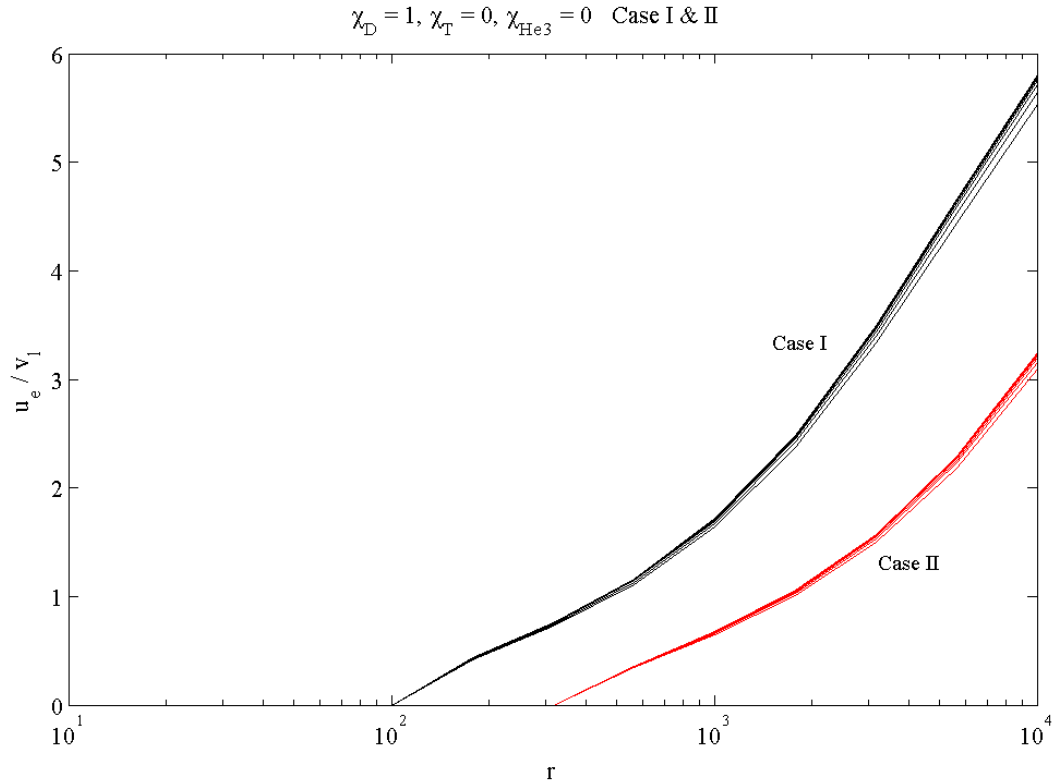


Figure 5.21: Exhaust/liner velocity vs. compression ratio for D-D fuel mixture.

As can be seen in Figure 5.20 through Figure 5.21, the quantity u_e/v_l is unaffected by changes in the fractional liner mass. For this reason, we color-coded the plots for each of the two cases we are studying, which illustrates how the liner velocity required for a given exhaust velocity is independent of the mass of the liner itself. As an example, for a given compression ratio of 200, say, and an exhaust velocity of 10^5 m/s, we would then require a liner velocity for case I of $\sim 6.7 \times 10^4$ m/s for D-T and $\sim 1.43 \times 10^5$ m/s for D-T in case II. For reference, current magnetized target fusion liner experiments have achieved liner implosion velocities exceeding $0.5 \text{ cm}/\mu\text{s}$, or 5000 m/s, although these were at much lower input currents (~ 12 MA) than those being considered here [38].

5.7 Case Study: Z-Pinch Fusion Reaction Engine Vehicle Design

The current state of the art in space propulsion system designs limits human exploration to bodies that are in Earth's vicinity in the inner solar system, with Mars considered as the most challenging destination. Additionally, the long flight times required to travel to other more distant destinations represent higher risk scenarios and are therefore not recognized as ideal missions for human exploration. The reduction of such risk is a high-priority objective to achieve so that human exploration of the outer solar system and beyond becomes viable. The high specific impulse and moderate accelerations possible with the z-pinch fusion propulsion system can enable the faster trip times needed in order to achieve this objective; furthermore with payload mass fractions similar to those predicted for state of the art chemical missions to Mars.

The benefits of developing z-pinch thruster technology can best be evaluated by characterizing its performance against potential missions of interest, a standard set of which has been offered in a 2004 AIAA special report title "Recommended Design Practices for Conceptual Nuclear Fusion Space Propulsion Systems" [39]. These missions are as follows:

1. Piloted Mars round trip, 150 mt total useful payload to Mars, total round trip transit time ≤ 6 months (not including planet stay time).
2. Piloted Jupiter round trip, 150 mt total useful payload to Jupiter, total round trip transit time ≤ 3 years (not including planet stay time).
3. Robotic mission to flyby a distance 550 AU from the sun, 150 mt useful payload, ≤ 35 year one-way trip time.

For the purposes of this thesis we will examine the first mission and the design requirements therein.

The design point chosen for this vehicle was a medium-thrust system with a pulse frequency of 10 Hz, D-T fuel mass of 100 mg, $I_{sp} \sim 28000$ s, and a thrust requirement of 55 kN.

With a pinch length of 1 m and radius of 10 cm (0.1 m) we refer to Figure 5.22 to estimate the required compression ratio of ~ 3500 , which corresponds to a linear compression ratio (R_1/R_2) of ~ 59.1 . From the gain curves in Figure 5-23 we see that this volumetric compression ratio corresponds to a gain of ~ 7.5 , which is excellent.

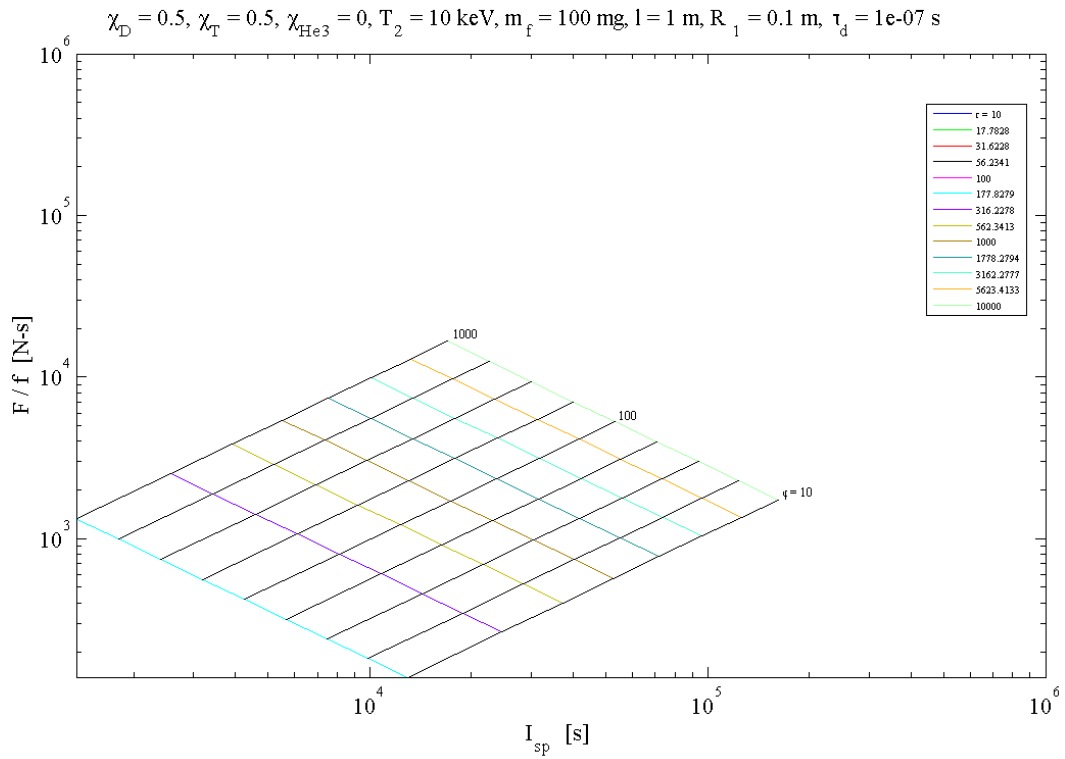


Figure 5.22: Thrust per unit frequency vs. specific impulse for NASA design study.

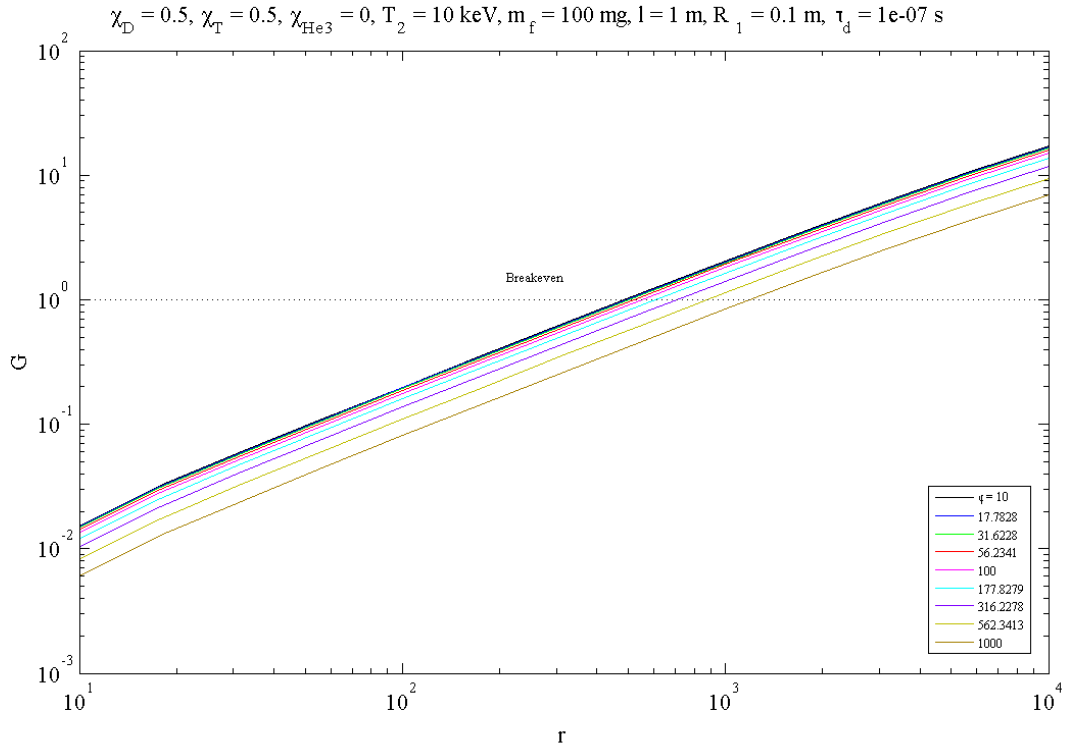


Figure 5.23: Gain curves for NASA design study.

Knowing the basic design points of the vehicle we can then examine the other design requirements such as the input current and liner velocity. For these design points we refer to Figure 5.24 and Figure 5.25 where we see that the required input current is $\sim 40 \text{ MA}$ and the required liner implosion velocity can be approximated from $u_e/v_l \sim 2.4$ as $v_l \sim 11.6 \text{ km/s}$ or 11600 m/s . Using the plot in Figure 5.26 we see that the driver charging energy required (assuming a charging efficiency of 80%, as before) can be estimated at $\sim 100 \text{ MJ}$.

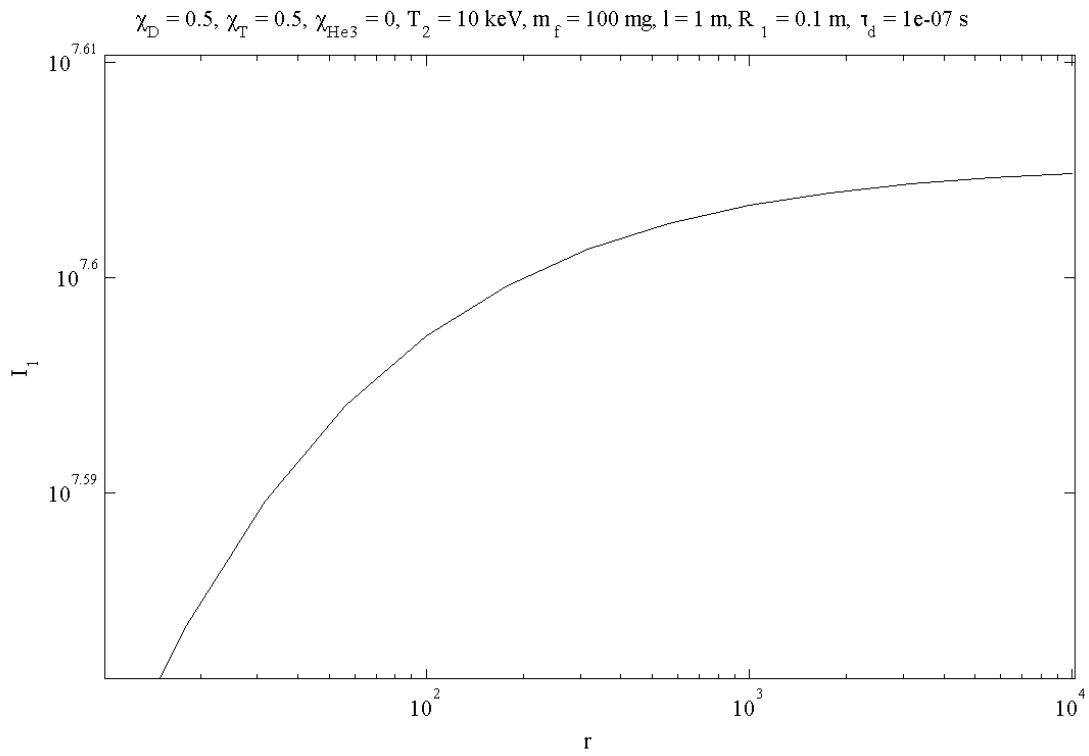


Figure 5.24: Required input current for NASA design study.

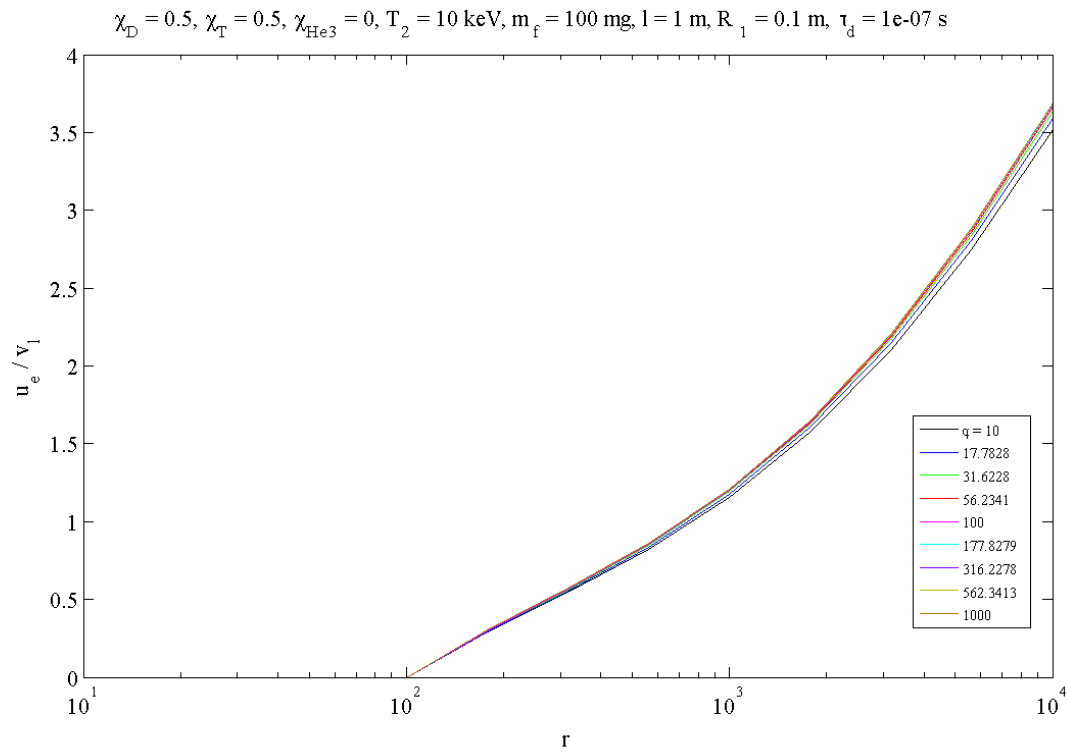


Figure 5.25: Exhaust/liner velocity vs. compression ratio for NASA design study.

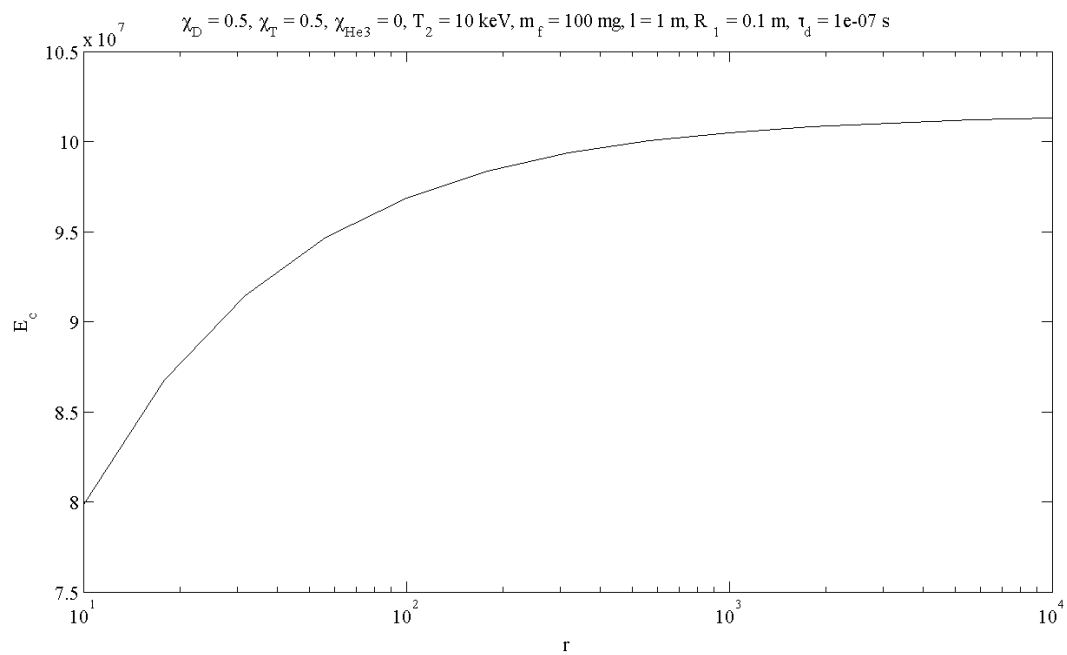


Figure 5.26: Charging energy required for NASA design study.

Chapter 6

Conclusions

6.1 Model Performance

From the cases depicted in Chapter 5 and the results considered therein, we may draw some important conclusions. First, the overall performance of a pulsed fusion reaction engine is heavily influenced by changes in the system geometry or configuration. This fact, in and of itself, is not surprising since the system size necessarily determines the work requirements to achieve fusion ignition. Second, due to the large range of parameters, the z-pinch system is highly configurable for multiple sets of mission requirements. In other words, for a given mission such as a routine trip to Mars, there is a wide array of design possibilities for this engine type that can accommodate different payload sizes, crew sizes, and trip times. We can draw this conclusion from the model depicted here based on the implications of our first conclusion: changes in system geometry, for example, have a large effect on the performance of the system. This in turn means that for a given thrust and specific impulse requirement there are multiple engine sizes and therefore propulsion system masses that can be utilized to accommodate changes in payload mass fraction or the number of crew members sent on the mission. Third, changes in the fuel composition affect the overall range of the system's performance, depending on the reactivity of the fuel mixture. The full effect of this point can be seen by comparing the size of the carpet plot for a D-T fuel mixture (see Figure 5.1, for example) with that of the corresponding carpet plot for a D-³He fuel mixture (Figure 5.2). Finally, as a direct consequence of the previous conclusion, we see that the difference between D-T and D-³He fuel mixtures (e.g., in Cases I and II) arises in the specific impulse. The higher specific impulse of the D-He³ fuel has a higher energy cost,

which will affect the driver energy storage size thus affecting the vehicle mass and payload mass fraction.

In addition to the previous conclusions, we also remark that design points illustrated by previous studies are also comparable to those produced by this analysis model. For example, Drake et al. [40] note that for a radial compression ratio of 10 (which corresponds to a volumetric compression ratio of 100 in cylindrical geometry) and an initial liner radius of 1 cm and length of 3 cm requires initial plasma energies of ~ 1 kJ and currents of ~ 5 MA to achieve a system with gain $G > 1$. In our model, the initial plasma energies required are of the same order, as well as the input currents required. Indeed, by scaling up from a volumetric compression ratio of 100 to one of 1000 (radial compression of ~ 33), the increase in system design requirements increases by one order of magnitude.

Although we have not considered design points from every previous study in the fusion propulsion community, the trends in system performance as a function of independent parameters like the compression ratio are found to be similar (to within an order of magnitude) to multiple study results in the MIF community. Indeed, even the most pessimistic studies of the MIF liner implosion concept have found that system gains greater than 1 are possible at driver energies as low as 20 MJ [41]. A full study of the comparison of results from this parametric model with those of other previous studies is not included here. However, we remark that this is indeed an important task to be completed in future work related to this design study.

6.2 Model Development & Future Work

This thesis is meant to be the beginning of a project with a much larger scope than what could be depicted here. The narrow focus of this particular study is meant to illustrate a straightforward design process that can be used to design the basic components of pulsed fusion reaction engines using a z-pinch geometry. As noted previously, the usefulness of parametric

cycle analysis is evident when looking to an abundant field such as the design of turbojets. It also comes as somewhat of a surprise that this method of analysis and design has not been applied to more advanced systems in order to compare, analyze, and develop them based on similar design points. Although the field of nuclear fusion propulsion is not quite as prevalent as that of gas turbine generator design, it is still surprising that there is no generalized process set forth for the design of these systems rooted in simple thermodynamic models. For all of the different fusion propulsion systems in existence today there is a one-to-one correspondence to the design methods used to analyze each specific engine. This makes it incredibly difficult to compare any of these systems with any level of objectivity or accuracy.

In an attempt to remedy this problem, this thesis serves as a starting point to develop this process for multiple fusion propulsion systems. We attempt here to enumerate the generic design process based on the thermodynamic Otto cycle followed by applying this process to a specific confinement method: the z-pinch. As presented above, the class of pulsed fusion confinement systems can be described using the same thermodynamic arguments that describe internal combustion engines. From the results presented in Chapter 5, we see that the performance of the z-pinch confinement scheme in this context is admirable and well suited to interplanetary travel throughout the solar system, perhaps even an interstellar precursor mission. With the multitude of changeable parameters and fuel mixtures there was not enough time or space within the scope of this project to investigate the many permutations that are possible with this system. However, it can be seen from the results presented that there are multiple ways that one can change the system (e.g., size, fuel mixture, liner mass, pulse frequency, etc.) that will enable a corresponding multitude of possible missions to be accomplished.

6.2.1 Liner Properties

For the purposes of the discussion promulgated here, there were other parameters that were not specifically investigated in this study that were nonetheless included in the model for

future use. One of these parameters that will become important in the future is the composition of the liner itself. In addition to the mass the liner adds to the exhaust for better thrust values (higher mass flow rate) we neglect to include the reactivity of the lithium liner with the fusion fuel and the fusion reaction products. Some of the possible reactions are numbers 6, 7a, 7b, 8, 10, and 11 shown in Table 1.1.

The reason these reactions will become important is that there will be much larger releases of energy once the plasma is compressed by the liner and the fuel, fusion products, and liner material have a chance to react, thus releasing even more energy adding to the overall useful work from the exhaust plume. This in turn enables higher gain values and thus better overall performance from the thruster, i.e. higher thrust, specific impulse, etc. By including these reactivities and enabling the composition of the liner to be changed, we create another parameter that can be modified to improve or adjust the propulsion system's performance for a given set of mission requirements.

6.2.2 Inductively Coupled Geometries: The θ -Pinch

Theta pinch experiments have been performed in different laboratories since the 1960s. The studies have encompassed diverse phenomena including: field annihilation and the resultant heating, axial contraction, tearing instability, $n = 2$ rotational instability, and various formation techniques. Early work reported from Los Alamos Scientific Laboratory (LASL) was primarily concerned with heating rather than with confinement. Comparison of negative, zero, and positive bias field experiments, showed that the negative bias field cases produced the largest neutron yields [43][40]. Axial contraction to an equilibrium profile and the destructive rotational instability are the typical characteristics found in most field-reversed experiments.

In the context of the study presented in this thesis, translation of the plasma from the formation region is a fundamental feature of a fusion reactor embodiment and thus becomes important when considering the design of a propulsion system based on the same concept. The

successful translation and capture of a FRC is the current objective of multiple experiments. Of note is the Field-Reversed configuration eXperiment with a Liner (FRX-L) at Los Alamos National Laboratory [6].

A FRC is an elongated prolate (cigar shaped) compact toroid (CT) formed without any toroidal field [43]. The basic structure of a FRC consists of two primary regions: a sheath outside what is called the separatrix with open field lines, and a torus inside the separatrix with closed field lines. The configuration was discovered by accident through theta pinch research when a bias field was applied in the reverse direction relative to that of the main magnetic field causing the plasma to turn “inside-out.” Formation of a FRC was shown to be possible through means other than the field reversed theta pinch method, such as rotating magnetic fields or a coaxial geometry. Generally, the majority of FRC research involves the theta pinch method.

The FRC offers many potential advantages as an MTF target plasma, including the promise of robust, closed flux surfaces that maintain their topology during compression, as has been observed in compression, translation, stability experiments, and models [6]. Efficient FRC translation has been demonstrated previously as well, and this is one of the most appealing features of CTs. Indeed, there are multiple models that have successfully described this phenomenon. In particular, Intrator et al. have shown that translation may be described using an adiabatic scaling model [44]. In many different conditions, FRC translation and trapping has been accomplished without any loss of confinement in the plasma. It is precisely this ability that prompts the further interest of using FRCs in propulsion research.

The parametric design method presented in this thesis is particularly useful when considering the more complex requirements of propulsion systems that are based on the FRC translation concept. One of the next steps to be taken with this model will be its application to this confinement method. The difficulties that could arise in doing so will more than likely be in

the description of the translation of the FRC, which occurs simultaneously with the compression. The ability to track the kinetic energy of the plasma while it is compressed and translates through a “burn region” will prove to be challenging, but not altogether impossible. The preliminary work for this stage of development of the model has already been performed, and the physics of such a concept has been investigated in multiple studies throughout the fusion community [45][46].

6.3 Final Thoughts

It is important to recognize the role that space propulsion will play in the future of humankind, and, in addition, the unequivocal role these technologies play in the minds and imaginations of those select individuals who see the vastness of space as opportunity rather than mere curiosity. Modern technological development encourages such a viewpoint in that, at our current state of development, we as a civilization are more than capable of pursuing such an endeavor with great boldness and a minimum of trepidation.

In the pursuit of such goals it becomes of great importance to enable our enterprise to thrive without being caught up in the tedium of having to re-create the basis from which we compare and analyze systems and designs each time a new set of mission requirements is set forth. This is not only undesirable; it is odious when one sees the extent to which the aviation industry has developed from its humble beginnings so long ago. The same explosive development is possible in the space industry once the community realizes the desideratum of raw resources can be provided in abundance by even the closest locations in the solar system, such as the moon, Mars, or the asteroid belt. In the cogitative words of Dr. Harrison H. Schmitt, the last man to have stepped on the moon:

As we reach toward the Moon and its resources, the development of fusion technologies will open new business opportunities in medical diagnostics and treatment, weapons detection, destruction of nuclear waste, and clean electrical power generation. Longer term, ancillary businesses will be possible because of low-cost access to space required to meet the demands of lunar resource acquisition. These additional business opportunities include providing services to the government for lunar and planetary exploration and science, national defense, and long-term on-call protection from asteroids and comets. Space and lunar tourism will also be enabled by the existence of such capabilities in the private sector [47].

It is the humble hope of the author that this work will provide an impetus to surpass the self-inflicted boundaries of the advanced propulsion community as a whole by pointing out the possibilities of the simple design process that is known so well to the aviation community and how this process is applicable to a much broader range of vehicles and technologies.

APPENDICES

APPENDIX A

Z-PINCH CYCLE SCRIPT: GO.M

```

%R. Cortez
%
%Script:  go.m
%
%This script sets up all loops to iterate through parameter space for
the
%Fusion Reaction Engine Cycle: Z-Pinch analysis. It calls the following
%functions (listed in the required syntax):
%
%       1. [input, properties] = in(X_D, X_He3)
%       2. [z] = zcycle(input, properties)
%
%Where X_D, X_He3 are the Deuterium and Helium-3 mole fractions,
%respectively. Function 1 returns two structures: input & properties;
these
%structures are set up to contain all the input values and fuel/liner
%properties required to run the analysis. See the help file for in.m
for
%the structure details.
%The script then inputs the two structures from 1 into the zcycle
function,
%which outputs a structure containing the calculated performance data,
%which is then stored in a 5-D structure array with fields containing
the
%input parameters for each particular case and each performance
parameter
%output by the model. This structure is then saved as a '.mat' file for
%future use.
%
%NOTE: The input structure for the zcycle function will be set up
%differently from the one built in the input function in.m. This is
because
%the zcycle function is not set up to use vectors for the input
properties.
%The computer runs out of memory very quickly if this function is
%vectorized.
%
%UPDATE (5/17/11): The input structure for the zcycle function is now
set
%up such that the compression ratio is input as a vector. The zcycle
%function is vectorized to handle this and the fractional liner mass so
%that the output structure gives performance values (e.g., ue, Isp) as
%arrays of size [phi,r].
%
%-----
----
%REACTIONS:
%
%(a = alpha)
%
%       Reaction  1: d(d,n)he3           Reaction  2: d(d,p)he3
%       Reaction  3: t(d,n)a - 10        Reaction  4: t(d,n)a - 11
%       Reaction  5: t(t,2n)a           Reaction  6: he3(d,p)a -
10
%       Reaction  7: he3(he3,2p)a        Reaction  8: he3(t,d)a -
10

```

```

%      Reaction  9: he3(t,n+p)a          Reaction 10: li6(d,a)a -
10
%      Reaction 11: li6(d,n)be7 - 10     Reaction 12: li6(d,p)li7 -
10
%      Reaction 13: li6(he3,d)be7 - 10   Reaction 14: li6(he3,p+a)a
%      Reaction 15: li6(n,tot)           Reaction 16: li6(p,he3)a -
10
%      Reaction 17: li7(n,tot)
%-----
----

%-----
----

%FUEL MIXTURE COMPOSITION
%Mole fraction of tritium component is determined based on the set
values
%of X_D and X_3He.

X_D    = 0.5;
X_He3  = 0.0;

%-----
----

%-----
----

%LINER MIXTURE COMPOSITION

X_Li    = 0.0;
X_Li6   = 1.0;
X_Li7   = 0.0;

%LINER THICKNESS
delta   = 0.01; %meters

%-----
----

%Load reaction rate data calculated from ENDF database
ddnhe3   = load('rxn1_sigv.mat');      %ddnhe3
dtna     = load('rxn3_sigv.mat');      %dtna
dhe3pa   = load('rxn6_sigv.mat');      %dhe3pa

%Energy units
J = 1;
MJ = J/1e6;
kilotons = J/4.184e12;
handgrenades = kilotons*1000*2000*.4536/.15;
littleboys = kilotons/15;
fatmans = kilotons/20;

%-----
----

%Run input function to set up and initialize parameter space

```

```

[input, properties] = in(X_D, X_He3, X_Li, X_Li6);

X_T = properties.t.X;

%-----
----
%Intialize parameter space

T2kev = input.T2kev;           %[4x1]
mf     = input.mf;             %[3x1]
L      = input.l;             %[6x1]
R      = input.R1;            %[4x1]
taud   = input.taud;          %[4x1]
r      = input.r;             %[100x1]

taui   = input.tau;           %[50x1]

%Initialize timing arrays
telapse1 = 0*T2kev;
telapse2 = 0*mf;
telapse3 = 0*L;
telapse4 = 0*R;
telapse5 = 0*taud;
telapse6 = 0*r;

%Initialize structures and arrays

ue      = zeros(length(properties.liner.phi),length(r));
Isp     = 0*ue;
F_f     = 0*Isp;
P_f     = 0*F_f;
v12_T2 = 0*P_f;
ue_v1   = 0*v12_T2;

G       = 0*r;
W12     = 0*G;
W34     = 0*W12;
Efus    = 0*W34;
etaP    = 0*Efus;
etaT    = 0*etaP;
etaO    = 0*etaT;
etat    = 0*etaO;
fb      = 0*etat;
nn      = 0*fb;
En      = 0*nn;
Ec      = 0*En;
I1      = 0*Ec;

z(length(T2kev),length(mf),length(L),length(R),length(taud)).T2 =
[];

```



```

z(length(T2kev),length(mf),length(L),length(R),length(taud)).mf      =
[];
z(length(T2kev),length(mf),length(L),length(R),length(taud)).l      =
[];
z(length(T2kev),length(mf),length(L),length(R),length(taud)).R1    =
[];
z(length(T2kev),length(mf),length(L),length(R),length(taud)).taud   =
[];
z(length(T2kev),length(mf),length(L),length(R),length(taud)).ue     =
ue;
z(length(T2kev),length(mf),length(L),length(R),length(taud)).Isp    =
Isp;
z(length(T2kev),length(mf),length(L),length(R),length(taud)).F_f    =
F_f;
z(length(T2kev),length(mf),length(L),length(R),length(taud)).P_f    =
P_f;
z(length(T2kev),length(mf),length(L),length(R),length(taud)).G      =
G;
z(length(T2kev),length(mf),length(L),length(R),length(taud)).W12    =
W12;
z(length(T2kev),length(mf),length(L),length(R),length(taud)).W34    =
W34;
z(length(T2kev),length(mf),length(L),length(R),length(taud)).Efus   =
Efus;
z(length(T2kev),length(mf),length(L),length(R),length(taud)).etaP   =
etaP;
z(length(T2kev),length(mf),length(L),length(R),length(taud)).etaT   =
etaT;
z(length(T2kev),length(mf),length(L),length(R),length(taud)).etaO   =
etaO;
z(length(T2kev),length(mf),length(L),length(R),length(taud)).etat   =
etat;
z(length(T2kev),length(mf),length(L),length(R),length(taud)).fb     =
fb;
z(length(T2kev),length(mf),length(L),length(R),length(taud)).nn     =
nn;
z(length(T2kev),length(mf),length(L),length(R),length(taud)).En     =
En;
z(length(T2kev),length(mf),length(L),length(R),length(taud)).Ec     =
Ec;
z(length(T2kev),length(mf),length(L),length(R),length(taud)).I1     =
I1;
z(length(T2kev),length(mf),length(L),length(R),length(taud)).vl2_T2  =
vl2_T2;
z(length(T2kev),length(mf),length(L),length(R),length(taud)).ue_vl  =
ue_vl;

```

```

%-----
%-----

```

```

%Set up loops to run through analysis through entire parameter space

```

```

for tt = 1:length(T2kev)

```

```

    tstart1 = tic;
    T2k = T2kev(tt);

```

```

disp(['T2k = ' num2str(T2k)]);

var1 = genvarname(['T2' num2str(tt)]);

for mm = 1:length(mf)

    tstart2 = tic;
    mfk = mf(mm);
    disp(['mfk = ' num2str(mfk)]);

    var2 = genvarname(['mf' num2str(mm)]);

    for ll = 1:length(L)

        tstart3 = tic;
        lk = L(ll);
        disp(['lk = ' num2str(lk)]);

        var3 = genvarname(['l' num2str(ll)]);

        for RR = 1:length(R)

            tstart4 = tic;
            R1k = R(RR);
            disp(['R1k = ' num2str(R1k)]);

            var4 = genvarname(['R1' num2str(RR)]);

            for dd = 1:length(taud)

                tstart5 = tic;
                tdk = taud(dd);
                disp(['tau_dk = ' num2str(tdk)]);

                var5 = genvarname(['td' num2str(dd)]);

                ink = struct('T2kev', {T2k},...
                    'mf', {mfk},...
                    'l', {lk},...
                    'R1', {R1k},...
                    'r', {r},...
                    'taud', {tdk},...
                    'taui', {taui},...
                    'delta', {delta});

                [zz] = zcycle(ink, properties, dtna, ddnhe3,
dhe3pa);

                z(tt,mm,ll,RR,dd).T2      = T2k;
                z(tt,mm,ll,RR,dd).mf     = mfk;
                z(tt,mm,ll,RR,dd).l      = lk;
                z(tt,mm,ll,RR,dd).R1     = R1k;

```

```

z(tt,mm,ll,RR,dd).taud      = tdk;
z(tt,mm,ll,RR,dd).delta    = delta;

z(tt,mm,ll,RR,dd).ue       = zz.ue;
z(tt,mm,ll,RR,dd).Isp      = zz.Isp;
z(tt,mm,ll,RR,dd).F_f      = zz.F_f;
z(tt,mm,ll,RR,dd).P_f      = zz.P_f;
z(tt,mm,ll,RR,dd).G        = zz.G;
z(tt,mm,ll,RR,dd).W12     = zz.W12;
z(tt,mm,ll,RR,dd).W34     = zz.W34;
z(tt,mm,ll,RR,dd).Efus     = zz.Efus;
z(tt,mm,ll,RR,dd).etaP     = zz.etaP;
z(tt,mm,ll,RR,dd).etaT     = zz.etaT;
z(tt,mm,ll,RR,dd).etaO     = zz.etaO;
z(tt,mm,ll,RR,dd).etat     = zz.etat;
z(tt,mm,ll,RR,dd).fb       = zz.fb;
z(tt,mm,ll,RR,dd).nn       = zz.nn;
z(tt,mm,ll,RR,dd).En       = zz.En;
z(tt,mm,ll,RR,dd).Ec       = zz.Ec;
z(tt,mm,ll,RR,dd).I1       = zz.I1;
z(tt,mm,ll,RR,dd).vl2_T2   = zz.vl2_T2;
z(tt,mm,ll,RR,dd).ue_vl    = zz.ue_vl;

telapse5(dd) = toc(tstart5);
disp(['telapse5 = ' num2str(telapse5(dd))]);
%   if dd==2
%       keyboard
%   end
end
telapse4(RR) = toc(tstart4);
disp(['telapse4 = ' num2str(telapse4(RR))]);
end
telapse3(ll) = toc(tstart3);
disp(['telapse3 = ' num2str(telapse3(ll))]);
end
telapse2(mm) = toc(tstart2);
disp(['telapse2 = ' num2str(telapse2(mm))]);
end
telapse1(tt) = toc(tstart1);
disp(['telapse1 = ' num2str(telapse1(tt))]);
end

%-----
----

time = struct('te1',{telapse1},'te2',{telapse2},'te3',{telapse3},...
             'te4',{telapse4},'te5',{telapse5},'te6',{telapse6});

if X_He3 == 0 && X_T > 0 && X_T < 1.0
    namestring = 'DT';
elseif X_He3 == 0 && X_D == 1.0
    namestring = 'DD';

```

```

elseif X_He3 ~= 0 && X_T == 0
    namestring = 'DHe3';
elseif X_He3 ~= 0 && X_He3 < X_T
    namestring = 'DThe3';
elseif X_He3 ~= 0 && X_He3 > X_T
    namestring = 'DHe3T';
elseif X_He3 ~= 0 && X_He3 == X_T
    namestring = 'D50_He325_T25';
elseif X_He3 == 0 && X_D == 0
    namestring = 'TT';
else
    namestring = input('Input fuel composition string for save file:
', 's');
    if isempty(namestring)
        namestring = 'unknown_fuel';
    end
end

datestring = datestr(clock, 30);
filestring = datestr(now, 'yyyymmdd'); %mkdir(filestring);

save(['/Users/serenity/Documents/MATLAB/cycle/data/' filestring
'/zdata_' namestring '_etat08_' datestring '.mat'], ...
      'z', 'time', 'input', 'properties');

```

APPENDIX B

Z-PINCH CYCLE INPUT FUNCTION: IN.M

```

%R. Cortez
%
%Input function to build structures required to run cycle analysis for
%fusion reaction engine model. Start with step sizes to determine
%resolution of each element in parameter space, then sets the size of
each
%vector for the given input parameters of the model. Then the input
%parameters are built into a structure called 'input'.
%
%Next structure function (nested function) builds input structure of
fuel
%& liner properties for fusion reaction engine cycle analysis. Will
take
%input of total fuel mass, mole fractions of deuterium and helium-3,
and
%will calculate tritium mole fraction followed by the mass of each
%substance in fuel mixture. The properties of the fuel mixture and
liner
%mixture are also calculated.
%
%Liner mass is output in terms of 'fractional liner mass', i.e. it is a
%vector containing values for liner mass as 1 to 1000 times the fuel
mass.
%
%Assumptions:
%
% 1. Currently we assume the only relevant fusion fuels to analyze
%     for now are Deuterium (D), Tritium (T), and Helium-3 (He3).
%
% 2. Liners will be made up of some mixture of lithium, lithium-6,
and
%     lithium-7.
%
%
%Syntax:
%
% function [input, p] = in(X_D, X_3He)
%
% function [properties] = fuelprops(M, X_D, X_3He, X_Li, X_Li6)
%
%
%INPUT:
%
% M          = total mass of the fuel [kg]
% X_D        = mole fraction of deuterium
% X_3He      = mole fraction of helium-3
% X_Li       = mole fraction of lithium in liner
% X_Li6      = mole fraction of lithium-6 in liner
%
%
%OUTPUT:
%
% input = structure containing fields corresponding to each
input
%         parameter for cycle analysis:
%
% Parameters:

```

```

%
%
%           T2kev   = ignition temperature, keV
%           r       = volumetric compression ratio, V1/V2
%           mf      = fuel mass, kg
%           l       = system length, m
%           R1      = initial system radius, m
%           taud    = dwell time, s
%           tau_i   = current rise time, s

```

```

%           p =      structure containing the following levels and
%                   corresponding substance properties:

```

```

%           Level 1: Substance name
%           [d,t,he3,li,li6,li7,fuel,liner]

```

```

%           Level 2: Substance mole fraction X (if specified)
%                   Charge number Z
%                   Molecular weight MW [mi/u]
%                   Molecular mass mi [kg]
%                   Density rho [kg/m^3] (if needed)
%                   Mixture mass m [kg]
%                   Gas constant R [J/kg-K]
%                   Constant volume specific heat cv [J/kg-K]
%                   Constant pressure specific heat cp [J/kg-K]

```

```

function [input, p] = in(X_D, X_He3, X_Li, X_Li6)

```

```

%-----
----
%Step sizes
dr   = 0.25;      %compression ratio
dT   = 5;         %ignition temperature
dR1  = 0.05;     %initial radius
dtaud = 5e-7;    %dwell time
dtaui = 3e-7;    %rise time

```

```

%-----
----
%INPUT:

```

```

X_T = 1-(X_D + X_He3);

```

```

if X_He3 == 0 && X_D < 1.0           %DT mixture
    T2_kev = (10:dT:20)';
elseif X_He3 == 0 && X_D == 1.0     %DD mixture
    T2_kev = (25:dT:40)';
elseif X_He3 == 0.5 && X_T == 0.0   %DHe3 mixture
    T2_kev = (25:dT:40)';
elseif X_He3 ~= 0 && X_He3 < 0.5    %DTHe3 mixture
    T2_kev = (10:dT:25)';

```

```

end

%-----
----
%Set up parameter space

r      = 10.^(1:dr:4)';
%compression ratio, V1/V2
mf     = [10e-6, 50e-6, 100e-6, 500e-6, 1e-3]';           %fuel
mass, kg
l      = [0.05, 0.25, 0.45, 0.65, 0.85, 1.0]';           %system
length, m
R1     = (5e-2:dR1:0.2)';                                   %initial
system radius, m
taud   = [100e-9, 200e-9, 500e-9, 1e-6, 1.5e-6, 2e-6];   %dwell
time, s
taui   = (5e-7:dtaui:2e-6)';                               %current
rise time, s

%-----
----

%Build input structure
input = struct('r',{r},...
              'T2kev',{T2_kev},...
              'mf',{mf},...
              'l',{l},...
              'R1',{R1},...
              'taud',{taud},...
              'taui',{taui});

%Build properties structure
M = input.mf;

[p] = fuelprops(M,X_D,X_He3);

%-----
----

%-----
----

function [properties] = fuelprops(M,X_D,X_3He)

%-----
----

%CONSTANTS:
u = 1.6605e-27;      %atomic mass unit, kg
k = 1.38054e-23;     %Boltzmann constant, J/K
NA = 6.0221e26;      %Avogadro number, kgmol^-1
Ru = NA*k;           %Universal gas constant, J/kgmol-K
gamma = 1.67;        %Ratio of specific heats

%-----
----

```



```

%-----
----
%Fuel properties

%Deuterium, D

D_X    = X_D;
D_Z    = 1;
D_MW   = 2.014;
D_mi   = D_MW*u;
D_rho  = 0.180;    %kg/m^3 at STP (0 C, 101.325kPa)

md     = D_X.*M;

    d =
struct('X',{D_X},'Z',{D_Z},'MW',{D_MW},'mi',{D_mi},'m',{md},'rho',{D_rho});

%Tritium, T

T_X    = 1 - (X_D + X_3He);
T_Z    = 1;
T_MW   = 3.016;
T_mi   = T_MW*u;

mt     = T_X.*M;

    t = struct('X',{T_X},'Z',{T_Z},'MW',{T_MW},'mi',{T_mi},'m',{mt});

%Helium-3, He3

He3_X  = X_3He;
He3_Z  = 2;
He3_MW = 3.016;
He3_mi = He3_MW*u;

m3he   = He3_X.*M;

    he3 =
struct('X',{He3_X},'Z',{He3_Z},'MW',{He3_MW},'mi',{He3_mi},'m',{m3he});
%-----
----

%-----
----
%Liner material properties

%Lithium, Li

```

```

Li_X    = X_Li;
Li_Z    = 3;
Li_MW   = 6.941;
Li_rho  = 535;
Li_mi   = Li_MW*u;

    li =
struct('X',{Li_X},'Z',{Li_Z},'MW',{Li_MW},'rho',{Li_rho},'mi',{Li_mi});

%Lithium-6, Li6

Li6_X   = X_Li6;
Li6_Z   = Li_Z;
Li6_MW  = 6.015;
Li6_mi  = Li6_MW*u;

    li6 = struct('X',{Li6_X},'Z',{Li6_Z},'MW',{Li6_MW},'mi',{Li6_mi});

%Lithium-7, Li7

Li7_X   = 1 - (X_Li + X_Li6);
Li7_Z   = Li_Z;
Li7_MW  = 7.016;
Li7_mi  = Li7_MW*u;

    li7 = struct('X',{Li7_X},'Z',{Li7_Z},'MW',{Li7_MW},'mi',{Li7_mi});
%-----
%-----
%-----
%Calculate fuel mixture properties
mf      = md + mt + m3he;

Zf      = d.Z*d.X + t.Z*t.X + he3.Z*he3.X;

MWf     = d.MW*d.X + t.MW*t.X + he3.MW*he3.X;

Rf      = Ru/MWf;

cvf     = Rf/(gamma-1);

cpf     = gamma*cvf;

mif     = d.mi*d.X + t.mi*t.X + he3.mi*he3.X;

    fuel = struct('mf',{mf},'Z',{Zf},'MW',{MWf},'R',{Rf},'cv',{cvf},...
                  'cp',{cpf},'mif',{mif});

```

```

%-----
-----

%-----
-----
%Calculate liner properties
phi = 10.^(1:0.25:3);      %liner mass fraction

Zl  = li.Z*li.X + li6.Z*li6.X + li7.Z*li7.X;

ml  = M*phi;

MWl = li.MW*li.X + li6.MW*li6.X + li7.MW*li7.X;

Rl  = Ru/MWl;

cvl = Rl/(gamma-1);

cpl = gamma*cvl;

mil = li.mi*li.X + li6.mi*li6.X + li7.mi*li7.X;

liner =
struct('phi',{phi},'ml',{ml},'Z',{Zl},'MW',{MWl},'R',{Rl},'cv',{cvl},...
      'cp',{cpl},'mil',{mil});

%-----
-----

%-----
-----
%Construct output structure of properties

properties = struct('d',{d},...
                   't',{t},...
                   'he3',{he3},...
                   'li',{li},...
                   'li6',{li6},...
                   'li7',{li7},...
                   'fuel',{fuel},...
                   'liner',{liner});

%-----
-----

end

end

```

APPENDIX C

Z-PINCH CYCLE CALCULATION FUNCTION: ZCYCLE.M

```

%R. Cortez
%
% Pulsed Fusion Reaction Engine Cycle Analysis: Z-Pinch
%
% This function will run the calculations for the parametric cycle
% analysis of the z-pinch fusion reaction engine.
% Pass in arguments using structures containing required inputs.
%
%Syntax:
%
% [z] = zcycle(input, properties)
%
%INPUTS:
%
% Input (structure):
%
% input.T2kev      = ignition temperature [keV]
% input.r          = volumetric compression ratio, V1/V2
% input.mf         = fuel mass, kg
% input.l          = system length [m]
% input.R1         = initial radius at state 1 [m]
% input.E          = elongation, l/R1
% input.f          = pulse frequency [Hz]
% input.taud       = dwell time [s]
% input.tau1       = current rise time (implosion time) [s]
%
%
% Properties (structure):
%
% Structure formed using fuelprops function containing the following
% levels and corresponding substance properties:
%
% Level 1: Substance name [d,t,he3,li,li6,li7,fuel,liner]
%
% Level 2: Substance mole fraction X (if specified)
%          Charge number Z
%          Molecular weight MW [mi/u]
%          Molecular mass mi [kg]
%          Density rho [kg/m^3] (if needed)
%          Mixture mass m [kg]
%          Gas constant R [J/kg-K]
%          Constant volume specific heat cv [J/kg-K]
%          Constant pressure specific heat cp [J/kg-K]
%
%-----
%-----

function [z] = zcycle(input, properties, dtna, ddnhe3, dhe3pa)
tic
%-----
%-----

%CONSTANTS:
mu0 = 4*pi*1e-7;    %permeability of free space, H/m

```

```

u = 1.6605e-27;      %atomic mass unit, kg
k = 1.38054e-23;    %Boltzmann constant, J/K
q = 1.6022e-19;     %fundamental charge, C
c = 2.9979e8;       %speed of light, m/s
NA = 6.0221e26;     %Avogadro number, kgmol^-1
Ru = NA*k;          %Universal gas constant, J/kgmol-K
gamma = 1.67;       %Ratio of specific heats
g0 = 9.8;           %acceleration of gravity, m/s/s
%energy units
J = 1;
MJ = J/1e6;
kilotons = J/4.184e12;
handgrenades = kilotons*1000*2000*.4536/.15;
littleboys = kilotons/15;
fatmans = kilotons/20;
%-----

%-----

%INPUTS:
T2kev = input.T2kev;      %[keV]
T2 = T2kev*1000*11605;    %[K]
mf = input.mf;           %fuel mass, kg
l = input.l;             %system length, m
R1 = input.R1;           %initial system radius, m
r = input.r;             %compression ratio, V1/V2
taud = input.taud;       %dwell time, s
taui = input.taui;       %current rise time, s

Z = properties.fuel.Z;    %fuel atomic number
phi = properties.liner.phi; %fractional liner mass, ml/mf
ml = phi.*mf;            %liner mass, kg
X_D = properties.d.X;    %deuterium mole fraction
X_T = properties.t.X;    %tritium mole fraction
X_3He = properties.he3.X; %helium-3 mole fraction
cv = properties.fuel.cv; %fuel cv, J/(kg-K)
cvl = properties.liner.cv; %liner cv, J/(kg-K)
Rf = properties.fuel.R;  %fuel gas constant, J/(kg-K)
Rl = properties.liner.R; %liner gas constant, J/(kg-K)
mif = properties.fuel.mif; %fuel ion mass, kg
MWf = properties.fuel.MW; %molecular weight of fuel
%-----

%-----

%Geometry
V1 = pi.*R1.^2.*l;
V2 = V1./r;

%fuel number density
n1 = mf./mif./V1;
n2 = n1.*r;

```

```

%-----
----
%Zpinch Cycle Analysis

%Thermal efficiency
etaT = 1 - (1./r).^(gamma-1);

%State 1 Internal Energy
U1 = zeros(length(r),length(ml));
for ii = 1:length(ml)
    U1(:,ii) = mf.*cv.*T2.*(1./r).^(gamma-1) + ml(ii).*cvl.*50*11605;
end

%Process [1-2]: Isentropic Compression
%Energy required for ignition
W12 = mf.*(cv + cvl).*T2.*(1-(1./r).^(gamma-1)); %This is within 10%
of calculated value above %Actual amount is off
by %~0.0746547756

%Input current required
I1 = sqrt((8*pi.*mf./mu0./l).*T2.*(cv + cvl).*(r./(r-1)).*(1-
(1./r).^(gamma-1)));
%keyboard
%-----
----
%Process [2-3]: Constant Volume Heat Addition
%Q23 = Efus = (mf.*cv+ml.*cvl).*(T3-T2)

%initial density of species
nD = n2.*X_D; %deuterium
nT = n2.*X_T; %tritium
n3He = n2.*X_3He; %helium-3
n4He = 0; %alpha
nn = 0; %neutron
np = 0; %proton

%rate equations
dt = taud/1000;
nn = taud/dt;
n_D = zeros(length(r),round(nn)); n_D(:,1) = nD;
n_T = n_D*0; n_T(:,1) = nT;
n_3He = n_D*0; n_3He(:,1) = n3He;
n_4He = n_D*0;
n_n = n_D*0;
n_p = n_D*0;

%for burnup fraction calculations
n_D_cold = n_D;
n_D_cold2 = n_D_cold;

```

```

n_T_cold      = n_T;
n_T_cold2     = n_T_cold;
n_3He_cold    = n_3He;
n_3He_cold2   = n_3He_cold;

time = (0:nn)*0;
%keyboard
E_3He = zeros(length(V2),1);
E_4He = zeros(length(V2),1);
E_T    = zeros(length(V2),1);
E_p    = zeros(length(V2),1);
E_n    = zeros(length(V2),1);

T2temp = T2kev;

T3 = T2;      %This sets the initial temperature for process [2-3] so
that
              %as the integration below proceeds, T3 increases
incrementally
              %and is capped at 100 keV in order for the estimate to stay
              %conservative.
%keyboard
%-----
----
%Relevant Species in Reactions:
%
%  1: D           5: Li6           9: n
%  2: T           6: Li7
%  3: He3         7: Be7
%  4: He4 (a)    8: p
%
%Functions to located reactivity for given temperature using data above
%Return reactivity in units of cm^3/sec
%ddnhe3_fun      = @(T2kev)
interp1(ddnhe3.sigv(:,2),ddnhe3.sigv(:,1),T2kev,'linear','extrap');
%dtna_fun        = @(T2kev)
interp1(dtna.sigv(:,2),dtna.sigv(:,1),T2kev,'linear','extrap');
%dhe3pa_fun      = @(T2kev)
interp1(dhe3pa.sigv(:,2),dhe3pa.sigv(:,1),T2kev,'linear','extrap');

%-----
----

for tt = 2:nn+1;

    %R = n_a * n_b * <sig_v>_ab
    %dt_rate      = nD.*nT      .*dtna_fun(T2kev)/1e6;
    dt_rate       = nD.*nT      .*fusion_react('DT',T2kev)/1e6;
    %d3he_rate    = nD.*n3He    .*dhe3pa_fun(T2kev)/1e6;
    d3he_rate     = nD.*n3He    .*fusion_react('DHe-3',T2kev)/1e6;
    %ddn3He_rate  = nD.*nD      .*ddnhe3_fun(T2kev)/1e6;
    ddn3He_rate   = nD.*nD      .*fusion_react('DD_nHe-3',T2kev)/1e6;

```



```

        ddpt_rate = nD.*nD .*fusion_react('DD_pT',T2kev)/1e6;
%don't have the ENDF data for this one

        dnDdt = - dt_rate - d3he_rate -2*ddpt_rate -
2*ddn3He_rate;
        dn3Hedt = - d3he_rate + ddn3He_rate;
        dnTdt = - dt_rate + ddpt_rate;

        dnDdt_cold = - dt_rate - d3he_rate -2*ddpt_rate -
2*ddn3He_rate;
        dn3Hedt_cold = - d3he_rate;
        dnTdt_cold = - dt_rate;

        %pure fusion products
        dn4Hedt = + dt_rate + d3he_rate;
        dnpdt = + d3he_rate + ddpt_rate;
        dnndt = + dt_rate + ddn3He_rate;
%keyboard
        %track energies
        E_3He = E_3He + ddn3He_rate.*V2 .*dt.*.82;
        E_4He = E_4He + dt_rate.*V2 .*dt.*3.5 + d3he_rate.*V2
.*dt.*3.6;
        E_T = E_T + ddpt_rate.*V2 .*dt.*1.01;
        E_p = E_p + d3he_rate.*V2 .*dt.*14.7 + ddpt_rate.*V2
.*dt.*3.02;
        E_n = E_n + dt_rate.*V2 .*dt.*14.1 + ddn3He_rate.*V2
.*dt.*2.45;
%keyboard
        %store species in array vs. time increment
        n_D(:,tt) = n_D(:,tt-1) + dnDdt*dt;
        n_T(:,tt) = n_T(:,tt-1) + dnTdt*dt;
        n_3He(:,tt) = n_3He(:,tt-1) + dn3Hedt*dt;
        n_4He(:,tt) = n_4He(:,tt-1) + dn4Hedt*dt;
        n_n(:,tt) = n_n(:,tt-1) + dnndt*dt;
        n_p(:,tt) = n_p(:,tt-1) + dnpdt*dt;

        n_D_cold(:,tt) = n_D_cold(:,tt-1) + dnDdt_cold*dt;
        n_T_cold(:,tt) = n_T_cold(:,tt-1) + dnTdt_cold*dt;
        n_3He_cold(:,tt) = n_3He_cold(:,tt-1) + dn3Hedt_cold*dt;
%keyboard
        %create logical array to prevent "negative densities" due to
the
        %higher compression ratios
        n_D_cold2(:,tt) = n_D_cold(:,tt) >= 0;
        n_T_cold2(:,tt) = n_T_cold(:,tt) >= 0;
        n_3He_cold2(:,tt) = n_3He_cold(:,tt) >= 0;

        time(tt) = time(tt-1) + dt;

        nD = n_D(:,tt);

        nT = n_T(:,tt);

        n3He = n_3He(:,tt);

```

```

Efus = (E_3He+E_4He+E_T+E_p) *1e6 *q;

T3 = (Efus + T3.*(mf.*cv))./(mf.*cv);           %Recalculate
T3 as reaction proceeds.
T2kev = min(T3./11605./1000,200);             %Determine if
T3 is >=100keV by taking minimum              %value
between T3 and 100, and set
    if ~isreal(T2kev)                          %T2kev equal
to the minimum value
    disp('T2kev not real...what now?');        %for the next
iteration.
    keyboard
end

%      keyboard

end

%-----
-----
%DT =          'DT';      D +   T -> 4He(3.5)  + n(14.1)
%DHe3 =        'DHe-3';   D + 3He -> 4He(3.6)  + p(14.7)
%DD_pT =       'DD_pT';   D +   D ->   T(1.01) + p(3.02)
%DD_nHe3 =     'DD_nHe-3'; D +   D -> 3He(0.82) + n(2.45)
%-----
-----

n_D_coldrange = logical(n_D_cold2(:,end));
n_T_coldrange = logical(n_T_cold2(:,end));
n_3He_coldrange = logical(n_3He_cold2(:,end));

n_D_cold(~n_D_coldrange,end) = 0;
n_T_cold(~n_T_coldrange,end) = 0;
n_3He_cold(~n_3He_coldrange,end) = 0;

%keyboard

%burnup fraction
%fb = 1 - (n_D_cold(:,end) +
n_T_cold(:,end)+n_3He_cold(:,end))./n2;
if n3He(:)==0
    fb = 1 - (n_D_cold(:,end) + n_T_cold(:,end))./n2;
elseif nD(:)==0
    fb = 1 - (n_T_cold(:,end) + n_3He_cold(:,end))./n2;
elseif nT(:)==0
    fb = 1 - (n_D_cold(:,end) + n_3He_cold(:,end))./n2;
else
    fb = 1 - (n_D_cold(:,end) + n_T_cold(:,end) +
n_3He_cold(:,end))./n2;
end

%keyboard

```

```

%fusion energy
Efus = (E_3He + E_4He + E_T + E_p) *1e6 *q;

%neutron count
Nn = n_n(:,end);

%neutron energy
Eneutron = E_n .*1e6*q;

T3 = (Efus + T2.*mf.*(cv+cvl))./(mf.*(cv+cvl));
%keyboard

%-----
----
%Process [3-4]: Isentropic Expansion
W34 = mf.*(cv + cvl).*T3.*(1-(1./r).^(gamma-1));

%Expansion provides useful work output for exhaust and re-charge
circuit
%W34 = (KE)_exhaust + E_charge
%
%AT THE MOMENT WE ASSUME COUPLING EFFICIENCY ETAX = 1.0 SO THAT ED =
W12
%AND CHARGING EFFICIENCY ETAC = 0.8

etat = 0.8;
etax = 1.0;
etac = 0.8;

%Charge energy
Ec = W12./etac./etax;

%Exhaust velocity
% ue = sqrt((2./(mf+ml)).*(etaT.*Efus + (I1.^2).*(mu0.*1./8./pi)).*((r-
1)./r).*...
%          (1 - (1./etat./etac))));

ue = sqrt(outer((2./mf./(phi+1)),(etaT.*Efus + W12.*(1-(1./etac))),2));

%Specific impulse
Isp = ue./g0;

%Thrust
%F_f = (mf+ml).*ue;

F_f = sqrt(outer((2.*mf.*(phi+1)),(etaT.*Efus + W12.*(1-
(1./etac))),2));

%Thrust power
%P = 0.5.*F.*ue;
%P = 0.5.*(mf+ml).*ue.^2;

```

```

P_f = etaT.*Efus + W12.*(1-(1./etac));

%Gain
%G = (8*pi/mu0./l).*(r./(r-1)).*Efus./I1.^2;
G = zeros(length(r),length(ml));
for ii = 1:length(ml)
    X = W12 + U1(:,ii);
    G(:,ii) = Efus./X;
end
%keyboard
%Propulsive efficiency
% etaP = (etaT.*Efus + (I1.^2).*(mu0.*l./8./pi).*((r-1)./r).*(1 -
(1./etat./etac)))...
%      ./ (etaT.*Efus + (I1.^2).*(mu0.*l./8./pi).*((r-1)./r));

etaP = (etaT.*Efus + W12.*(1-(1./etac)))./(etaT.*Efus + W12);

%Overall efficiency
eta0 = etaT .* etaP .* etat .* etax .* etac;

%Liner Velocity
vl2_T2 = outer((2./phi./etat),(cvl.*etaT + cv.*(1 -
(1+etax).*(1./r).^ (gamma-1))),2);

vl = sqrt(vl2_T2 .* T2) ;

%Exhaust Velocity / Liner Velocity
ue_vl = ue ./ vl;

%-----
----
%Output structure
z.ue      = ue';
z.Isp     = Isp';
z.F_f     = F_f';
z.P_f     = P_f';
z.G       = G;
z.W12     = W12;
z.W34     = W34;
z.Efus    = Efus;
z.etaP    = etaP;
z.etaT    = etaT;
z.eta0    = eta0;
z.etat    = etat;
z.fb      = fb;
z.nn      = Nn;
z.En      = Eneutron;
z.Ec      = Ec;
z.I1      = I1;
z.vl2_T2  = vl2_T2;
z.ue_vl   = ue_vl;

toc
end

```

REFERENCES

- [1] Terry Kammash, Ed., *Fusion Energy in Space Propulsion*. Washington, DC: AIAA, 1995.
- [2] Jack D. Mattingly, *Elements of Propulsion: Gas Turbines and Rockets*. Reston, VA: AIAA Education Series, 2006.
- [3] A. A. Harms, G. H. Miley, K. F. Schoepf, and D. R. Kingdon, *Principles of Fusion Energy*. London, UK: World Scientific Publishing Co. Pte. Ltd., 2000.
- [4] K. F. Schoenberg and R. E. Siemon, "Magnetized Target Fusion: A Proof-of-Principle Research Proposal," Los Alamos National Laboratory, proposal 1998.
- [5] J. T. Cassibry, R. J. Cortez, S. C. Hsu, and F. D. Witherspoon, "Estimates Of Confinement Time And Energy Gain For Plasma Liner Driver Magnetoinertial Fusion Using An Analytic Self-Similar Converging Shock Model," *Physics of Plasmas*, vol. 16, no. 112707, 2009.
- [6] T. P. Intrator et al., "A High-Density Field Reversed Configuration Plasma For Magnetized Target Fusion," *IEEE Transactions on Plasma Science*, vol. 32, no. 1, pp. 152-160, 2004.
- [7] Irvin R. Lindemuth and Richard E. Siemon, "The Fundamental Parameter Space Of Controlled Thermonuclear Fusion," *American Journal of Physics*, vol. 77, no. 5, pp. 407-416, 2009.
- [8] R. C. Kirkpatrick, "Magnetized Target Fusion - An Overview of the Concept," in *1st International Symposium for Evaluation of Current Trends in Fusion Research*, Washington, DC, 1994.

- [9] Y. C. F. Thio, Magneto-Inertial Fusion: An Emerging Concept For Inertial Fusion And Dense Plasmas In Ultrahigh Magnetic Fields, 2008.
- [10] Michael A. Liberman, John S. De, Arthur Toor, and Rick B. Spielman, *Physics of High-Density Z-Pinch Plasmas*: Springer, 1999.
- [11] L. Tonks, *Transactions of the Electrochemical Society*, vol. 72, no. 37, p. 167.
- [12] C. A. Coverdale et al., "Deuterium Gas-Puff Z-Pinch Implosions On The Z Accelerator," *Physics of Plasmas*, vol. 14, no. 5, p. 056309, 2007.
- [13] J. P. Chittenden, S. V. Lebedev, B. V. Oliver, E. P. Yu, and M. E. Cuneo, "Equilibrium Flow Structures And Scaling Of Implosion Trajectories In Wire Array Z Pinches," *Physics of Plasmas*, vol. 11, no. 3, pp. 1118-1127, 2004.
- [14] S. V. Lebedev et al., "Physics of Wire Array Z-Pinch Implosions: Experiments at Imperial College," *Plasma Physics and Controlled Fusion*, vol. 47, no. 5A, p. A91, 2005.
- [15] D. J. Ampleford et al., "Dynamics of Conical Wire Array Z-Pinch Implosions," *Physics of Plasmas*, vol. 14, no. 10, p. 102704, 2007.
- [16] S. N. Bland, S. V. Lebedev, J. P. Chittenden, D. J. Ampleford, and G. Tang, "Use of Linear Wire Array Z Pinches To Examine Plasma Dynamics In High Magnetic Fields," *Physics of Plasmas*, vol. 11, no. 11, pp. 4911-4921, 2004.
- [17] W. M. Parsons et al., "The Atlas Project - A New Pulsed Power Facility for High Energy Density Physics Experiments," *IEEE Transactions on Plasma Science*, vol. 25, no. 2, pp. 205-211, 1997.

- [18] R. E. Reinovsky et al., "Pulsed-Power Hydrodynamics: An Application of Pulsed-Power and High Magnetic Fields to the Exploration of Material Properties and Problems in Experimental Hydrodynamics," *IEEE Transactions on Plasma Science*, vol. 36, no. 1, pp. 112-124, 2008.
- [19] L. Christensen et al., "Decade Radiation Test Facility - Plans and Capabilities," *Space Technology Conference & Exhibit*, 1999.
- [20] M. S. Derzon et al., "An Inertial-Fusion Z-Pinch Power Plant Concept," Albuquerque, NM, Technical Report SAND2000-3132J, 2000.
- [21] S. A. Slutz et al., "Z-Pinch Driven Fusion Energy," Albuquerque, NM, Technical Report SAND2000-1342C, 2000.
- [22] S. DeSouza-Machado, A. B. Hassam, and Ramin Sina, "Stabilization of Z Pinch By Velocity Shear," *Physics of Plasmas*, vol. 7, no. 11, pp. 4632-4643, 2000.
- [23] Niansheng Qi et al., "Two-Dimensional Gas Density and Velocity Distributions of a 12-cm-Diameter, Triple-Nozzle Argon Z-pinch Load," *IEEE Transactions on Plasma Science*, vol. 33, no. 2, pp. 752-762, 2005.
- [24] N. F. Roderick et al., "Hydromagnetic Rayleigh--Taylor Instability In High-Velocity Gas-Puff Implosions," *Physics of Plasmas*, vol. 5, no. 5, pp. 1477-1484, 1998.
- [25] Y. Zhang and N. Ding, "Effects of Various Axial Flow Profiles On The Magneto-Rayleigh-Taylor Instability In Z-Pinch Implosions," *Physics of Plasmas*, vol. 13, 2006.

- [26] Yang Zhang and Ning Ding, "Effects of Compressibility On The Magneto-Rayleigh-Taylor Instability In Z-Pinch Implosions With Sheared Axial Flows," *Physics of Plasmas*, vol. 13, no. 2, p. 022701, 2006.
- [27] U. Shumlak et al., "Equilibrium, Flow Shear And Stability Measurements In The Z-pinch," *Nuclear Fusion*, vol. 49, no. 7, p. 075039, 2009.
- [28] N. Qi et al., "Magnetic Rayleigh--Taylor Instability Mitigation In Large-Diameter Gas Puff Z-Pinch Implosions," *Physics of Plasmas*, vol. 15, no. 2, p. 022703, 2008.
- [29] R. P. Golingo, U. Shumlak, and B. A. Nelson, "Formation of a sheared flow Z pinch," *Physics of Plasmas*, vol. 12, no. 6, p. 062505, 2005.
- [30] U. Shumlak and N. F. Roderick, "Mitigation of the Rayleigh--Taylor Instability By Sheared Axial Flows," *Physics of Plasmas*, vol. 5, no. 6, pp. 2384-2389, 1998.
- [31] Rina B. Baksht et al., "On the Stabilization of Gas Puff Implosion: Experiment and Simulation," *IEEE Transactions on Plasma Science*, vol. 26, no. 4, pp. 1259-1266, 1998.
- [32] H. Sze et al., "Magnetic Rayleigh-Taylor instability mitigation and efficient radiation production in gas puff Z-pinch implosions," *Physics of Plasmas*, vol. 14, no. 5, p. 056307, 2007.
- [33] M. J. Moran and H. N. Shapiro, *Fundamentals of Engineering Thermodynamics*, 6th ed.: Wiley, 2007.

- [34] M.B. Chadwick et al., "ENDF/B-VII.0: Next Generation Evaluated Nuclear Data Library for Nuclear Science and Technology," *Nuclear Data Sheets*, vol. 107, no. 12, pp. 2931-3118, 2006.
- [35] W. J. Sarjeant and R. E. Dollinger, *High-Power Electronics*: Tab Books, Inc., 1989.
- [36] T. Polsgrove et al., "Z-Pinch/Dense Plasma Focus Thermonuclear Propulsion System," NASA MSFC Advanced Concepts Office (ED04), Final Report 2010.
- [37] U. Shumlak and N. F. Roderick, "Mitigation of the Rayleigh--Taylor Instability By Sheared Axial Flows," *Physics of Plasmas*, vol. 5, no. 6, pp. 2384-2389, 1998.
- [38] J. H. Degnan et al., "Experimental and Computational Progress on Liner Implosions for Compression of FRCs," *IEEE Transactions on Plasma Science*, vol. 36, no. 1, pp. 80-91, 2008.
- [39] Craig H. Williams, "Application of Recommended Design Practices for Conceptual Nuclear Fusion Space Propulsion Systems," *40th AIAA/ASME/SAE/ASEE Joint Propulsion Conference & Exhibit*, 2004.
- [40] R. P. Drake, J. H. Hammer, C. W. Hartman, L. J. Perkins, and D. D. Ryutov, "Submegajoule Liner Implosion Of A Closed Field Line Configuration," *Fusion Technology*, vol. 30, no. 3, pp. 310-325, 1996.
- [41] J. Dahlin and J. Scheffel, "Self-Consistent Zero-Dimensional Numerical Simulation of a Magnetized Target Fusion Configuration," *Physica Scripta*, vol. 70, pp. 310-316, 2004.

- [42] Brookhaven National Laboratory (BNL). (2011) Evaluated Nuclear Data File (ENDF).
[Online]. HYPERLINK "<http://www.nndc.bnl.gov/exfor/endl00.jsp>"
<http://www.nndc.bnl.gov/exfor/endl00.jsp>
- [43] M. Tuszewski, "Field Reversed Configurations," *Nuclear Fusion*, vol. 28, no. 11, pp. 2033-2092, 1988.
- [44] T. P. Intrator, R. E. Siemon, and P. E. Sieck, "Adiabatic Model And Design Of A Translating Field Reversed Configuration," *Physics of Plasmas*, vol. 15, no. 4, p. 042505, 2008.
- [45] John Slough, "Performance Capability and Mission Analysis for a Pulsed High Density FRC Fusion Rocket," *37th AIAA/ASME/SAE/ASEE Joint Propulsion Conference \& Exhibit*, 2001.
- [46] Adam K. Martin, Richard H. Eskridge, Peter J. Fimognari, and Michael H. Lee, "FIREBALL: Fusion Ignition Rocket Engine with Ballistic Ablative Lithium Liner," *AIP Conference Proceedings*, vol. 813, no. 1, pp. 783-794, 2006.
- [47] H. Schmitt, *Return to the Moon: Exploration, Enterprise, and Energy in the Human Settlement of Space*: Praxis Publishing, Ltd., 2006.
- [48] M. M. Basko, A. J. Kemp, and J. Meyer-ter-Vehn, "Ignition conditions for magnetized target fusion in cylindrical geometry," *Nuclear Fusion*, vol. 40, pp. 59-68, 2000.
- [49] EMC2. [Online]. HYPERLINK "<http://www.emc2fusion.org>" <http://www.emc2fusion.org>

- [50] N. B. Dhote, "Numerical Modeling of Alpha Particle Deposition in Field Reversed Configuration," The University of Alabama in Huntsville, 2008.
- [51] [Online]. HYPERLINK "<http://www.udintsev.com/science/science.html>"
<http://www.udintsev.com/science/science.html>
- [52] [Online]. HYPERLINK "<http://www.answers.com/topic/pinch-effect-1>"
<http://www.answers.com/topic/pinch-effect-1>
- [53] U. Shumlak et al., "Sheared Flow Stabilization Experiments In The Zap Flow Z Pinch," *Physics of Plasmas*, vol. 10, no. 5, pp. 1683-1690, 2003.
- [54] H. Sze et al., "Initial Results For An Argon Z Pinch Using A Double-Shell Gas Puff," *Physics of Plasmas*, vol. 7, no. 10, pp. 4223-4226, 2000.
- [55] Y. Song et al., "Valve And Nozzle Design For Injecting A Shell-On-Shell Gas Puff Load Into A [Bold Z] Pinch," *Review of Scientific Instruments*, vol. 71, no. 8, pp. 3080-3084, 2000.
- [56] G. A. Wurden et al., "FRCHX Magnetized Target Fusion HEDLP Experiments," 2008.